

Abstract

Title of Document: SOURCE DEPENDENT VARIATION IN HYDROXYL RADICAL PRODUCTION BY AIRBORNE PARTICULATE MATTER AND THE IMPACT ON BEAS-2B AND JB6 CELLS.

Marjan Alaghmand, Doctor of Philosophy, 2007

Directed By: Professor Neil V. Blough,
Department of Chemistry and Biochemistry

Numerous studies have shown an association between increased levels of particulate matter (PM) and the exacerbation of lung diseases. The exact means by which PM produces these effects remain unclear. Generation of reactive oxygen species such as the hydroxyl radical ($\cdot\text{OH}$), is one of the hypothesized mechanisms. However, the importance of $\cdot\text{OH}$ production by PM remains uncertain due to a lack of sensitive and selective methods for its determination.

In this work, a highly-sensitive fluorescence-based technique was employed to quantify the magnitude of $\cdot\text{OH}$ generated by a wide range of airborne particulate matter. The generated $\cdot\text{OH}$ was measured in the presence and absence of biological electron donor. Little or no production of $\cdot\text{OH}$ was observed in the absence of the added electron donor. For some but not all particles, $\cdot\text{OH}$ production was increased

substantially when a biological electron donor was present. No detectable $\cdot\text{OH}$ was produced by kaolinite or silica.

The mechanism(s) of $\cdot\text{OH}$ generation by airborne particulate matter were investigated. The presence of dioxygen, hydrogen peroxide, superoxide and metal chelators significantly affected $\cdot\text{OH}$ production by the particles. The results indicate that metals and organic constituents are involved in $\cdot\text{OH}$ production by particles and occur through both homogeneous and heterogeneous reactions.

The effect of different airborne particles on $\cdot\text{OH}$ generation in the presence of two different cell lines, lung epithelial cells (BEAS-2b) and mouse epidermal cells (JB6) were investigated. In addition, two different toxicological methods were employed to investigate cell viability in the presence of different airborne particles. Based on our results, some $\cdot\text{OH}$ production was observed in the presence of these cell lines when exposed to diesel particulate matter and urban dust, but rates of cell death did not correlate with the $\cdot\text{OH}$ production rate. Further, silica particles, which exhibited no evidence of $\cdot\text{OH}$ production, produced the most rapid cell death.

On the other hand, both cell death and hydroxyl radical formation were dramatically enhanced when an external biological reductant, NADPH, was added to a suspension of cells and urban dust. In this situation, the high flux of $\cdot\text{OH}$ is the likely factor causing cell death.

SOURCE DEPENDENT VARIATION IN HYDROXYL RADICAL PRODUCTION
BY AIRBORNE PARTICULATE MATTER AND THE IMPACT ON BEAS-2B
AND JB6 CELLS.

By

Marjan Alaghmand

Dissertation submitted to the Faculty of the Graduate School of the
University of Maryland, College Park, in partial fulfillment
of the requirements for the degree of
Doctor of Chemistry
2007

Advisory Committee:

Professor Neil V. Blough, Chair/ Adviser
Professor Peter L. Gutierrez
Professor George R. Helz
Professor Catherine Fenselau
Professor John Ondov
Professor Mohamad Al-Sheikhly

© Copyright by
Marjan Alaghmand
2007

Dedication
to my parents & sister

Acknowledgements

I would like to express my sincere gratitude to my adviser Professor Neil Blough for his continuous guidance, encouragement, kindness and patience during my PhD studies. Professor Blough's vision and personality make him a great adviser. I, as his student, had a great opportunity to learn a lot about science, research and method of thinking from him. His extraordinary editorial skills also effectively helped me to improve my technical writing skills. I highly appreciate these values, which help my future academic advancement.

I sincerely thank to all my advisory committee members Professor Peter Gutierrez, Professor Catherine Fenselau, Professor George Helz, Professor John Ondov and Professor Mohamad Al-Sheikhly for their support, encouragement, guidance and time.

Special thanks to Professor Peter Gutierrez for his continual advice, support and encouragement. I have learned a lot about science and research, specially cell biology and laboratory techniques such as cell culture from him.

I thank to member of the Blough group (Rossana, Matt, Gan, Nixon, Pramila, Yu, Qing, Min, Lynn, Luca, Tammy and Sarah) for their support and friendship over the years.

I would like to thank my dear uncle and aunt, Dr. Mohamadi and Mrs. Nahid, who have been taking care of me like their daughter from the time that I came to USA for my PhD studying. I will never forget their love and support and I always respect them as the best people in the world.

I would like to thank to my dearest angels, my Mom and Dad, who have been endless source of support, encouragement and love. They always motivated me to improve my knowledge and my personality. I really appreciate their continuous love and patience.

I thank to my sister, Dr. Morvarid, who is everything that is good and beautiful in this world. I really appreciate her endless love, moral support as well as her scientific helps during my PhD studies.

Table of Contents

Abstract.....	1
Acknowledgements.....	iii
Table of Contents.....	v
List of Tables.....	viii
List of Schemes.....	ix
Chapter 1: Introduction.....	1
1.1. Previous studies on particulate matter adverse health effects.....	1
1.2. How does PM lead to adverse health effects?	3
1.3. How is ROS generated by particulate matter?.....	7
1.4. Factors influencing the ROS production and toxicity of particulate matter	14
1.4.1. Solubility of particles.....	14
1.4.4. Surface area of particles.....	17
1.5. Evidence of ·OH involvement in particle induced ROS and cell toxicity.....	17
1.5.1. Spin trapping with Electron Spin Resonance (ESR).....	18
1.5.2. Formation of 8-oxo-dG.....	24
1.5.3. Aromatic hydroxylation.....	27
1.5.4. Other indirect ·OH detection methods.....	29
1.6. New Approach: detection of particle induced ·OH using nitroxide scavenging	
.....	30
Chapter 2: Source Dependent Variation in Hydroxyl Radical Production	
by Airborne Particulate Matter	34
Abstract.....	34
2.1. Introduction.....	35
2.2. Experimental section.....	39
2.2.1. Materials	39
2.2.2. Particle sources	40
2.2.3. Apparatus	42
2.2.4. Determination of hydroxyl radical generated by airborne particles	43
2.2.5. Hydroxyl radical detection and quantification.....	46
2.2.5.1. Preparation and purification of Me-3apf standard for HPLC calibration	
.....	46
2.2.5.2. DMSO and 3ap dependence.....	47
2.2.5.3. Competitive study of methanol and DMSO.....	51
2.2.5.4. Time course for integrated ·OH formation by different airborne particles	
.....	53
2.2.5.5. Precision, accuracy and detection limit (D.L.)	55
2.3. Results.....	56
2.3.1. ·OH formation in particle suspensions in the absence and presence of	
biological reductant.....	56
2.3.2. Dependence of hydroxyl radical formation on type of particle, pH, ionic	
strength and buffer content	61

2.3.3. Dependence of hydroxyl radical formation rate on NADPH.....	65
2.3.4. The origin of hydroxyl radical	66
2.4. Discussion	76
Chapter 3: Impact of Airborne Particulate Matter on Cellular Toxicity .	79
Abstract.....	79
3.1. Introduction.....	80
3.2. Experimental section.....	83
3.2.1. Materials	83
3.2.2. Particle source.....	84
3.2.3. Apparatus	84
3.2.4. Cell culture.....	85
3.2.4.1. Preparation of culture medium for lung epithelial cells (BEAS-2b)	85
3.2.4.2. Preparation of culture medium for mouse epidermal cells (JB6)	85
3.2.4.3. Maintenance of cell culture for BEAS-2b cells	86
3.2.4.4. Maintenance of cell culture for JB6 cells	86
3.2.4.5. Preparation and counting cell suspension	87
3.2.4.6. Dye exclusion test for the viability of cells	88
3.2.4.7. Preparation of the BEAS-2b and JB6 cells for experiments.....	88
3.2.5. Toxicological studies	89
3.2.5.1. Toxicological method I.....	89
3.2.5.2. Toxicological method II.....	90
3.2.6. Synthesis of 3apf.....	90
3.2.7. Kinetics of the probe bioreduction.....	92
3.2.8. Hydroxyl radical determination	93
3.2.9. Hydroxyl radical detection and quantification.....	94
3.2.10. Precision, accuracy and detection limit (D.L.)	95
3.3. Results.....	96
3.3.1. Toxicity of diesel particulate matter, urban dust and Aerosil.....	96
3.3.2. Effect of DMSO concentration on cell viability.....	103
3.3.3. Results of bioreduction of 3apf.....	104
3.3.4. Dependence of Me-3apf and $\cdot\text{OH}$ production on DMSO and 3apf concentration.....	105
3.3.5. Determination of hydroxyl radical production	111
3.3.5. Cell Viability and $\cdot\text{OH}$ production in the presence of external biological reductant.....	118
3.4. Discussion.....	121
Chapter 4: Conclusion and Future Work.....	124
4.1. Conclusion	124
4.2. Future work.....	127
4.2.1. Seasonal and regional studies on $\cdot\text{OH}$ production by PM.....	127
4.2.2. Screening $\cdot\text{OH}$ production by PMs in the presence of other reductants .	127
4.2.3. Determining $\cdot\text{OH}$ produced by PM in the presence of macrophage or other cell lines	128
4.2.4. Physiochemical analysis for diesel particles.....	128
4.2.5. Protein analysis for the cell lines exposed to PM	129
Appendix A: Preliminary work on SRM 2975 analysis	130

Appendix B: Particles properties	143
B.1. Standard Reference Material 1649 (urban dust)	143
B.1.1. Sample collection and preparation	143
B.1.2. Particle size	143
B.1.3. Chemical constituents	144
B.1.3.1. Organic constituents	144
B.1.3.2. Inorganic constituents	148
B.1.4. Toxicity of SRM 1649	149
B.2. Standard Reference Material 1648	150
B.2.1. Sample collection and preparation	150
B.2.2. Chemical constituents	150
B.2.2.1. Inorganic constituents	150
B.2.3. Toxicity of SRM 1648	152
B.3. Standard Reference Material 2975	152
B.3.1. Sample collection and preparation	152
B.3.2. Particle size	152
B.3.3. Chemical constituents	153
B.3.3.1. Organic constituents	153
B.3.4. Toxicity of SRM 2975	154
B.4. Standard Reference Material 2689	154
B.4.1. Sample collection and preparation	154
B.4.2. Chemical Constituents	155
B.4.2.1. Inorganic constituents	155
B.5. Standard Reference Material 1632b	156
B.5.1. Sample collection and preparation	156
B.5.2. Chemical constituents	156
B.5.2.1. Inorganic constituent	157
B.6. KGa-1b (kaolinite)	158
B.6.1. Particle source	158
B.6.2. Chemical constituents	159
B.7. Aerosil	159
B.7.1. Particle source and constituent	159
Bibliography	160

List of Tables

Table 1-1. Particulate matter inorganic and organic constituents.....	13
Table 1-2. A selection of spin trapping molecules.....	18
Table 2-1. Source and description of particles.....	41
Table 2-2. Effect of biological reductant (NADPH and Glutathione) on R_{OH}	60
Table 2-3. Dependence of R_{OH} phosphate concentration, pH and ionic strength.....	64
Table 2-4. Stability constants for metal complexes at physiological pH.....	67
Table 3-1. Viability of BEAS-2b cells in the presence of different concentration of DMSO.....	103
Table 3-2. Rates of $\cdot OH$ formation by different particles in the presence of BEAS-2b and JB6 cells.....	112
Table B-1. Values for particle-size characteristics for SRM 1649.....	145
Table B-2. PAHs and nitro-PAHs and their concentrations in SRM 1649.....	146
Table B-3. PCBs and their concentrations in SRM 1649.....	147
Table B-4. Dibenzo- <i>p</i> -dioxins & Dibenzofurans & their concentration.....	148
Table B-5. Chlorinated Pesticides and their concentrations in SRM 1649.....	149
Table B-6. Quinones & their concentrations in SRM 1649.....	149
Table B-7. Concentration of inorganic constituents in SRM 1649.....	149
Table B-8. Concentration of inorganic constituents in SRM 1648.....	152
Table B-9. Values for particle-size characteristics for SRM 2975.....	153
Table B-10. PAHs and their concentrations in SRM 2975.....	154
Table B-11. Concentration of inorganic constituents in SRM 2986.....	156
Table B-12. Concentration of inorganic constituents in SRM 1632b.....	158

List of Schemes

Scheme 1-1. Mechanistic pathways of particulate matter adverse health effect.....	4
Scheme 1-2. Redox cycle by airborne particles in the presence of biological reductant.....	10
Scheme 1-3. Chemical structure of NADPH.....	11
Scheme 1-4. Keto (I) and enol (II) form of 8-oxo-2'-deoxyguanosine from deoxyguanosine.....	25
Scheme 1-5. The reactions of $\cdot\text{OH}$ addition to benzoic acid.....	28
Scheme 1-6. $\cdot\text{OH}$ trapping method.....	31
Scheme 2-1. $\cdot\text{OH}$ trapping method.....	38
Scheme 2-2. Possible oxidation/ reduction reactions for particle constituents.....	66
Scheme 3-1. $\cdot\text{OH}$ trapping method.....	82

List of Figures

Figure 1-1. The reaction of $\cdot\text{OH}$ with DMPO spin trap and the formation of DMPO-OH spin adduct.....	20
Figure 1-2. Effect of OFA and ROFA concentration on 8-oxo-dG.....	26
Figure 2-1. Chromatogram illustrating formation of Me-3apf (after 60min) in solutions containing 3 mg/ml SRM 2975.....	44
Figure 2-2. Chromatogram illustrating formation of Me-3apf (after 60min) in solutions containing 3 mg/ml SRM 1649.....	45
Figure 2-3. Dependence of Me-3apf formation rate on DMSO concentration.....	48
Figure 2-4. Dependence of Me-3apf formation on the concentration of 3ap.....	50
Figure 2-5. Effect of ethanol on Me-3apf formation rate.....	52
Figure 2-6. Effect of different airborne particles.....	54
Figure 2-7. Time course for formation of hydroxyl radical by SRM 1649 (A) and SRM 2975 (B).....	58
Figure 2-8. Time course for formation of hydroxyl radical by SRM 1649 (A) and SRM 2975 (B) in the presence of 3 mM NADPH.....	59
Figure 2-9. Dependence of R_{OH} on particle concentration.....	62
Figure 2-10. Dependence of R_{OH} on NADPH concentration for SRM 1649 (A) and SRM 2975 (B).....	63
Figure 2-11. Production rate of $\cdot\text{OH}$ (R_{OH}) for airborne particles (reaction mixture) and with addition of.....	68
Figure 2-12. Time course for formation of hydroxyl radical by SRM 1649 (A) and SRM 2975 (B) (\bullet), with addition of 3000 U/mL SOD.....	69
Figure 2-13. Dependence of R_{OH} on NADPH concentration for the supernatant (\circ), the resuspended particles (\blacktriangledown) and the original suspension (\bullet).....	72
Figure 2-14. R_{OH} for the supernatant, the resuspended particles and original suspension of (A) SRM 1649 and (B) SRM 2975	73

Figure 2-15. R_{OH} for the supernatant, the resuspended particles and original suspension of (A) SRM 1649 and (B) SRM 2975.....	74
Figure 2-16. R_{OH} for the supernatant (\square) and the resuspended particles (\blacksquare) of (A) SRM 1649 and (B) SRM 2975.....	75
Figure 3-1. Kinetics of the bioreduction of 3apf by BEAS-2b cells.....	93
Figure 3-2. Graphs A, B and C illustrating BEAS-2b cells growth.....	97
Figure 3-3. Time course for viability of BEAS-2b and JB6 cells in PBS (\bullet); 1 mg/ml suspension of.....	101
Figure 3-4. Time course for viability of BEAS-2b and JB6 cells in PBS (\bullet); 0.1 mg/ml suspension of.....	102
Figure 3-5. Dependence of the product formation rate on DMSO concentration...	107
Figure 3-6. Dependence of Me-3apf formation on the concentration of 3apf.....	110
Figure 3-7. Time course for formation $\cdot OH$ in suspension BEAS-2b or JB6 cells treated with 1 mg/mL SRM 1649 (UD).....	113
Figure 3-8. Dependence of $\cdot OH$ formation rates on cell density.....	114
Figure 3-9. Time course for formation OH in suspension BEAS-2b or JB6 cells treated with 0.5, 1, 2 mg/ml SRM 1649 (UD).....	115
Figure 3-10. Dependence of cell viability on $\cdot OH$ formation rate generated with urban dust at different concentrations.....	116
Figure 3-11. Time course for formation OH in suspension of BEAS-2b or JB6 cells treated with 0.15 mg/ml SRM 2975 (DPM).....	117
Figure 3-12. Time course for OH formation in a cell suspension 2×10^6 cells/mL containing 1 mg/mL SRM 1649 (UD) in the presence of 1 mM NADPH.....	119
Figure 3-13. Time course for viability of BEAS-2b (A) or JB6 (B) cells in PBS...	120
Figure A-1. UV-Visible spectrum of extracted diesel particulate matter in 5 mM phosphate buffer and 0.9% NaCl.....	132
Figure A-2. 3-D fluorescence spectrum of extracted diesel particulate matter in 5 mM phosphate buffer and 0.9% NaCl at pH 7.5 for 24 hours. After the extraction the pH was adjusted to 2.....	133

Figure A-3. Same spectrum as in previous figure, viewed in contour.....	134
Figure A-4. 3-D fluorescence spectrum of extracted diesel particulate matter in 5 mM phosphate buffer and 0.9% NaCl at pH 7.5 for 24 hours. After the extraction pH was adjusted to 4.....	135
Figure A-5. Same spectrum as in previous figure, viewed in contour.....	136
Figure A-6. 3-D fluorescence spectrum of extracted diesel particulate matter in 5 mM phosphate buffer and 0.9% NaCl at pH 7.5 for 24 hours. After the extraction pH was adjusted to 10.....	137
Figure A-7. Same spectrum as in previous figure, viewed in contour.....	138
Figure A-8. (A) UV-Visible spectrum of extracted diesel particulate matter in 5 mM phosphate buffer and 0.9% NaCl.....	139
Figure A-9. (A) UV-Visible spectrum of extracted diesel particulate matter in 5 mM phosphate buffer and 0.9% NaCl.....	140
Figure A-10. (A) UV-Visible spectrum of extracted diesel particulate matter in 100 mM phosphate buffer.....	141
Figure A-11. (A) UV-Visible spectrum of extracted diesel particulate matter in 5 mM phosphate buffer.....	142
Figure A-12. (A) UV-Visible spectrum of extracted diesel particulate matter in water for 24 hours.....	143

List of Abbreviations

ACN	acetonitrile
3ap	3-amino-2,2,5,5-tetramethyl-1-pyrrolidinyloxy
AP1	activator protein 1
BAL	bronchioalveolar Lavage
BEAS-2b	human lung epithelial cell
CAT	catalase
$\cdot\text{CH}_3$	methyl radical
CFA	coal fly ash
DFX	deferoxmine
DEP	diesel exhaust particles
DETAPAC	diethylaminepentaacetic acid
DMPO	5,5-dimethyl-1-pyrroline-N-oxide
DMSO	dimethyl sulfoxide
DMTU	diemethylthiourea
DNASSB	DNA double strand break
DPM	diesel particulate matter
DTPA	diethylenetriamine pentaacetic acid
EDTA	ethylenediaminetetraacetic acid
EMEM	earl modified essential medium
EtOH	ethanol
ESR	electron spin resonance

EPR	electron paramagnetic resonance
GSH	glutathione
GSSG	oxidized form of glutathione
JB6	mouse epidermal cell
HPLC	high performance liquid chromatography
IL-6	interleukin-6
IL-8	interleukin-8
KBM	keratinocyte basal medium
KGM	keratinocyte growth medium
LDH	lactate dehydrogenase
MAPK	mitogen-activated protein kinases
MeOH	methanol
MIP-2	macrophage inflammatory protein-2
MWCNT	multi-walled carbon nanotube
NAC	N-acetylcysteine
NADPH	nicotinic adenine dinucleotide phosphate reduced form
NF- κ B	nuclear factor kappa B
OFA	oil fly ash
O ₂ ⁻	superoxide
·OH	hydrogen peroxide
8-oxo-dG	8-oxo-2'-deoxyguanosine
PAH	polycyclic aromatic hydrocarbons
PBN	<i>a</i> -Phenyl- <i>tert</i> -butylnitron

PBS	phosphate buffer saline
PM	particulate matter
4-POBN	a-(4-Pyridyl 1-oxide)-N-tert-butyl nitron
ROFA	residual oil fly ash
RNS	reactive nitrogen species
ROS	reactive oxygen species
SRM	standard reference material
SOD	superoxide dismutase
SWCNT	single walled carbon nanotubes
TNF- α	tumor necrosis factor
UD	urban dust
UV-Vis	ultraviolet or visible light

Chapter 1: Introduction

1.1. Previous studies on particulate matter adverse health effects

Exposure to airborne particles presents a serious risk to human health with significant increases in both morbidity and mortality rates (Dockery et al. 1992). The current levels of airborne particulate matter increases mortality as a result of chronic bronchitis, pneumonia, asthma attacks, cardiovascular disease and lung cancer (Whittemore and Korn 1980; Schwartz et al. 1992; Dockery et al. 1993). In the past few decades, different studies have been conducted to understand the origin of adverse health effects of particulate matter (PM) from external factors such as smoking, exposure to asbestos, quartz particles, urban dust, coal dust, and diesel particles. Early studies focused on severe air pollution episodes such as that in the Meuse Valley, Belgium (Firket 1931) and the London fog incident (Logan 1953) dating back to the 1930's. By 1970, a link between respiratory disease and air pollution particles was established and some efforts were applied to reduce the air pollution and improve the air quality. Despite the air quality improvements over the past few decades, associations between current ambient pollution levels and excess morbidity and mortality have been consistently detected.

Over the last decade, epidemiological and clinical studies have provided additional evidence for the potential negative effect of airborne particles on health (Brook et al. 2002; Samet et al. 1999). The current level of PM has been positively

associated with the exacerbation of asthma and an increase in airway inflammation, a decrease in pulmonary function and increase in chronic obstructive pulmonary disease (Dye et al., 1997; Sunyer et al. 2001). Several studies have also reported adverse cardiovascular outcomes in relation to long-term particulate matter exposure (Brook et al., 2004). Airborne particulate matter has been associated with the increase in cancer, especially lung cancer (Pope et al., 2002). These particles were also found to produce heritable genetic changes that can be passed to the next generation (Samet et al., 2004; Somers et al., 2004). In addition, the rapid development of nanotechnology has provided considerable attention to research about the health impact of ultrafine particles (Maynard and Kuempel, 2005). In sum, numerous epidemiological studies have shown increased risk of respiratory and cardiovascular morbidity and mortality due to exposure to particles.

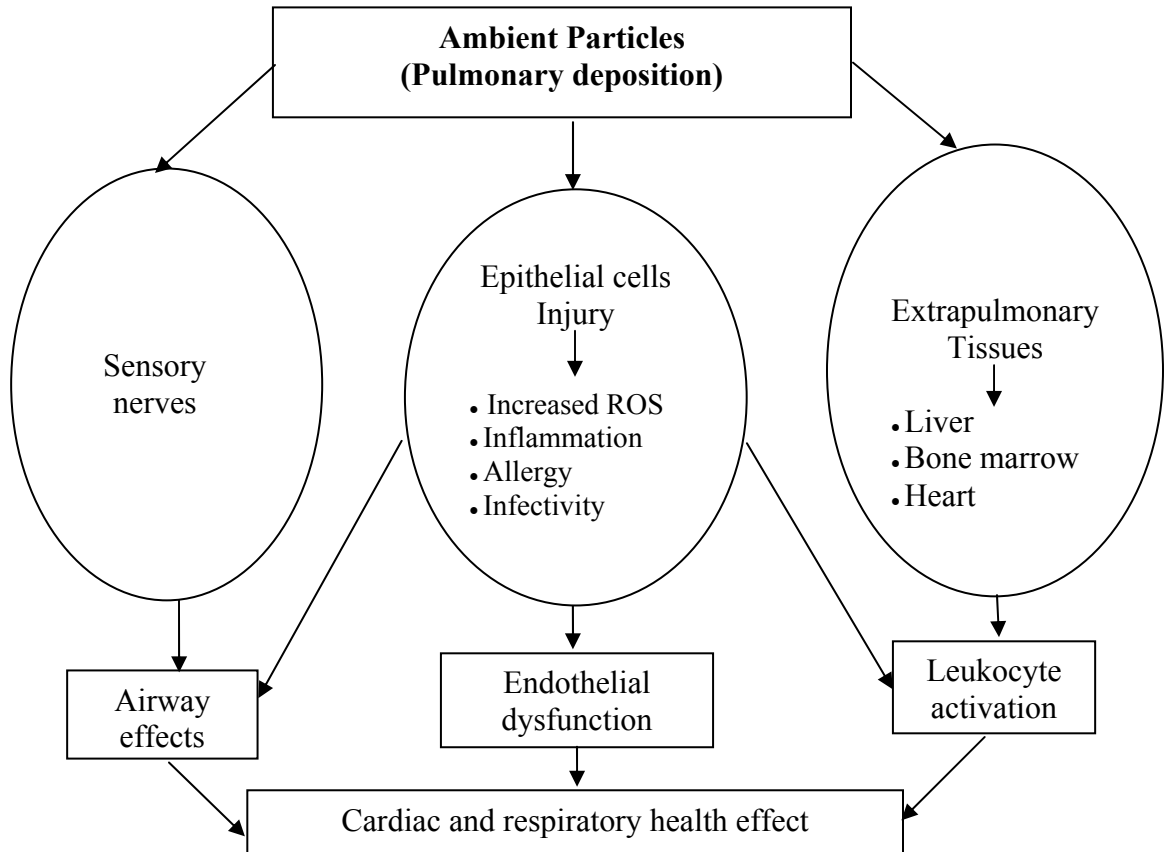
To develop methods that could be employed to mitigate the adverse health effects induced by particulate matter, it is important to understand the mechanisms that are involved in PM interactions with lung or other tissues. The mechanisms by which PM produce these detrimental health effects are under investigation but are still not fully defined. Because of the heterogeneity in PM composition, it is often difficult to identify a single causative mechanism.

1.2. How does PM lead to adverse health effects?

In this section, we briefly review the hypothetical mechanisms that explain adverse health effects caused by PM. Utell and Frampton (2000) provide a summary of possible pathways that may link PM exposure with adverse health effects (Scheme 1-1). In this scheme, three different mechanisms were suggested:

- 1) Particulate matter may stimulate airway sensory nerves, which causes cardiopulmonary dysfunction.
- 2) Ultrafine particles may enter pulmonary capillary blood and be transported to other tissues such as liver, bone marrow and heart. Ultimately, adverse health effects develop because of the activation of the immune system.
- 3) Particulate matter causes epithelial cell injury through production of reactive oxygen species such as $\cdot\text{OH}$ by either the particles themselves or through inflammatory response which ultimately results in endothelial dysfunction, airway effects and leukocyte activation.

Scheme 1-1. Mechanistic pathways of particulate matter adverse health effect (Utell & Frampton, 2000).



Although different pathways for particulate-matter induced health effects have been suggested, past work suggests that production of reactive oxygen species (ROS) is one of the most important mechanisms in particulate-related adverse health effects.

Various studies have reported that ROS generated by PM provides pro-inflammatory stimuli to lung epithelial cells and macrophages. These studies have shown that ROS or the particles themselves activates the immune system with cytokine and chemokine production (such as Interleukin-6 (IL-6), Interleukin-8 (IL-

8), tumor necrosis factor (TNF- α), macrophage inflammatory protein-2 (MIP-2)) which subsequently cause more inflammation, cell death or proliferation leading to adverse health effects (Tao et al., 2003; Huang et al. 2003; MacNee and Donaldson, 2003; Shukla et al., 2000; Mossman and Churg, 1998; Castranova, 2000; Tao and Kobzik, 2002; Utell and Frampton, 2000).

In general, cytokines and chemokines are small secreted proteins which regulate the immune response. Researchers have employed techniques to measure immune response of cells (through chemokine and cytokine production) as an evidence for presence of ROS. For example, Li et al. (2002) tested the sensitivity of a bronchial epithelial cell line (BEAS-2b) and macrophages to diesel exhaust particles (DEP) to determine whether there is a link between the level of ROS production and cellular response. They reported that in presence of 100 $\mu\text{g/mL}$ of DEP, approximately 75% of the BEAS-2b cells were killed with a decline in GSH/GSSG ratio (ratio of reduced to oxidized disulphide-linked glutathione) and increase in IL-8 level, which are a representative marker for oxidative stress. Veranth et al. 2004 also reported an increase in inflammatory cytokines (IL-6 and IL-8) and cell death when BEAS-2b cells were treated with soil dust.

ROS generated by particulate matter is also thought to activate several redox-responsive signaling pathways (such as Nuclear Factor Kappa B (NF- κ B), Mitogen-Activated Protein Kinases (MAPKs) and Activator Protein 1 (AP-1)) that are involved in gene expression and play a role in pathological changes. For instance, it has been reported that transition metals (Jiménez et al. 2000), diesel particulate matter (Takizawa et al. 1999) and silica (Kang et al. 2000) activate NF- κ B in cells and

macrophages. These studies concluded that generation of ROS is the major factor in the activation of NF- κ B.

In other studies, radical scavengers and inhibitors were applied to further investigate the role of generated ROS in NF- κ B activation. For example, Shi et al. (1999) found that catalase and radical scavengers such as DMSO inhibited silica induced-NF- κ B activation. On the other hand, other studies (Chen et al. 1995, Takizawa, et al. 2003) showed that antioxidant N-acetylcysteine (NAC) did not inhibit NF- κ B activity generated by silica. Huang et al. (2002) reported that metal chelators such as deferoxamine (DFX), ethylenediaminetetraacetic acid (EDTA) or diethylenetriamine pentaacetic acid (DTPA) did not affect NF- κ B activity generated by urban dust (SRM 1649), but Jiménez et al. 2000 provided evidence that DFX was an inhibitor for NF- κ B activity. Clearly, these studies do not provide consistent results, linking PM-induced NF- κ B activation with ROS generation.

It has also been reported that MAPKs and AP1 are activated by exposure to airborne particles such as asbestos and silica. For example, Ding et al. (1999) reported that freshly fractured silica activates MAPK, leading to increase in AP1 activity in mouse epidermal cells (JB6) and rat lung epithelial cells. Shukla et al. (2001) showed that α -quartz (silica) causes production of AP-1 and this production was inhibited with catalase (CAT) and hydroxyl radical scavengers such as diemethylthiourea (DMTU). They concluded that ROS generated by particles is the major factor to activate MAPKs and AP1 in these systems.

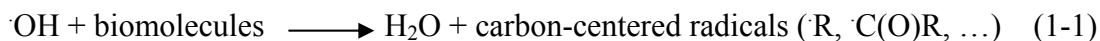
Although many studies have been performed to correlate increase in cytokines, chemokines and other redox representative signaling pathways to

generated ROS by airborne particulate matter, none of these studies have directly measured PM-induced ROS.

1.3. How is ROS generated by particulate matter?

Free radicals can be defined as any species containing one or more unpaired electrons. Particles consist of different components that may produce variety of free radicals through different reaction. Oxygen-centered radicals such as hydroxyl radical ($\cdot\text{OH}$), superoxide anion ($\text{O}_2^{\cdot-}$) alkoxy radicals ($\cdot\text{OR}$), peroxy radicals ($\cdot\text{OOR}$), as well as carbon-centered radicals such as alkyl radical ($\cdot\text{R}$), α -keto radicals ($\cdot\text{C}(\text{O})\text{R}$) may be produced.

Hydroxyl radical is highly reactive oxygen-centered radical which reacts rapidly with all biomolecules. Reaction of $\cdot\text{OH}$ produces secondary radicals which are usually less reactive than $\cdot\text{OH}$ (Rxns 1-1 through 1-3).

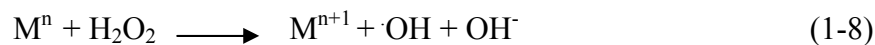
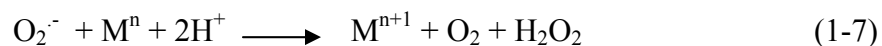
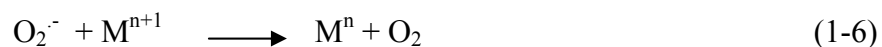
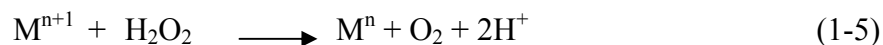


Superoxide, by comparison with $\cdot\text{OH}$, is far less reactive with non-radical species in aqueous solution. The rapid disappearance of $\text{O}_2^{\cdot-}$ in aqueous solution is due to the dismutation reaction. In this reaction, one $\text{O}_2^{\cdot-}$ is oxidized to O_2 and another is reduced to H_2O_2 (Rxn 1-4).



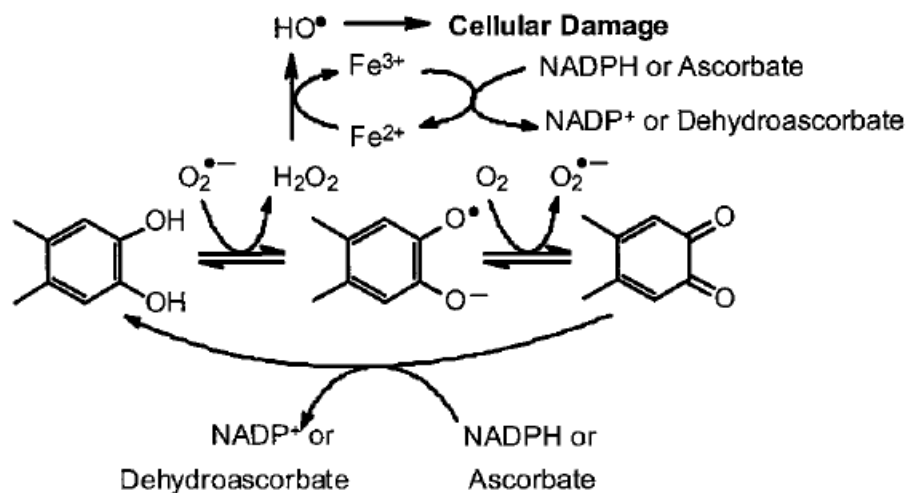
Peroxy and alkoxy radicals are good oxidizing agents although alkoxy radicals formed in biological systems often undergo rapid molecular rearrangement to other species. Carbon-centered radicals are important reactive intermediate formed in a certain reduction and oxidation of organic and biological materials. The preferred fate of many of these radicals, under aerobic conditions, is direct reaction with O_2 (Rxn 1-2, 1-3; Halliwell and Gutteridge, 1999).

Based on different studies, oxidative stress is a central hypothetical mechanism for adverse health effect of airborne particles. Oxidative stress is defined as a situation when the production of ROS or reactive nitrogen species (RNS) exceeds the antioxidant defenses of the cell, thus affecting cell function. Dellinger et al. (2001) suggested that oxidative stress caused by the production of ROS is a fundamental mechanism of particulate toxicity. ROS are a class of compounds which includes hydroxyl radical ($\cdot OH$), superoxide anion ($O_2^{\cdot -}$), hydrogen peroxide (H_2O_2) and singlet oxygen (1O_2). Hydroxyl radical is the most highly reactive ROS that can kill cells through reaction with biomolecules. Although hydroxyl radical can be generated by ionizing radiation (X-ray or γ -ray), it is thought to be formed in vitro and in vivo by Fenton reaction (1-7) and Haber-Wiess reaction (1-8), which is sum of reactions 1-5 through 1-7.



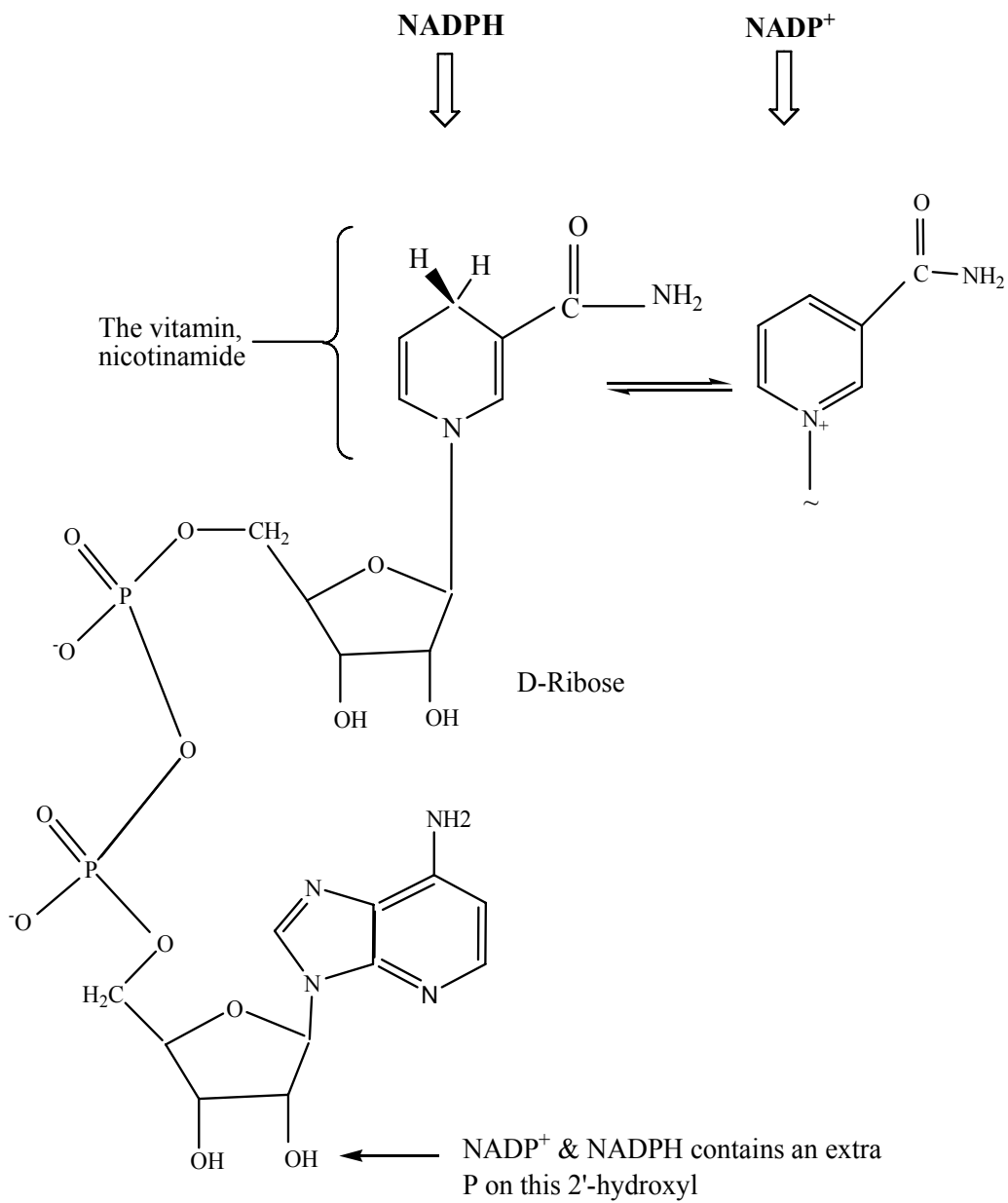
where M^{n+} and M^{n+1} represent reduced and oxidized metal species, respectively, In this reactions, transition metals such as iron (Fe^{+3}), copper (Cu^{+2}), cobalt (Co^{+2}), nickel (Ni^{+2}), titanium (Ti^{+3}), vanadium (vanadyl) , as ions or chelates, are known or have been postulated to produce $\cdot OH$ (Halliwell and Gutteridge, 1999). Pure hydrogen peroxide has limited reactivity, but it is able to cross cell membranes. Superoxide crosses cell membranes very slowly due to its charge and is generally assumed poorly reactive, but is known to react specifically with certain enzymes (Halliwell and Gutteridge, 1999).

Dallinger et al. (2001) first proposed a hypothetical reaction scheme in which particle constituents form the highly reactive ROS, $\cdot OH$ (Scheme 1-2).



Scheme 1-2. Redox cycle by airborne particles in the presence of biological reductant (Dellinger et al. 2001)

This scheme indicates that two different pathways are involved in ROS formation, especially $\cdot\text{OH}$. First, the organic component of particles is involved in redox cycling under aerobic condition. In this cycle, quinone derivatives are reduced by biological electron-transfer chains or reducing enzymes to form the hydroquinone (Lind et al. 1982). Subsequent electron transfer to $\text{O}_2^{\bullet-}$ and dioxygen generates H_2O_2 and $\text{O}_2^{\bullet-}$ regenerating the quinone (Powis et al. 1981). Second, transition metals catalyze formation of $\cdot\text{OH}$ by participating in Fenton reaction. In this reaction, a reduced metal ion reacts with H_2O_2 to produce $\cdot\text{OH}$ and OH^- (Powis et al. 1989). Both the first (organic constituents) and second (trace metal) pathways are enhanced in the presence of reducing agents or enzymes such as ascorbate, NADPH, NADH or other reductants. Chemical structures of NADH and NADPH are presented in Scheme 1-3.



Scheme 1-3. Chemical structure of NADPH and NADP⁺

Airborne particles contain a wide variety of inorganic compounds (eg., minerals, and transition metals) and organic compounds (eg., polycyclic aromatic hydrocarbons (PAHs), polychlorinated biphenyls (PCBs) and quinones). Table 1-1 and Appendix B present the certified reports on particulate matter chemical compositions. The SRMs certificate of analysis (National Institute of Standard and Technology, 2006) shows that these particles contain various minerals and organic components such as metals, PAHs, PCBs, quinones and pesticides whose concentrations vary in range (see Appendix B). Although there are numbers of toxic and known chemical carcinogens among those reported chemicals, the specific compounds which cause cellular toxicity and adverse health effect have not been identified. On the other hand, some studies have shown that inhalation of high concentration of particles containing few toxic compounds (little or no quinones, PAHs, trace metals, ...) also results in adverse health effects. The possible mechanism behind such effects may be due to the overloading of the lung with poorly soluble particles, thus resulting in chronic inflammation.

Table 1-1. Particulate matter inorganic and organic constituents

Particulate Matter	Inorganic Constituents	Organic Constituents
Urban Dust SRM 1649a	Br, Cl, Fe, Pb, Mg, S, Zn, Sb, As, Ba, Cd, Ce, Cs, Cr, Co, Cu, La, Mn M Ni, Se, Ag, W, V, Sn	Chlorinated Pesticides , PAHs
Urban Dust SRM 1648	Cl, I, Fe, Pb, Mg, Al, S, Zn, Sb, As, Ba, Cd, Ce, Cs, Cr, Co, Cu, La, Mn Ni, Se, Ag, W, V, In, K, Na	Not Reported
Coal Fly Ash SRM 2689	Al, Ca, Fe, K, Mg, Na, P, Si, S, Ti, Ba, Mn, Sr, Zn, Se, Ni, Pb, Ce, Cr, Be, As, Sb, Sc.	Not Reported
Coal Fly Ash (Bituminous) SRM 1632b	C, S, Al, Ca, Fe, K, Mg, Na, Ti, As, Ba, Cd, Co, Cu, F, Pb, Mn, Ni, Rb, Se U, Zn, Sb, Br, Ce, Cs, Cl, La, Li, Mo, Sc, Si, St, W. V	Not Reported
Diesel Particulate Matter SRM 2975	Not Reported	PAHs, Quinones
Uncommon Commercial Asbestos SRM 1867a	Si, Fe, Ca, Mg	Not Reported
Kaolinite	Si, Fe, Ca, Mg	-
Aerosil	Si	-

In addition to the particle constituents, other key factors influencing the biological reactivity and toxicity of airborne particulate matter are its solubility, size, shape and surface area. A more complete discussion about these chemical and

physical properties that influence ROS production and toxicity of inhaled particles is provided, in the next sections.

1.4. Factors influencing the ROS production and toxicity of particulate matter

1.4.1. Solubility of particles

Airborne particles usually consist of both soluble and insoluble components. A large number of studies have been performed to examine whether the soluble or insoluble constituents play a greater role in generating ROS. The major portion of the soluble component appears to be mostly metal ions, which can participate in toxicity of particles (Knaapen et al. 2002). In addition, particles treated with metal chelators such as EDTA and DTPA mobilized metal ions that resulted the production of ROS and DNA strand breaks (Smith and Aust, 1997; Imrich et al. 2000). Adding deferoxamine (DFX), which strongly chelates Fe ions, inhibited the production of ROS and cellular damage (Molinelli et al. 2002, Knaapen et al. 2002). Brunner et al. (2006) investigated toxicity of different nanoparticle, such as silica, asbestos, iron oxide (Fe_2O_3), ceria (CeO_2), zinc oxide (ZnO) and zirconia (ZrO). They reported that redox active and relatively soluble particles (such as Fe_2O_3 and asbestos) showed more cytotoxicity and caused less cell viability due to participating in Fenton like reactions. Antonini et al. (2004) found that presence of specific water soluble metals in residual oil fly ash (ROFA) is associated with inflammation. For example, they

reported that water-soluble metals such as nickel and iron cause an increase in lactate dehydrogenase (LDH; indicating tissue damage). Adamson et al. (1999) also reported that the soluble fraction of particles alone exhibits pulmonary toxicity.

Antonini et al. (1999) reported that both soluble and insoluble fractions of particulate matter induced lung injuries as measured by bronchioalveolar lavage (BAL) fluid proteins and LDH activity. It was also shown that a combination of ultrafine carbon black and transition metals produces ROS and the production of ROS in the presence of two components is more than each individually (Wilson et al. 2002).

Other studies have shown that some particles that are poorly soluble also cause oxidative stress, either directly from free radical production or indirectly by triggering the influx of immune cells into the lungs, leading to inflammation.

1.4.2. Size of particles

Particle size has also been shown to influence both biological responses and cytotoxicity to cells and tissues (Osornio-Vargas et al. 2003). Smaller particles have more highly toxic effect, presumably due to their larger surface area. For instance, ultrafine particles composed of a low-toxicity material such as polystyrene showed proinflammatory activity (greater number of neutrophils in the lung and greater oxidant activity) due to their large surface area (Brown et al. 2001).

Another potential reason for the higher toxicity of smaller particles is their ability to enter lung cells. Oberdörster et al. 1992 have observed that smaller ultrafine

particles (~20 nm) can penetrate the alveolar epithelial lining and enter the lung tissues to a greater extent than the larger size particles (>200 nm). Li et al. (2003) reported that nanometer-sized particles may enter cells and localize in mitochondria, producing oxidative damage of the mitochondrial membrane. Furthermore, there is some evidence that nanometer particles can pass from lungs into bloodstream. In one study, translocation of particles from lung into the blood or other organs was traced by using labeled ultrafine carbon particles (^{13}C) (Nemmer et al. 2002). There is a hypothesis that the interaction of particles with proteins influences the translocation of inhaled nanoparticles (Kreyling et al. 2002).

Kleeman et al. (2000) showed that particles with a diameter of 0.1 μm or less mostly consist of organic and elemental carbon rather than sulfate, ammonium, nitrate, sodium and chloride and this could be an additional reason behind the toxicity of ultrafine particles. This conclusion is very consistent with the results obtained by Möller et al. (2002) who reported that ultrafine particles such as carbon black and diesel particulate matter (having more organic components) caused cytoskeletal dysfunction and decreased cell viability in primary alveolar macrophage cell line.

1.4.3. Shape of particles

The shape of particles can be generally defined as isotropic (identical in all directions) or anisotropic (non-identical in all directions). Exposure to both isotropic and anisotropic particles has been associated with adverse health effects (Maynard, and Kuempel, 2005). Other work has indicated that the morphology of nanoparticles

is also important. For example, specific attention has been paid to single walled carbon nanotubes (SWCNT) which caused inflammation in mice (Lam et al. 2004) and mortality in rats due to airway blockage (Warheit et al. 2004). Shvedova et al. (2003) also reported generation of oxidative stress, cellular toxicity and loss of cell viability in the presence of human cells and unpurified SWCNT (containing 30% iron by mass). A recent study of multi-walled carbon nanotube (MWCNT) showed that the particles can penetrate human epidermal cells and produce cytokines (Monteiro-Riviere et al. 2005).

1.4.4. Surface area of particles

The surface area of airborne particles has been long known to be an important factor influencing the toxicity of inhaled particles (Duffin et al. 2002; Brown et al. 2001, Tran et al. 2000; Tran et al. 1999) . Particle surface area expresses the real dose of particles. Smaller particles can provide a larger reactive surface area and this will be more toxic.

1.5. Evidence of $\cdot OH$ involvement in particle induced ROS and cell toxicity

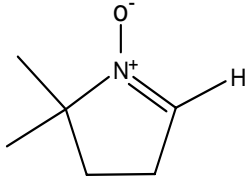
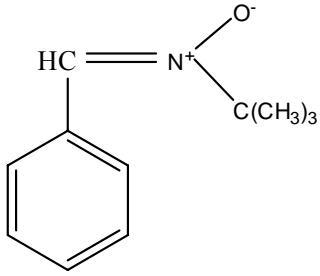
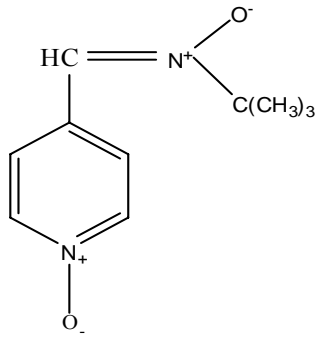
Different studies have shown that airborne particles can cause cellular toxicity and the production of ROS. However, relatively few studies have quantified the

hydroxyl radical production by particles. One of the most widely used methods is spin trapping with electron spin resonance (ESR) detection which was employed by different groups to detect formation of hydroxyl radical by particles. Other methods employed measure the formation of 8-oxo-2'-deoxyguanosine (8-oxo-dG), aromatic hydroxylation and some other indirect methods. A summary of studies that have been performed to detect hydroxyl radical by airborne particles is provided below.

1.5.1. Spin trapping with Electron Spin Resonance (ESR)

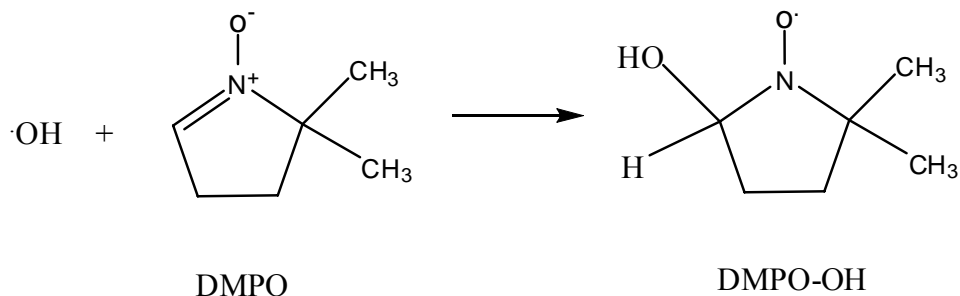
The most widely employed method for detecting the ·OH produced by airborne particles is spin trapping with electron spin resonance detection (ESR; Briedé et al. 2005; Valavanidis et al. 2005, Baulig et al. 2004, Shi et al. 2003a, Kadiiska et al. 1997, Dalal et al. 1995, Dalal et al. 1990, Shi et al. 1988, Vallyathan et al. 1988).

Table 1-2. A selection of spin trapping molecules

Name	Abbreviation	Structure
5,5- Dimethylpyrroline-N-oxide	DMPO	
<i>a</i> -Phenyl- <i>tert</i> -butylnitronone	PBN	
<i>a</i> -(4-Pyridyl 1-oxide)- <i>N</i> - <i>tert</i> -butylnitronone	4-POBN	

In this technique, a transient radical reacts with the trap (such as DMPO, PBN and 4-POBN; Table 1-2) to produce a radical that has a longer lifetime. This enhanced stability is due in part to electron delocalization between nitrogen and oxygen atoms. The most used spin trap for detecting oxygen-centered radical is 5, 5-dimethyl-1-pyrroline-N-oxide (DMPO; Janzen et al. 1990). DMPO, a diamagnetic species, reacts with $\cdot\text{OH}$ to generate a paramagnetic product (DPMO-OH), which has a four line

(1:2:2:1) ESR signal (Figure 1-1). DMPO also reacts with O_2^- to form a product with different ESR spectra, but this product (DMPO-OOH) is unstable and can decompose to the DMPO-OH product, thus complicating the interpretations. However, the rate constants for these two reactions are very different ($10 \text{ M}^{-1} \text{ s}^{-1}$ for O_2^- ; $3.4 \times 10^9 \text{ M}^{-1} \text{ s}^{-1}$ for OH), therefore, OH is trapped more efficiently than O_2^- .



DMPO-OH EPR spectrum

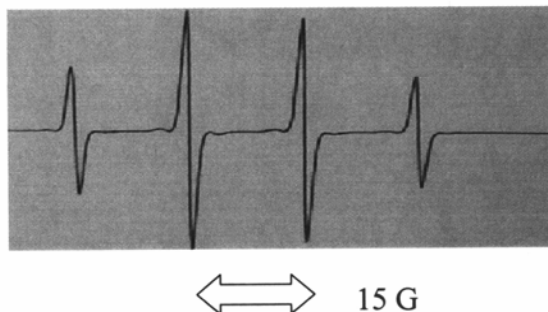


Figure 1-1. The reaction of $\cdot\text{OH}$ with DMPO spin trap and the formation of DMPO-OH spin adduct.

In both past and more recent studies, spin trapping employing DMPO with ESR detection was widely used to detect $\cdot\text{OH}$ generated by airborne particulate matter. Briedé et al. (2005) used DMPO to test the formation of $\cdot\text{OH}$ by particulate matter (PM_{10} and $\text{PM}_{2.5}$) in the presence of either NADPH or ascorbate. They reported that DMPO-OH signal was enhanced in the presence of low concentrations

of biological reductant, but this signal did not increase at concentrations of reductant higher than 50 μM .

Valavanidis et al. (2005) examined the possible mechanisms and parameters influencing the formation of ROS by diesel vehicle exhaust soot, gasoline vehicle exhaust soot and samples of fresh soot from wood combustion. They detected by ESR five different semi-quinones originating from 1,2-naphthoquinone, 1,4-naphthoquinone and 1,4 benzoquinone in particulate matter extracted in aqueous phase (phosphate buffer pH=7.4). They also detected DMPO-OOH and DMPO-OH and concluded that the detected quinones were in part responsible for generating ROS, especially $\cdot\text{OH}$.

Baulig et al. (2004) observed DMPO-OH adduct generation in a suspension of $\text{PM}_{2.5}$ in the absence and presence of H_2O_2 . Shi et al. (2003a) also used ESR to measure hydroxyl radical formation by different particulate matter (PM_1 , $\text{PM}_{2.5}$, PM_{10}) in the presence and absence of H_2O_2 and radical scavengers. Based on their results, higher concentration of H_2O_2 provided more hydroxyl radical generation whereas $\cdot\text{OH}$ scavengers (DMSO and ethanol) suppressed the $\cdot\text{OH}$ formation. From DPMO-OH detection with different metal-coated carbon black particles, they found that particles coated with Cu^{+2} , Fe^{+2} , V^{+2} , V^{+5} generated more $\cdot\text{OH}$ than those coated with Fe^{+3} , Ni^{+2} , Zn^{+2} .

Kadiiska et al. (1997) tested the hypothesis that exposure to air pollution particles is associated with in vivo free radical production. In this work, ESR in conjunction with the spin trap α - (4- pyridyl- 1- oxide)- N- tert- butylnitrone (4- POBN) was used to detect radicals. Incubation of rat lung with an oil fly ash (OFA) sample provided spectra consistent with a carbon-centered (phenyl or ethyl) radical

adduct. They concluded that peroxy radicals were formed, through reaction of O₂ with these carbon-centered radicals.

Dalal et al. (1995) employed DMPO to determine hydroxyl radical formation from a mixture of coal dust and H₂O₂. They observed the characteristic 1:2:2:1 hyperfine quartet of the DMPO–OH adduct consistent with ·OH. Addition of metal chelators such as EDTA, diethylaminepentaacetic acid (DETAPAC) enhanced the ESR signal whereas CAT and DFX suppressed the ESR signal, suggesting the formation of ·OH via the Fenton reaction.

Using spin trapping, Dalal et al. (1990) detected ·OH and provided evidence for role of Fenton reaction in hemolysis and lipid peroxidation by quartz particles. They reported a reduction in ·OH signal in the presence of CAT, superoxide dismutase (SOD) and some metal ion chelators, consistent with the involvement of the Fenton reaction. On the other hand, they reported that addition of a metal reductant did not increase the signal, inconsistent with the Fenton reaction acting as the source of ·OH.

In contrast to the results of Dalal et al. (1990), Shi et al. (1988) and Vallyathan et al. (1988) employed spin trapping to determine ·OH produced by quartz particles and found that the Fenton reaction was not responsible for ·OH generation. Their studies did not show any decrease in ·OH formation in the presence of DETAPAC, as a strong metal chelator. They reported that if the Fenton reaction occurred, there would have been a significant decrease in ESR signal in the presence of DETAPAC.

Although all of these studies have provided important information, the levels of ·OH produced are always reported in arbitrary units and thus do not provide

quantitative estimate of $\cdot\text{OH}$ formation rate. Spin trapping with ESR detection also suffers from a number of additional limitations.

First, spin adducts participate in secondary reaction such as disproportionation (Willson 1971) and secondary radical or redox reactions of the nitroxide (Mehlhorn et al. 1984, Gascoyne et al. 1987, Swartz et al. 1986, 1987, 1990). Therefore, radical production rates can not be determined quantitatively due to spin adduct instability.

Second, the breakdown of an unstable spin-adduct (Finkelstein et al. 1979) or non-radical reaction of the parent spin trap (Rosen et al. 1984) can artificially produce spin adducts. For example, when DMPO reacts with superoxide, the superoxide spin adduct (DMPO-OOH) is decomposed into several products including the hydroxyl radical spin adduct (DMPO-OH; Finkelstein et al. 1982). Therefore, production of DMPO-OH can not be used as a proof of hydroxyl radical formation in biological systems, unless additional tests are performed.

Third, in some instances, the rate constant for spin trapping is low thus necessitating the use of high concentrations of spin traps to quantitatively trap the radical. These high concentrations of spin trap may alter reaction mechanisms and in cell studies produce toxicity.

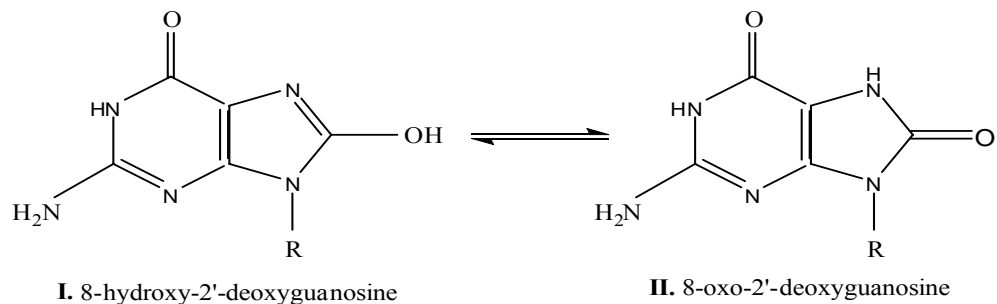
Fourth, nitrones can participate in oxidation reactions with transition metals such as iron and copper. For example, DMPO can be oxidized to its hydroxamic acid in the presence of ferric chloride solution.

Fifth, mixture of spin adducts with similar structure can not be distinguished by ESR due to their very similar g-value and hyperfine splitting constants (Janzan

1984). Sixth, the ESR sensitivity is low ($\sim\mu\text{M}$) relative to other detection methods (see below).

1.5.2. Formation of 8-oxo-dG

Karlsson et al. 2005, Shi et al. 2003b, Parahald et al. 2000, Ball et al. 2000, Ichinose et al. 1997 and Chao et al. 1996 tested for the formation of $\cdot\text{OH}$ by airborne particles through detection of 8-oxo-2'-deoxyguanosine (8-oxo-dG) formation. 8-oxo-dG is a marker of oxidative damage to DNA. It has been demonstrated that hydroxylation at the C-8 position of 2'-deoxyguanosine (dG) residues in DNA by either $\cdot\text{OH}$ or a species with a similar reactivity results in the formation of 8-oxo-2'-deoxyguanosine (8-oxo-dG), which is mutagenic and it is used as a biomarker for oxidative stress. This compound can exist in either an enol (I) or keto (II) form; hence its designation is 8-oxo-dG or 8-hydroxyl-2'-deoxyguanosine (8-OH-dG; Scheme 1-4).



Scheme 1-4. Enol (I) and keto (II) form of 8-oxo-2'-deoxyguanosine from deoxyguanosine.

Karlsson et al (2005) exposed the cultured human lung epithelial cells (A549) to subway particles, and subsequently analyzed for DNA damage using single cell gel electrophoresis (the comet assay) and the formation of 8-oxo-dG. Shi et al. (2003b) measured production of 8-oxo-dG when calf thymus DNA or human lung epithelial cells (A549) were exposed to either coarse or fine particulate matter. Based on their results, they concluded that coarse PM generates more ROS including $\cdot\text{OH}$. Prahalad et al. (2001) determined formation of 8-oxo-dG in calf thymus DNA and human airway epithelial cells (BEAS-2b) in the presence of airborne particulate matter. They reported the amount of 8-oxo-dG/ 10^5 dG generated by oil fly ash (OFA) and residual oil fly ash (ROFA) when their concentration varied from 0.1 to 1 mg/mL (Figure 1-2).

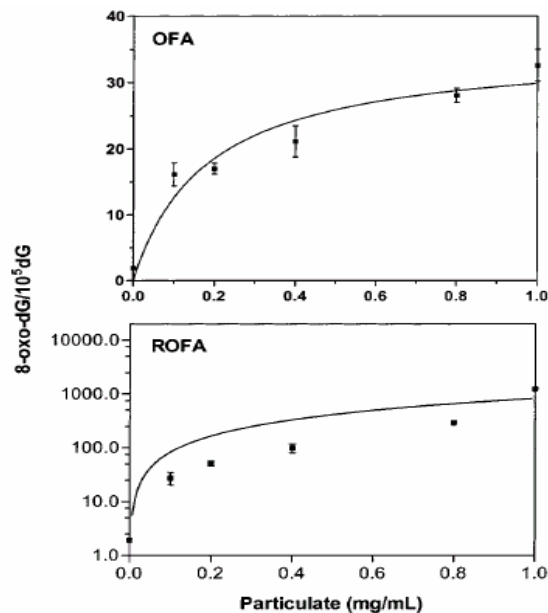


Figure 1-2. Effect of OFA and ROFA concentration on the formation of 8-oxo-dG (Pralhad et al., 2001).

Pralhad et al. (2001) also showed that addition of DFX, a metal ion chelator, resulted in significant inhibition of 8-oxo-dG production for some type of fly ashes like OFA and ROFA. Adding DMSO, as an $\cdot\text{OH}$ scavenger, also suppressed 8-oxo-dG formation. Treating OFA and ROFA with CAT suppressed 8-oxo-dG formation significantly. On the other hand, addition of SOD slightly enhanced 8-oxo-dG formation in DNA. These results showed that 8-oxo-dG could be produced by ROS, possibly $\cdot\text{OH}$, generated from particulate matter. In 2000, Prahalad et al showed the ability of OFA and coal fly ash (CFA) to hydroxylate the C-8 position of dG as a sign for presence of ROS. In addition, they examined the ability of different metal species

in 8-oxo-dG formation at the same concentrations of metals in airborne particles. The soluble and reduced metal ions V (IV) and Fe (II) enhanced 8-oxo-dG production relative to V (V) and Fe (III) ions. The involvement of transition metals in the generation of $\cdot\text{OH}$ as well as 8-oxo-dG was also confirmed by inhibition of 8-oxo-dG formation in the presence of metal ion chelators such as DFX, DTPA and ferrozine.

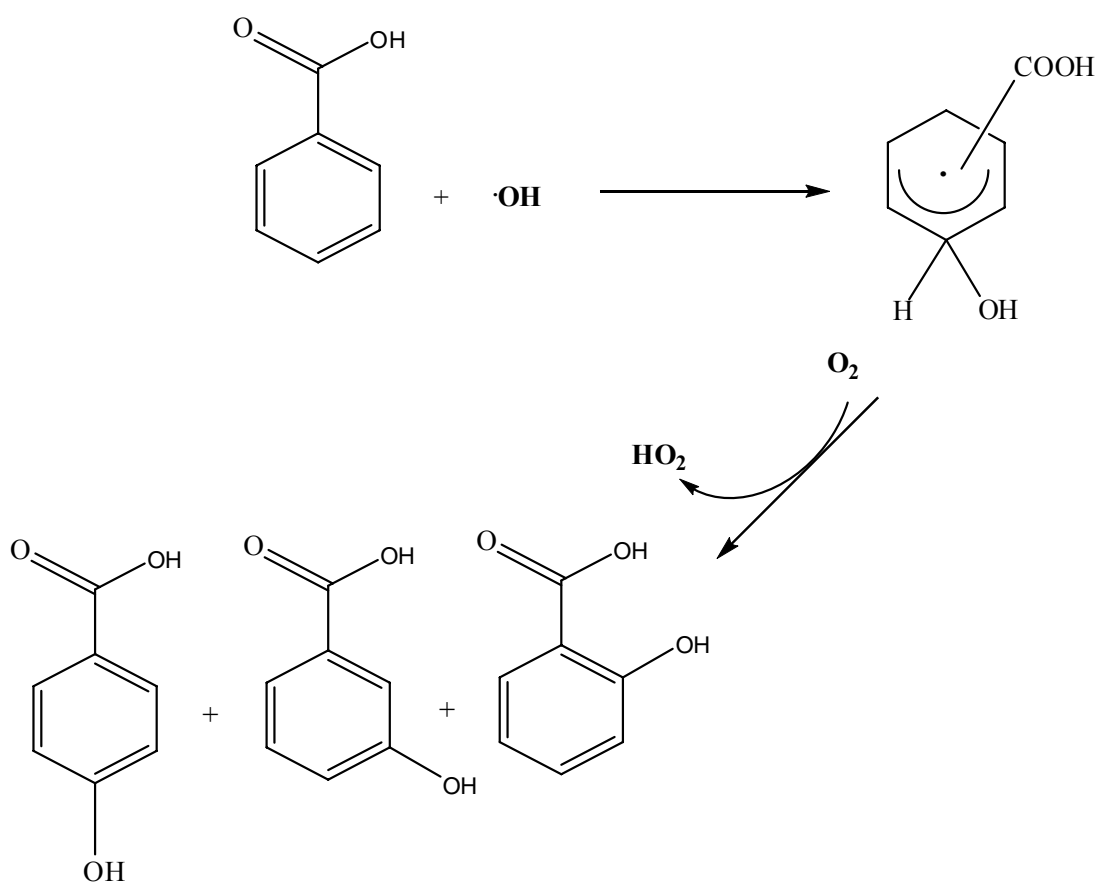
Ichinose et al. (1997) determined 8-oxo-dG in lung DNA to clarify the involvement of oxygen radicals in lung carcinogenesis induced by diesel exhaust particles (DEP). They observed the increase in lung tumor and 8-oxo-dG while different concentrations of DEP were injected into mice trachea. Chao et al. (1996) also reported that treatment of human lung epithelial cells with crocidolite, a form of asbestos, resulted in an increased 8-oxo-dG level leading to tumor formation.

Although the formation of guanine oxidized adduct (8-oxo-dG) was used as a marker for OH-induced DNA damage, it is not necessarily selective technique to detect the hydroxyl radical among all other reactive species. In addition, this method can be subject to artifacts, because guanine is susceptible to oxidation during sample preparation (Collins et al. 2004)

1.5.3. Aromatic hydroxylation

There is only one report in which a relatively specific technique, aromatic hydroxylation, was employed to quantify the formation of $\cdot\text{OH}$ by particles. In this technique, addition of $\cdot\text{OH}$ to benzoic acid ring gives rise to three mono-hydroxylated benzoic acid isomers (*meta*, *para*, *ortho* hydroxylated benzoic acid; Scheme 1-5). In

this reaction, the initial step is fast addition of $\cdot\text{OH}$ to the aromatic ring to form an intermediate radical. The intermediate radical will be oxidized by an electron acceptor (oxygen) to produce the hydroxylated benzoic acid. The ratio of these three isomers is close to 1:1:1 for reaction with $\cdot\text{OH}$. To analyze these products, each one of the hydroxylated product can be separated by HPLC and detected spectrophotometrically.



Scheme 1-5. The reactions of $\cdot\text{OH}$ addition to benzoic acid.

Jung et al (2006) employed this technique to measure $\cdot\text{OH}$ formation by flame soot particles, carbon black and ambient fine particles in a surrogate lung fluid. They reported the integrated concentration of $\cdot\text{OH}$ generated by flame soot, carbon black and other particulate matter ($\text{PM}_{2.5}$) in the presence of 1.0 mM of H_2O_2 are 0.91, 0.096 and 21 nmol mg^{-1} , respectively, over 2 hours reaction time. This method can be highly sensitive for measuring $\cdot\text{OH}$, but there are several problems with employing this technique in biological systems. These include: (1) multiple products require separation (2) cellular toxicity at high levels of benzoic acid, that actually is required to scavenge $\cdot\text{OH}$ effectively (3) inhibition of some enzymes such as cyclooxygenase by benzoic acid (4) high affinity of iron ion for benzoic acid and perturbation in iron-dependent hydroxyl radical production (5) incomplete scavenging of $\cdot\text{OH}$ due to limited solubility of benzoic acid.

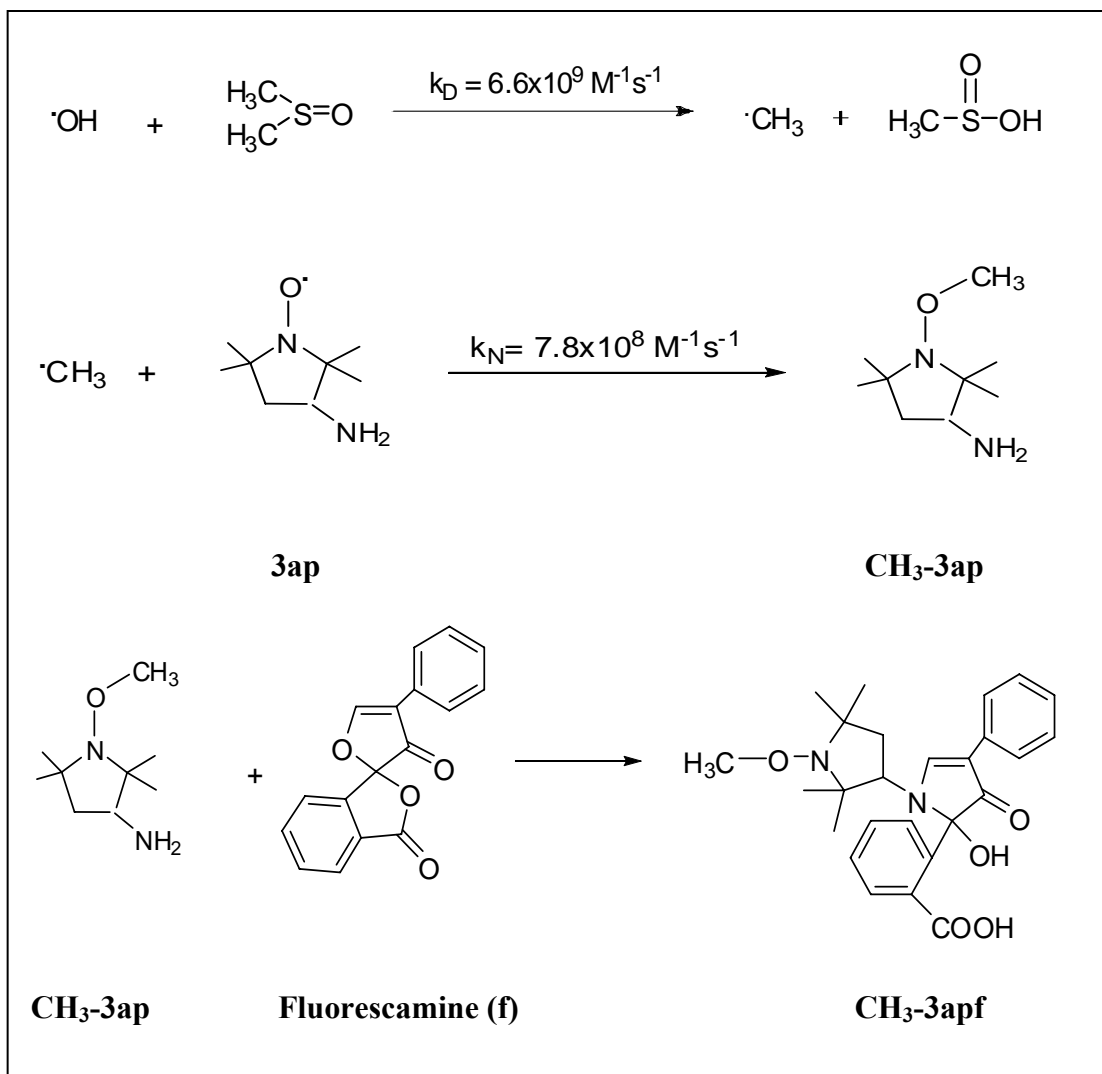
1.5.4 Other indirect $\cdot\text{OH}$ detection methods

Generation of DNA single strand breaks (DNASSBs) (Smith and Aust 1997, Pan et al. 2004), production of chemokines and cytokines such as IL-6, IL-8 and TNF- α (Carter et al. 1997, Frampton et al. 1999, Imrich et al. 2000) and activation of several redox-responsive signaling pathways such as NF- κB (Shukla et al. 2000) were employed as a markers of hydroxyl radical production by particulate matter in the cell systems. Cytokine production was also inhibited by inclusion of metal chelators such as DFX, catalase, and free radical scavengers such as (DMTU) or dimethyl sulfoxide (DMSO). However, determining DNASSBs, cytokine and chemokine production and

their inhibition in the presence of some reagents are not selective methods to detect and measure $\cdot\text{OH}$ formation directly.

1.6. New Approach: detection of particle induced $\cdot\text{OH}$ using nitroxide scavenging

Over the past few years, the use of nitroxide with fluorescence detection (Scheme 1-5) , a sensitive and simple fluorescence detection method, has been developed by Blough and co-workers to determine hydroxyl radical (Li et al. 1997, 1999 a&b, 2000, Petigara et al. 2002, Gan 2004, Mwebi 2005) and carbon centered radicals (Blough and Simpson 1988, Kieber and Blough 1990a & b, Kieber et al. 1992, Johnson et al. 1996, Vaughan and Blough 1998) in both biological and environmental systems.



Scheme 1-6. $\cdot\text{OH}$ trapping method; (Kieber and Blough, 1990b; Li et al. 1997)

In this work, dimethyl sulfoxide (DMSO) is to react with the hydroxyl radical generated by airborne particles to produce methyl radical ($\cdot\text{CH}_3$). The $\cdot\text{CH}_3$ is then trapped with 3-amino-2,2,5,5-tetramethyl-1-pyrrolidinyloxy (3ap) to form $\text{CH}_3\text{-3ap}$ which is subsequently derivatized with fluorescamine to produce the $\text{CH}_3\text{-3apf}$. The resulting highly-fluorescent stable adduct ($\text{CH}_3\text{-3apf}$ or *O*-methylhydroxylamine) is separated by HPLC and determined fluorometrically (Scheme 1-5; Kieber and Blough 1990a & b). To measure generation of $\cdot\text{OH}$ in the presence of cells, fluorescamine derivatized 3-amino-2,2,5,5-tetramethyl-1-pyrrolidinyloxy (3apf) is used to react with $\cdot\text{CH}_3$ and produce $\text{CH}_3\text{-3apf}$ (Li et al. 1999b).

Using DMSO to react with $\cdot\text{OH}$ and generate carbon centered radical has several advantages such as (1) high water solubility (2) low toxicity to cells and tissues (3) rapid reaction with hydroxyl radical to generate methyl radical ($6.6 \times 10^9 \text{ M}^{-1} \text{ s}^{-1}$).

There are also some advantages for using 3ap, pyrrolidinyl nitroxide. For instance, 3ap reacts rapidly ($7.8 \times 10^8 \text{ M}^{-1} \text{ s}^{-1}$) with methyl radical and the rate of this reaction is an order of magnitude higher than those for spin trapping (Schmid and Ingold, 1978). Therefore, much lower concentration of nitroxides, which is normally used in vivo and vitro (Kocherginsky and Swartz 1995), can be employed for an equivalent trapping efficiency. Pyrrolidinyl nitroxides also show lower rates of bioreduction (Kocherginsky and Swartz 1995), reaction with superoxide (Krishna 1992 and 1994), and reaction with metal ions (Mitchell et al. 1990).

In the following chapters, this method is used to measure the production of hydroxyl radical by wide range of airborne particles in the absence and presence of

biological reductants, as well as in the presence of human lung epithelial (BEAS-2b) and mouse epidermal (JB6) cells.

In the second chapter, the results of an investigation of the mechanisms and magnitude of hydroxyl radical production by different airborne particulate matter in the absence and presence of biological electron donor such as NADPH are presented. Our results are largely consistent with the redox cycling mechanism proposed by Pryor and co-workers. Further investigation on both soluble and insoluble portion of airborne particles suggests that $\cdot\text{OH}$ is produced through both homogenous and heterogeneous reaction.

In the third chapter, results on the effect of particles on the viability of human lung epithelial (BEAS-2b) and mouse epidermal (JB6) cells are presented. In addition, the magnitude of hydroxyl radical production in the presence of different particles and BEAS-2b or JB6 cells and different particulate matter is presented. In addition, the correlation between the cell death and $\cdot\text{OH}$ production is discussed.

The results presented in the appendix provided preliminary information on the optical properties (absorption and fluorescence) of material extracted from diesel particulate matter in phosphate buffer at different pHs.

Chapter 2: Source Dependent Variation in Hydroxyl Radical Production by Airborne Particulate Matter

Abstract

Epidemiological studies suggest exposure to airborne particles is responsible for a wide range of adverse health effects, potentially arising from particle-induced oxidative stress. A highly-sensitive fluorescence method was employed to measure the production of hydroxyl radical by a broad range of particle types including urban dust, diesel particulate matter, coal fly ash, kaolinite and silica. Little or no production of $\cdot\text{OH}$ was observed in the absence of an added electron donor or H_2O_2 . In the presence of a biological electron donor (NADPH, 3 mM), the rate of $\cdot\text{OH}$ production (R_{OH}) for 3 mg/mL of these particles varied from 23 nM s^{-1} for diesel particulate matter (SRM 2975) to 0.20 nM s^{-1} for coal fly ash (SRM 2689). No detectable $\cdot\text{OH}$ was produced by kaolinite or silica. Hydroxyl radical formation was eliminated under anaerobic conditions and in the presence of catalase, indicating that O_2 and H_2O_2 are required for its generation. Partial inhibition of $\cdot\text{OH}$ formation by superoxide dismutase (SOD) was also observed in some cases, suggesting that superoxide ($\text{O}_2^{\cdot-}$) is also involved. The metal chelator, deferoxamine mesylate (DFX) in most cases suppressed $\cdot\text{OH}$ formation, but diethylenetriaminepentaacetic acid (DTPA) generally enhanced it, implicating metal ion reactions in $\cdot\text{OH}$ generation as

well. The dependence of R_{OH} on NADPH concentration further implicates particle surface reactions in $\cdot OH$ formation. To our knowledge, these measurements provide the first quantitative estimate of R_{OH} for a broad range of particle types.

2.1. Introduction

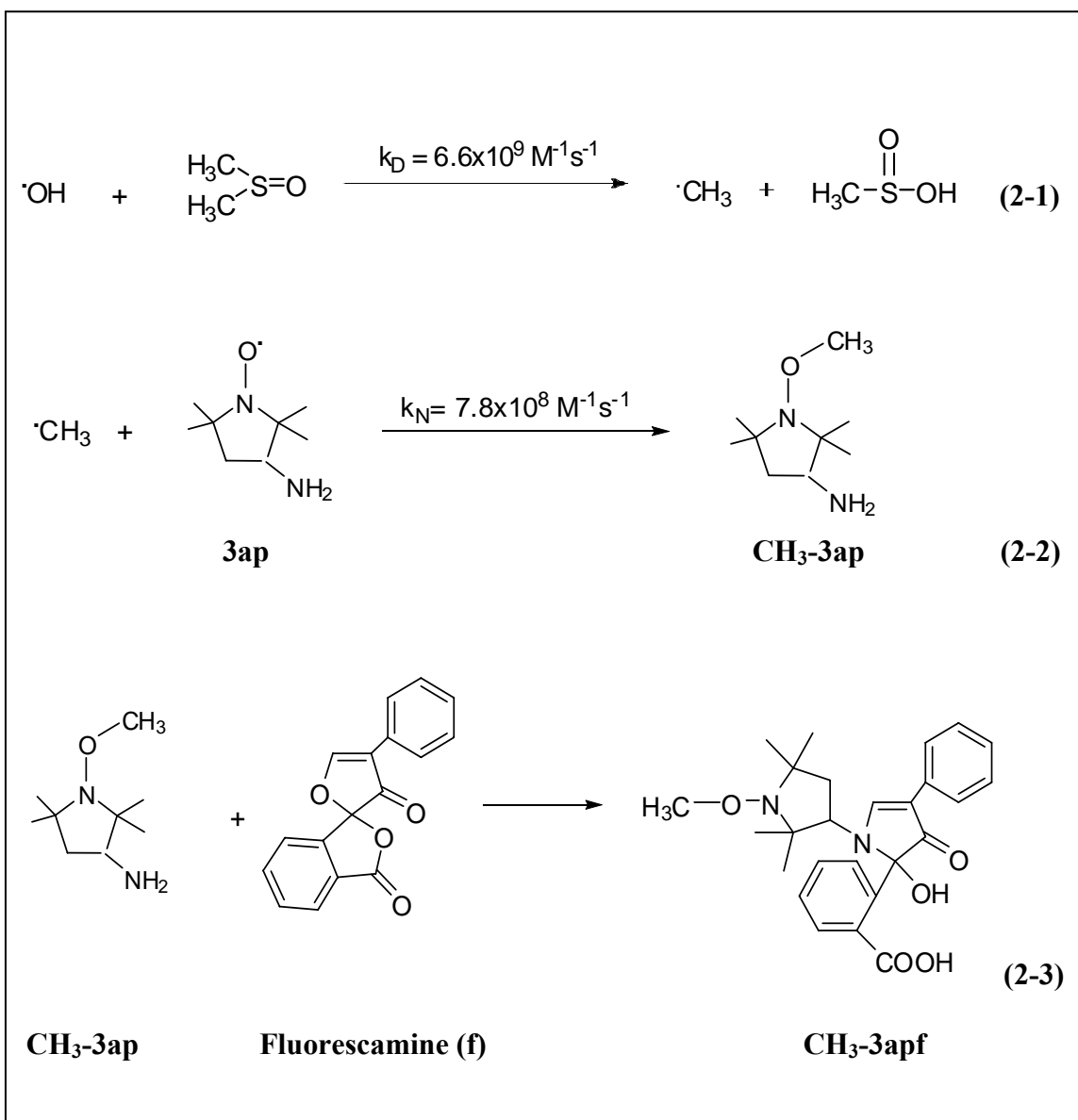
Epidemiological studies indicate that airborne particulates increase the incidence of respiratory diseases such as pneumonia, emphysema, chronic bronchitis and asthma (Lebowitz 1996; Sunyer and Bassagana 2001; Schwartz 1994; Porteney and Mullahy 1990; Tseny et al. 1992). Further, both epidemiological and clinical studies have implicated airborne particulates in cardiovascular disease and stroke (Brook et al. 2004). Long-term exposure to particulate air pollution has also been associated with increased rates of lung cancer (Pope III et al. 2002) and production of heritable genetic changes (Somers et al. 2004). Over the past few decades, a broad spectrum of studies have been conducted to understand the origins of the adverse health effects of particulate matter from sources such as smoke, asbestos, quartz particles, coal dust and vehicular air pollution (Hwang et al. 1999; Hardy and Aust 1995; Vallyathan et al. 1988; Dalal et al. 1995; Flicker and Green 2001, Karlsson et al. 2005). Although the precise biochemical mechanisms for particulate-induced health effects are poorly understood, it has been hypothesized that exposure to air pollutants gives rise to oxidative stress within lung cells (Kelly 2003) through production of reactive oxygen species (ROS), including the highly damaging hydroxyl radical, thus leading to pulmonary and cardiovascular injury (MacNee and

Donaldson 2003). ROS can be generated not only by particle-activated polymorphonuclear leukocytes, but also by the particles themselves and their constituents (Pralhad et al. 1999; Dellinger et al. 2001; Squadrito et al. 2001). Among the ROS, the hydroxyl radical is one of the strongest oxidants and has been implicated in the cellular damage.

Most past efforts to detect the production of ROS, particularly $\cdot\text{OH}$, by airborne particles have employed spin trapping with electron paramagnetic resonance (EPR) detection (Briedé et al. 2005; Valavanidis et al. 2005; Antonini et al. 2004; Shi et al. 2003a; Shi 2003b; Kumagai et al. 1997). However, this method is not particularly sensitive (Pou et al. 1989; Li et al. 1997; Li et al. 1999a; Li et al. 1999b; Li et al. 2000; Kieber and Blough 1990b), is subject to artifacts (Pou et al. 1989; Finkestein et al. 1979; Pou et al. 1994; Samuni et al. 1989; Janzan et al. 1990; Kieber and Blough 1990a&b), and generally can not be used to obtain quantitative estimates of radical generation due to numerous secondary reactions of the spin adducts (Li et al. 1990b; Kieber and Blough 1990b; Samuni et al. 1989; Janzan et al. 1990). The formation of 8-hydroxy-2'-deoxyguanosine (8-OHdG) from deoxyguanosine (dG) has also been used as a sensitive indicator of ROS formation by particles in the presence of cells (Karlsson et al. 2005; Shi et al. 2003b; Prahalad et al. 2001). As with spin trapping, the approach is not necessarily selective for $\cdot\text{OH}$ and does not readily provide a quantitative estimate of the rate of radical generation (Collins et al. 2004; Prise et al. 1993).

Here, a highly sensitive, fluorescence-based approach (Blough and Simpson 1988; Li et al. 1997; Li et al. 1999a; Kieber and Blough 1990a; Kieber and Blough

1990b; Vaughan and Blough 1998; Thomas-Smith and Blough 2001; Li et al. 2000; Li et al. 1999b; Petigara et al. 2002) is employed to measure hydroxyl radical production by particulate matter, including diesel particles, urban dust and coal fly ash. In this technique, the hydroxyl radical reacts with added dimethylsulfoxide (DMSO) to form a methyl radical, which is then trapped with 3-amino-2,2,5,5-tetramethyl-1-pyrrolidinyloxy (3ap) to produce a stable O-methyl-hydroxylamine adduct (Me-3ap). This adduct is then derivatized with fluorescamine (f) to form a highly fluorescent product (Me-3apf) which is separated by reversed phase high performance liquid chromatography (HPLC) and quantified fluorometrically (Scheme 2-1; Kieber and Blough 1990b; Vaughan and Blough 1998; Thomas-Smith and Blough 2001; Petigara et al. 2002). This technique was employed to investigate the mechanism(s) and magnitude of hydroxyl radical production from a broad spectrum of airborne particles in the absence and presence of a biological electron donor (NADPH).



Scheme 2-1. $\cdot\text{OH}$ trapping method; (Kieber and Blough, 1990b; Li et al. 1997)

2.2. Experimental section

2.2.1. Materials

The reduced form of β -nicotinamide adenine dinucleotide phosphate (NADPH), fluorescamine, catalase (CAT), superoxide dismutase (SOD) and deferoxamine mesylate (DFX) were purchased from Sigma. Dimethyl sulfoxide (DMSO) (99.9%), sodium hydroxide (99.998%), sodium hydrogen phosphate (99.999%), sodium dihydrogen phosphate (99.995%), sodium chloride (99.999%), hydrochloric acid (99.999%), boric acid, ethanol 200 proof (HPLC grade) and acetonitrile were obtained from Aldrich. 3-Amino-2,2,5,5-tetramethyl-1-pyrrolidinyloxy (3ap) was purchased from Acros. Diethylenetriamine pentaacetic acid (DTPA) was obtained from Fluka. Hydrogen peroxide was purchased from Fisher. Acetic acid and methanol (HPLC grade) were purchased from J.T.Baker. Ultra High Pure (UHP) grade nitrogen was obtained from Airgas Inc. All chemicals were used as received. A Millipore MilliQ system provided water for all experiments. Standard phosphate buffers used in all experiments were either 100 (pH 7.5) or 5 mM sodium phosphate (pH 4.8, 6.0, 6.8, 7.5, 7.9, 8.5).

2.2.2. Particle sources

Standard reference materials (SRM) 1649, 1648, 1632b, 2689 and 2975 were obtained from National Institute of Standard and Technology, Gaithersberg, MD. Other airborne particles, Fly Ash (I), Fly Ash (II) and Fly Ash (III) were obtained from different power plants in US. The Clay standard kaolinite (KGa-1b) and silica (Aerosil) were received from the Clay Mineral Society and the Degussa Corporation, respectively. All airborne particulate matter was used without pretreatment. More detailed information about particle type, size and source is available in Table 2-1.

Table 2-1. Source and Description of Particles

	Particle Type	Particle Size	Particle Source
SRM 1649	Urban Dust	<125 µm	Washington DC area over one year period (1975-1976)
SRM 1648	Urban Dust	<125 µm	St. Louis, MO area over one year period.
SRM 1632b	Bituminous Coal	<250 µm	Bailey Mine of the Consol Coal Company in southwestern Green county, PA.
SRM 2689	Coal Fly Ash	<145 µm	Georgia Coal-fired Power Co. Plant Bowen Stilesboro, GA. Coal Mine: Western Kentucky coal mine.
SRM 2975	Diesel Particulate Matter	<110 µm	M.E. Wright of the Donaldson Company, Inc., Minneapolis, MN.
Fly Ash (I)	Conventional Pulverized Coal(I)	-	a Power Plant in USA
Fly Ash (II)	Conventional Pulverized Coal(II)	-	a Power Plant in USA
Fly Ash (III)	Conventional Pulverized Coal(III)	-	a Power Plant in USA
Aerosil	amorphous, fumed, crystalline free Silicon Dioxide	-	Degussa Corporation, NJ.
KGa-1b	well-crystallized kaolinite	-	Washington county, GA.

2.2.3. Apparatus

The high-performance liquid chromatography system (HPLC) consisted of an Eldex Model B-100-S single piston pump (Eldex Scientific CA) followed by 0-5000 psi pressure gauge, a Valco Model C10W injection valve (Valco Inc., Texas), and a RCM 8 X 10 cm Waters radial compression module containing a 5 X 100 mm Nova - PAK C₁₈ 4- μ m reversed phased column (Waters, Massachusetts). 0.5- μ m filters (Upchurch) were placed after the pump and before the column. A 50 μ L loop was used in all measurements. A Dionex UV/Vis detector set to 390 nm (maximum absorption of Me-3apf) and a L-7480 Hitachi fluorescence detector set to 390 nm (excitation) and 490 nm (emission maximum of Me-3apf) were employed for the detection system. Elab software was used for acquisition and analysis (OMS Tech). Chromatographic separations were done isocratically with 35% sodium acetate buffer (50 mM, pH 4.0)/ 65% methanol (v/v) as mobile phase with flow rate 1 ml/min.

All absorption spectra were measured with a Hewlet-Packard 8452A diode array or a Shimadzu 2401 UV-PC spectrophotometers. A Mettler AT261 Delta Range electronic balance was used for all mass measurements. An ORION model 720A pH meter was used to measure the pH of all solutions.

2.2.4. Determination of hydroxyl radical generated by airborne particles

Appropriate weights of airborne particles were first suspended in 5 or 100 mM phosphate buffer (pH 7.5). DMSO (5% v/v) and 3ap (1500 μ M) were then added to the suspension, which was subsequently vortexed for 60 seconds. These solutions were incubated at room temperature in the dark under aerated conditions for an appropriate reaction time. In some experiments, other reagents such NADPH, SOD, CAT, H₂O₂, DFX or DTPA were added immediately prior to DMSO and 3ap addition and the vortex mixing. The concentrations of these reagents are provided in the figure captions. Following incubation, a sufficient amount of borate buffer (200 mM) was added to adjust the pH to 8. Fluorescamine (2.5 mM) was then added to the reaction mixture to derivatize the adduct (Kieber and Blough 1990b; Vaughan and Blough 1998; Thomas-Smith and Blough 2001; Petigara et al. 2002). The final suspension was centrifuged for 4 minutes at 14000 rpm (5415c Eppendorf centrifuge), and the supernatant then injected (50 μ L) onto Nova-PAK C₁₈ reversed phased column and separated isocratically at room temperature using a flow rate of 1 ml/min (Kieber and Blough 1990; Li et al. 2000, Li et al. 1999b). The mobile phase composition was 35% sodium acetate buffer (50 mM, pH 4.0)/ 65% methanol (v/v). Following the separation, Me-3apf was quantified fluorometrically as described previously (Fig. 2-1, 2-2; Blough and Simpson 1988; Kieber and Blough 1990a).

For anaerobic samples, reagent solutions were deoxygenated by bubbling with ultra-high purity N₂ (Airgas Inc.) for 15 minutes prior to addition to anaerobic suspensions of particles deoxygenated in the same fashion.

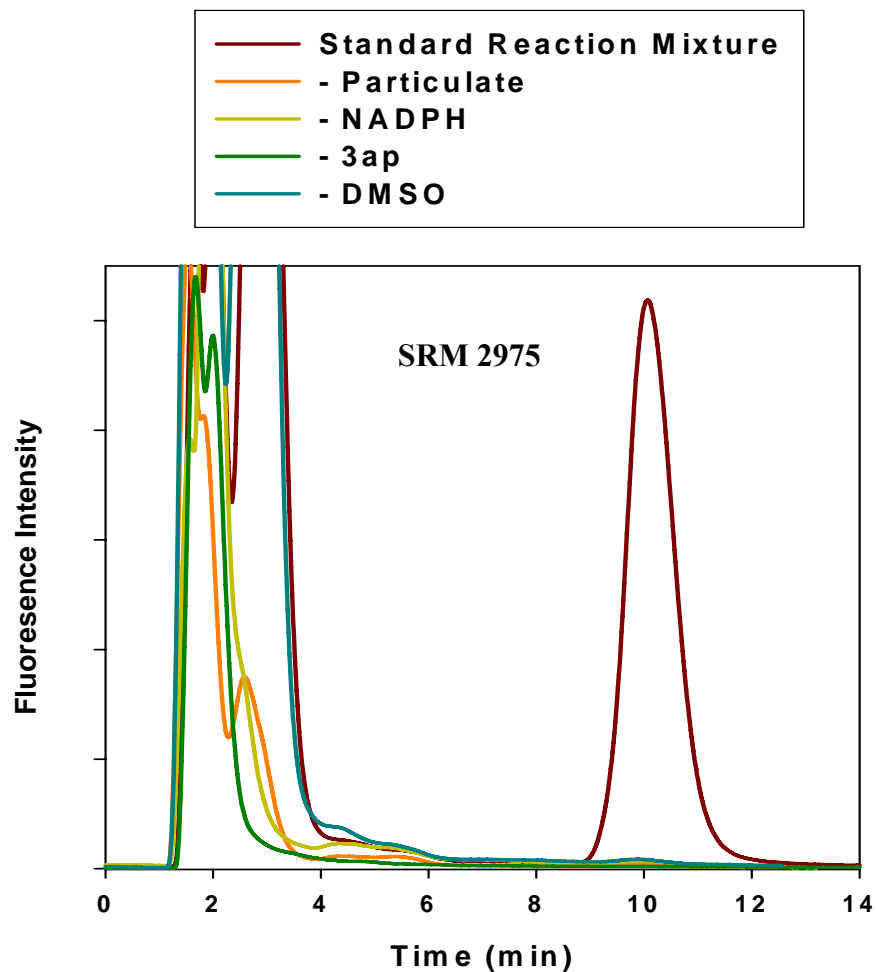


Figure 2-1. Chromatogram illustrating formation of Me-3apf (after 60 min) in solutions containing 3 mg/ml **SRM 2975**, 1500 μ M 3ap, 5% DMSO and 3 mM NADPH in 100 mM phosphate buffer, pH=7.5 (standard reaction mixture), following derivatization with 2.5 mM fluorescamine in 200 mM borate buffer. Chromatograms obtained in the absence of particles, NADPH, 3ap or DMSO are also provided.

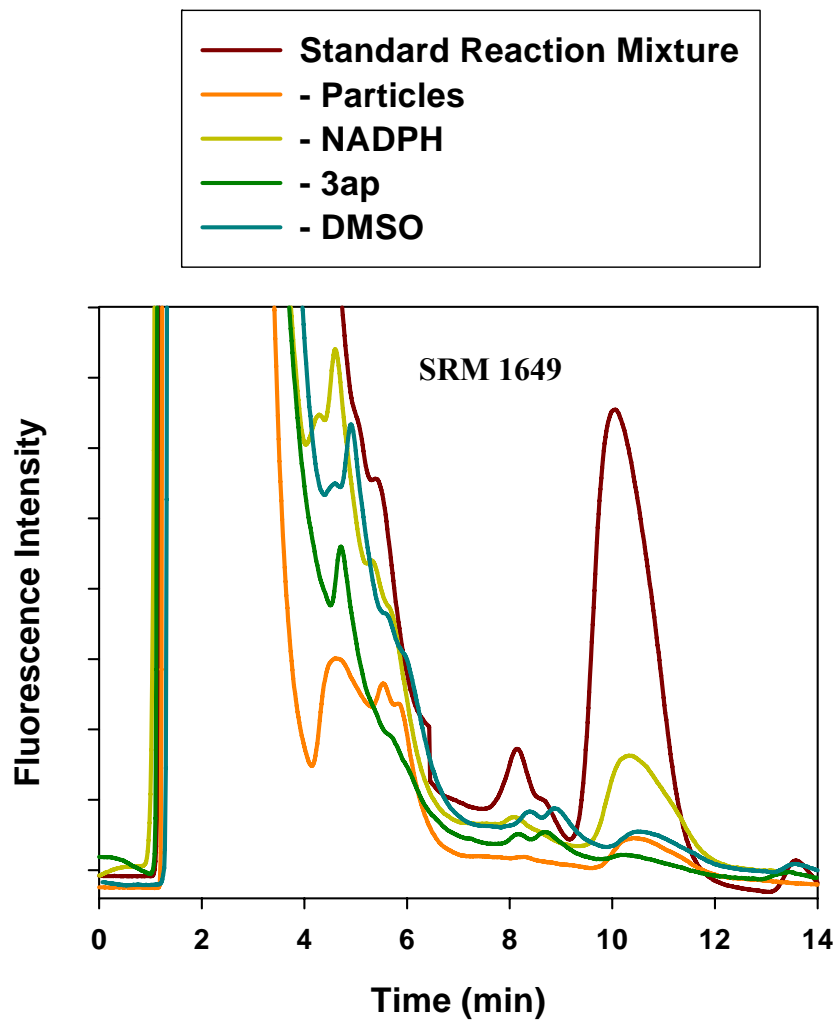


Figure 2-2. Chromatogram illustrating formation of Me-3apf (after 60min) in solutions containing 3 mg/mL **SRM 1649**, and other experimental conditions were identical to figure 2-1.

2.2.5. Hydroxyl radical detection and quantification

2.2.5.1. Preparation and purification of Me-3apf standard for HPLC calibration

Me-3apf standard was prepared by Fenton reaction as previously described (Li et al. 1997), with the exception that 3ap was used as the reactant to form Me-3ap, which was subsequently derivatized with fluorescamine to form the Me-3apf. First, 3 mM of 3ap, 5% DMSO and 3 mM H₂O₂ were mixed in 100 mM phosphate buffer at pH 7.5 in a container with a Teflon seal. The mixture was purged with N₂ for 5 minutes before 3 mM N₂ purged Fe(II)-EDTA was added via a gas-tight syringe. The reaction was initiated by immediate addition of Fe(II)-EDTA and allowed to proceed anaerobically in dark for at least 30 minutes. An aliquot of the product was then drawn and its pH rose to 8.0 by addition of 200 mM botare buffer. The product was then derivatized with 12 mM fluorescamine solution and the reaction was allowed to proceed in dark for 5 minutes. The pH was then adjusted to 4 by acetic acid and the derivatized sample was extracted (solid-phase) using Water C₁₈ Sep-Pak. The C₁₈ Sep-Pak was first rinsed with MilliQ water and methanol before loading with the reaction product. The reaction product was concentrated as a yellow band which was eluted with a small volume of methanol and reduced by flushing with dry nitrogen.

The product, Me-3apf, was separated and collected directly from the HPLC (mobile phase: 65% methanol and 35% acetate buffer, pH=4.0) and then extracted in 2 ml of chloroform. After evaporation of the chloroform, the bright yellow adduct was stored in dark at -20C. For HPLC calibration, the concentration of Me-3apf

standard was determined spectrophotometrically ($\epsilon_{386} = 5225 \text{ M}^{-1} \text{ cm}^{-1}$; Li et al. 1997) and calibration standard curve obtained from it by serial dilution. These were run on the HPLC and detected fluorometrically. The fluorescence response increased linearly with concentration over the range 5-14070 nM, and they were used to report the concentration of Me-3apf.

2.2.5.2. DMSO and 3ap dependence

To establish the conditions for determining hydroxyl radical quantitatively, the dependence of Me-3apf formation rate on the concentration of DMSO was first examined. The dependence of Me-3apf formation rate on DMSO concentration is shown in Figure 2-3 (Li et al. 1997; Li et al. 1999a; Vaughan and Blough 1998; Li et al. 1999b). The formation rate of Me-3apf was found to be independent of DMSO at concentrations $\geq 50 \text{ mM}$ in the presence of 3 mg/mL SRM 1649, 3 mM NADPH and 1500 μM 3ap in 100 mM phosphate buffer. However, to ensure quantitative determination of $\cdot\text{OH}$ in the presence of the particles, DMSO concentration was set to 705 mM (5% DMSO by volume).

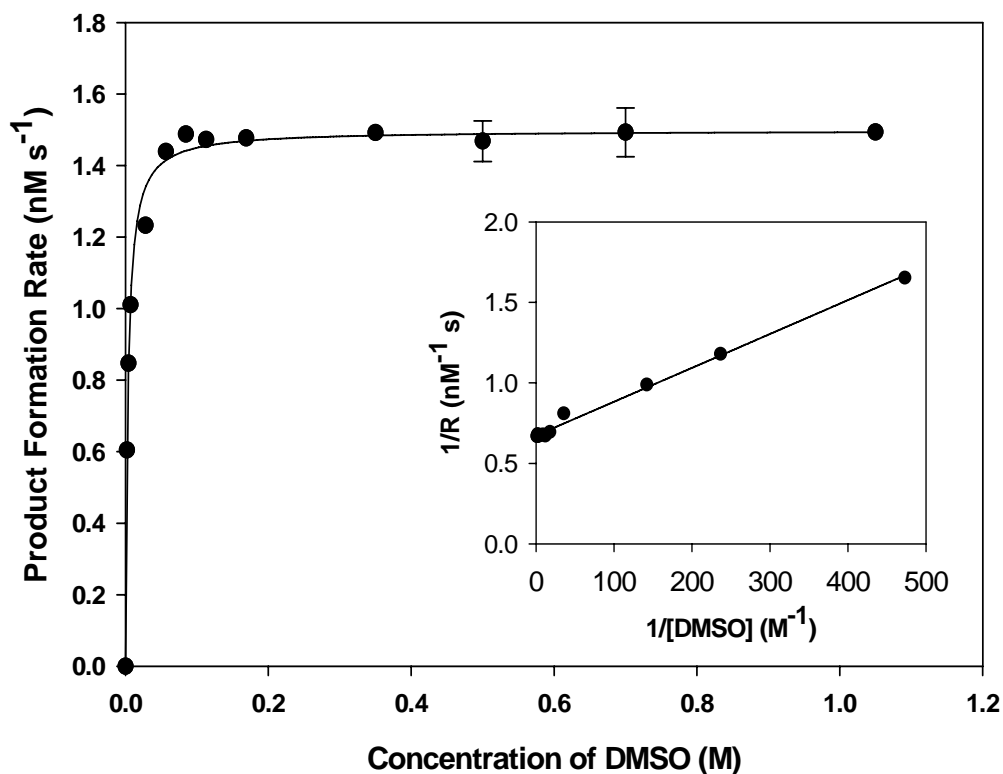
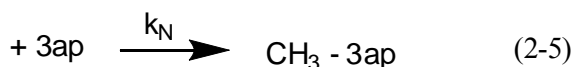
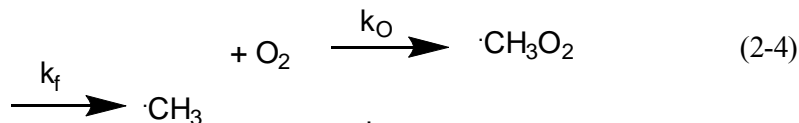


Figure 2-3. Dependence of the rate of Me-3apf formation on DMSO concentration in a suspension containing 3 mg/ml SRM 1649, 3 mM NADPH and 1500 μ M 3ap in 100 mM phosphate buffer (pH=7.5). Inset is the linearized form of the data. Error bars represent one standard deviation from the mean value (n=3).

The dependence of the formation rate of Me-3apf on the concentration of 3ap was then determined. Since dioxygen competes with 3ap for methyl radical, it is necessary to test the dependence of Me-3apf formation on 3ap concentration to define the condition that provides quantitative measurement of methyl radical.



If DMSO concentration is sufficient, the initial rate of product Me-3apf formation at steady state is given by the expression

$$R = \left(\frac{d[\text{Me-3apf}]}{dt} \right) = \frac{k_f k_N [3\text{ap}]}{k_O [\text{O}_2] + k_N [3\text{ap}]} = \frac{k_f [3\text{ap}]}{k_f S + [3\text{ap}]} \quad (2-6)$$

where k_f is the $\cdot\text{OH}$ formation rate and $S = (k_O [\text{O}_2]) / (k_f k_N)$. k_f and $k_f S$ were obtained from a nonlinear least-square fit to hyperbolic curve (Figure 2-4). Assuming an $[\text{O}_2] = 250 \mu\text{M}$, k_f and $k_f S$ from Figure 2-4 can be substituted into above equation to calculate k_O/k_N , which are the rate constant for the reaction of the methyl radical with O_2 and 3ap, respectively. This value, 3.6 ± 0.4 , is in a reasonable agreement with the result reported previously (Li et al. 1997; Vaughan and Blough 1998; Li et al. 1999b). Since this experiment indicates that O_2 is the only major competitor for methyl radical, a rearranged form of eq 2-6, eq 2-7 can be used to calculate k_f under conditions in which methyl radical and 3ap do not react quantitatively.

$$k_f = R \left(1 + \frac{k_O[\text{O}_2]}{k_N[\text{3ap}]} \right) = R \left(1 + \frac{k_f S}{[\text{3ap}]} \right) \quad (2-7)$$

In this study, based on the dependence of Me-3apf yield on 3ap concentration, Me-3apf concentration in aerated samples was converted to integrated ·OH formation through multiplication by a factor of 1.6 ± 0.07 obtained at $[\text{3ap}] = 1500 \mu\text{M}$ and $[\text{O}_2] = 250 \mu\text{M}$ (Li et al. 1999b; Li et al. 1997; Vaughan and Blough 1998), the concentration employed in all subsequent analyses.

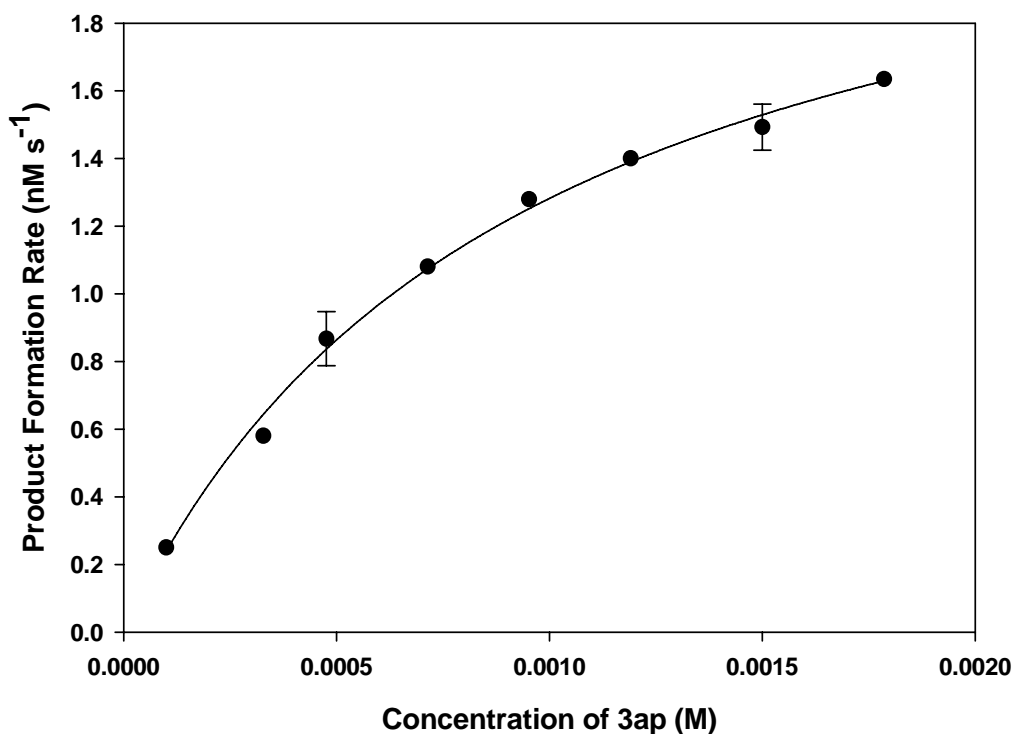
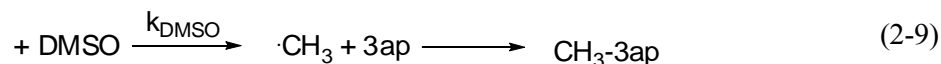


Figure 2-4. Dependence of Me-3apf formation rate on 3ap concentration under aerobic condition in a solution containing 3 mg/ml SRM 1649, 3 mM NADPH, and 5% DMSO in 100 mM phosphate buffer (pH=7.5). Error bars represent one standard deviation from the mean value (n=3).

2.2.5.3. Competitive study of methanol and DMSO

To test further that $\cdot\text{OH}$ was the species being detected; we examined the competition between DMSO and ethanol. In this test, ethanol was added to a reaction mixture containing a constant DMSO concentration. Reaction of ethanol with $\cdot\text{OH}$ forms radical intermediates other than methyl radical, thus producing a decrease in the formation of Me-3apf due to the competitive reaction between ethanol and DMSO.



Under these conditions, the formation rate of Me-3apf is expected to decrease with increasing ethanol concentration according to the following equation,

$$R = \frac{k_{\text{DMSO}} [\text{DMSO}]_0 R_0}{k_{\text{DMSO}} [\text{DMSO}]_0 + k_{\text{EtOH}} [\text{EtOH}]} = \frac{R_0 C_1}{C_1 + [\text{EtOH}]} \quad (2-10)$$

where R_0 is the formation rate of Me-3apf in the absence of ethanol at a constant DMSO concentration, $[\text{DMSO}]_0$, and R is the formation rate at ethanol concentration, $[\text{EtOH}]$. $C_1 = k_{\text{DMSO}} [\text{DMSO}]_0 / k_{\text{EtOH}}$ was derived from a nonlinear least-square fit to

the data (Figure 2-5), with the rate constant ratio $k_{\text{EtOH}}/k_{\text{DMSO}} = 0.30 \pm 0.05$ obtained at constant DMSO concentration of 0.5 M. This ratio agrees well with rate constant ratio, $k_{\text{EtOH}}/k_{\text{DMSO}} = 0.29$, calculated from the rate constants for the reaction of $\cdot\text{OH}$ with ethanol ($1.9 \times 10^9 \text{ M}^{-1} \text{ s}^{-1}$) and DMSO ($6.6 \times 10^9 \text{ M}^{-1} \text{ s}^{-1}$) obtained from the literature (Buxton et al. 1988).

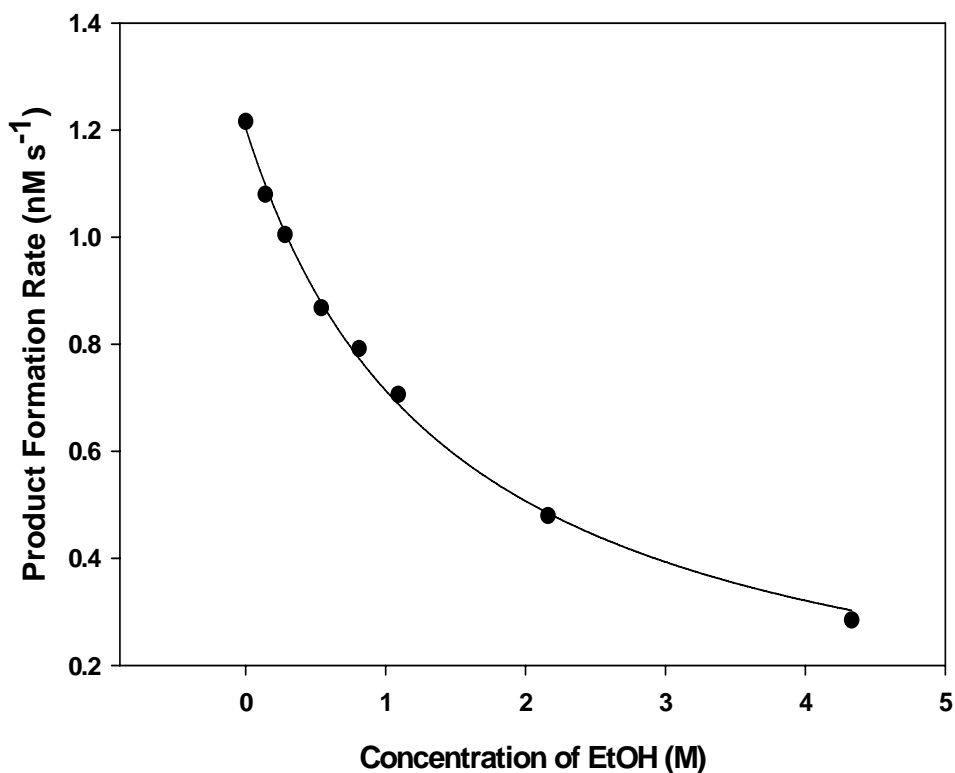


Figure 2-5. Effect of ethanol on the rate of Me-3apf formation rate in the presence of constant DMSO concentration (500 mM). Other solution conditions were 3 mg/ml SRM 1649, 3 mM NADPH and 1500 μM 3ap in 100 mM phosphate buffer (pH=7.5).

2.2.5.4. Time course for integrated $\cdot\text{OH}$ formation by different airborne particles

In the presence of NADPH, integrated $\cdot\text{OH}$ formation increased linearly with time versus time for all tested particles except SRM 1632b (Figure 2-6). Rates of $\cdot\text{OH}$ formation (R_{OH}) were obtained from the slope of plots of integrated $\cdot\text{OH}$ formation versus time over the first 60 minutes (minimally 3 time points). In the case of SRM1632b, the formation rate was calculated over the first 20 minutes (having linear response).

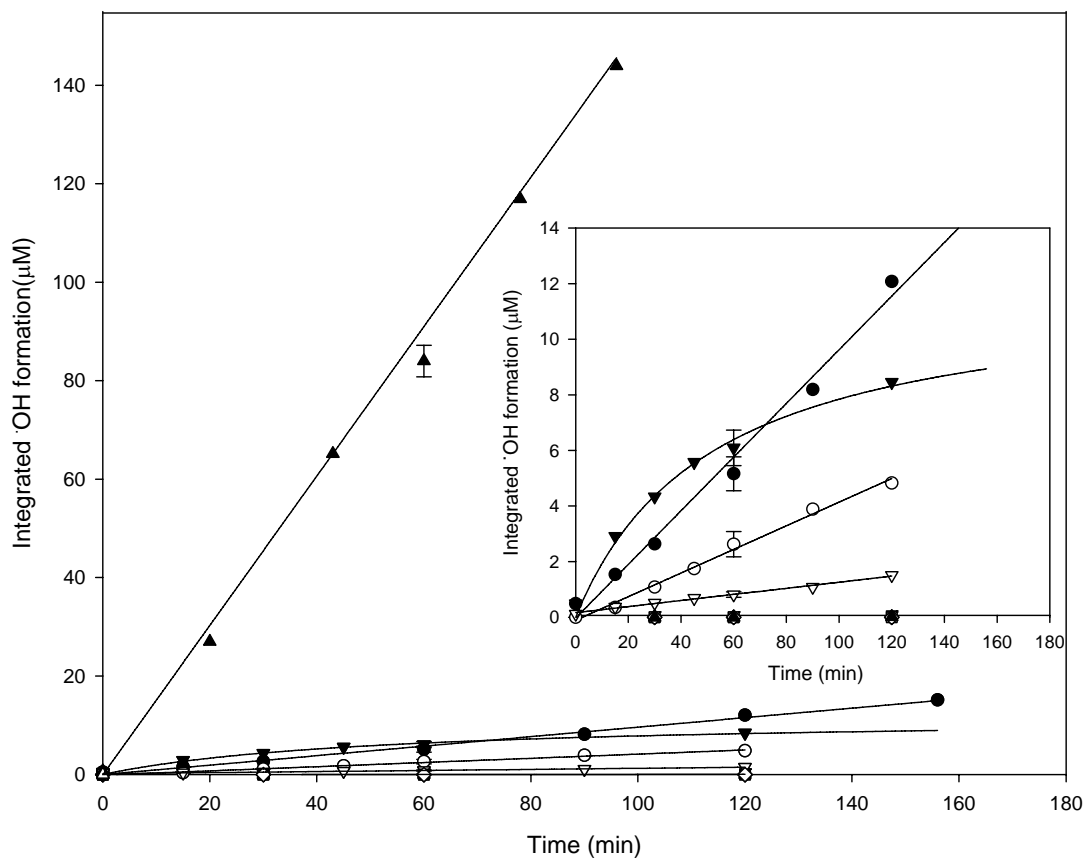


Figure 2-6. Effect of different airborne particles SRM 2975(▲); SRM 1649 (●); SRM1648 (○); SRM 1632b (▼); SRM 2689 (▽); Fly Ash I (■); Fly Ash II (□); Fly Ash III (◆); Aerosil (◇); KGa-1b (Δ) on hydroxyl radical formation as a function of time. The reaction mixture contains 3 mg/mL airborne particle, 3 mM NADPH, 5% DMSO and 1500 μ M 3ap in 100 mM phosphate buffer (pH=7.5) under aerobic condition. Error bars represent one standard deviation from the mean value (n=3).

2.2.5.5. Precision, accuracy and detection limit (D.L.)

The precision of the method was determined from the reproducibility of multiple HPLC injections (≥ 3) for a given experimental condition over multiple days. The maximum %RSD was 8.8 %, which includes the reproducibility of the measurements from day to day. Error bars reported in the figures represent \pm one standard deviation.

The accuracy of the method depends on the molar extinction coefficient of CH₃-3apf because the peak area of chromatograms was converted to concentration of CH₃-3apf obtained by using UV-Vis method as explained in section 2.2.5.1. For this purpose, a calibration curve (peak area from injecting to HPLC versus concentration of CH₃-3apf) was provided to find a factor to calculate concentration of CH₃-3apf, but the accuracy of this factor is completely related to reported extinction coefficient for CH₃-3apf (Li et al 1997). Moreover, the accuracy of the method mainly depends on the accuracy of a coefficient which was used to convert Me-3apf concentration in aerated samples to integrated ·OH formation through multiplication by a factor of 1.6 ± 0.07 obtained at [3ap]=1500 μ M and [O₂]=250 μ M.

Defining the detection limit as twice the standard deviation of the blank (1500 μ M 3ap, 705 mM DMSO; $n \geq 8$), values of 5.7 and 11 nM were estimated for Me-3apf (50 μ L injection volume) for samples containing no and 3 mM NADPH, respectively. These values are similar in magnitude to the detection limits previously reported for this method when applied to other systems (Kieber and Blough 1990; Vaughan and Blough 1998; Thomas-Smith and Blough 2001; Li et al. 1997).

2.3. Results

2.3.1. $\cdot\text{OH}$ formation in particle suspensions in the absence and presence of biological reductant

No signal was observed in the absence of either 3ap or DMSO (Figure 2-7). In the presence of these compounds, only very low levels of $\cdot\text{OH}$ formation were detected for SRM 1649 and SRM 2975 over the first 50 minutes and none thereafter. Other particles, such as the coal fly ashes, kaolinite (KGa-1b) and silica (Aerosil), showed little or no production of $\cdot\text{OH}$. Formation of $\cdot\text{OH}$ was eliminated under anaerobic conditions, but was substantially enhanced in the presence of H_2O_2 under both aerobic and anaerobic conditions for SRM 1649 and 2975 (Figure 2-7). Although formation of $\cdot\text{OH}$ from SRM 2975 increased linearly with time in the presence of H_2O_2 , $\cdot\text{OH}$ formation from SRM 1649 did not significantly increase beyond ~50 minutes. In the case of SRM 2975, the high, linear production suggests that $\cdot\text{OH}$ is being generated catalytically in the presence of H_2O_2 .

Addition of the biological reductant, NADPH, greatly enhanced the production of $\cdot\text{OH}$ for both SRM 1649 and 2975, producing a linear increase in $\cdot\text{OH}$ over time (Figure 2-8). As in the absence of NADPH, this production was eliminated under anaerobic conditions, but was further increased in the presence of H_2O_2 under either aerobic or anaerobic conditions. For SRM 2975, the decline in $\cdot\text{OH}$ formation beyond 50 minutes under anaerobic conditions may be due to a limiting concentration of H_2O_2 at this high level of $\cdot\text{OH}$ formation. Addition of NADPH also enhanced

production of $\cdot\text{OH}$ by SRM 1648 and 1632b, but had little effect on SRM 2689 and Fly Ash (I) and (III), and no effect on Fly ash (II), silica or kaolinite.

Rates of $\cdot\text{OH}$ production by airborne particles are also reported in Table 2-2. In the presence of glutathione as compared with NADPH, R_{OH} is 2 to 4 fold higher for all particles except SRM 2975. R_{OH} is about 38-fold lower when SRM 2975 is reacted with glutathione instead of NADPH.

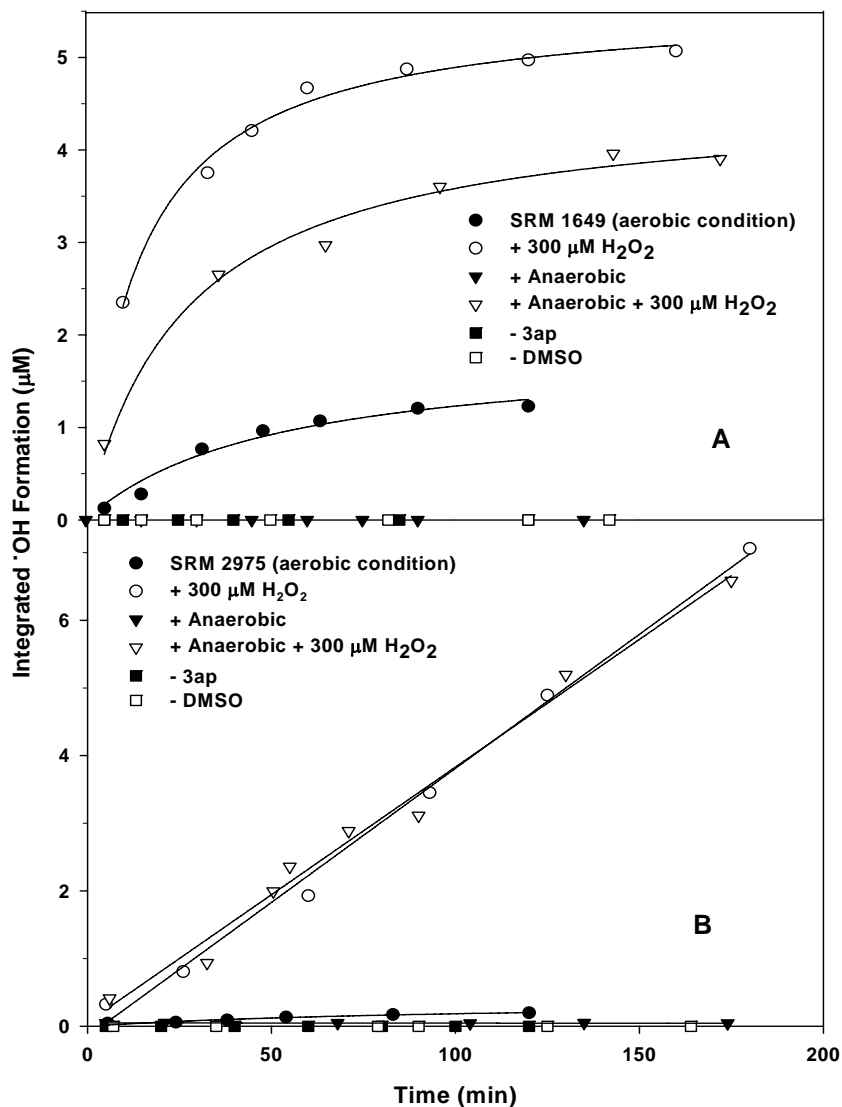


Figure 2-7. Time course for formation of hydroxyl radical by SRM 1649 (A) and SRM 2975 (B) under aerobic (●), and anaerobic (▼) conditions, and with addition of 300 μM H_2O_2 under aerobic (○), and anaerobic (▽) conditions. Particles (3 mg/mL) were suspended in 100 mM phosphate buffer, pH 7.5 in the presence of 1500 μM 3ap and 5% DMSO. Controls include the absence of 3ap (■), and DMSO (□) under aerobic conditions.

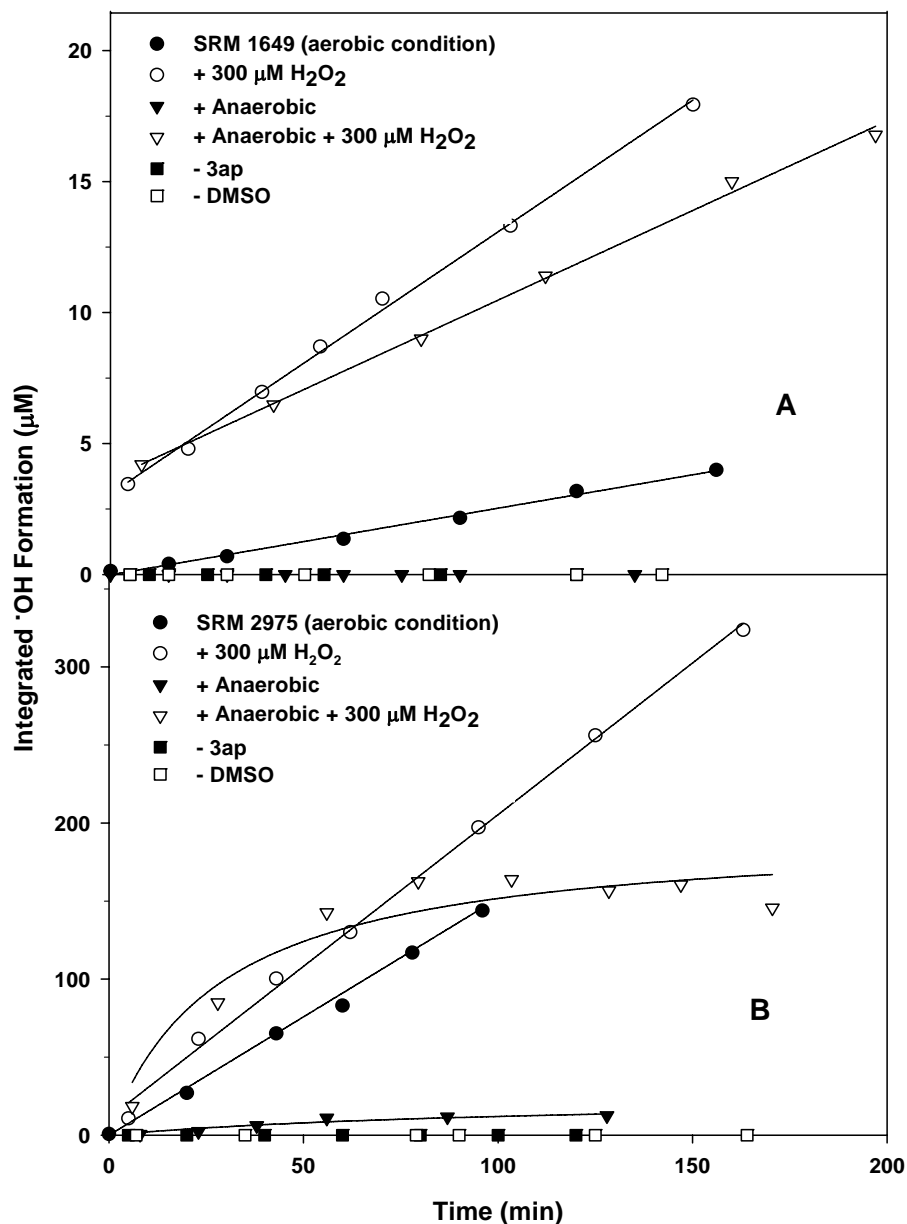


Figure 2-8. Time course for formation of hydroxyl radical by SRM 1649 (A) and SRM 2975 (B) in the presence of 3 mM NADPH under aerobic (●), and anaerobic (▼) conditions, and with addition of 300 μM H₂O₂ under aerobic (○), and anaerobic (▽) conditions. Other conditions are provided in Fig. 2-7. Controls include the absence of 3ap (■), and DMSO (□) under aerobic conditions.

Table 2-2. Effect of reductant (NADPH and glutathione) on R_{OH} . In these experiments, 3 mg/mL of particles was suspended in 100 mM phosphate buffer, pH 7.5, in the presence of 1500 μ M 3ap and 5% DMSO.

Particles Type	R_{OH} (nM s ⁻¹)	
	NADPH (0.3 mM)	Glutathione (0.3 mM)
SRM 2975	6.04	0.16
SRM 1649	0.13	0.55
SRM 1632b	0.24	0.58
SRM 2689	0.00	0.16
KGa-1b	0.00	0.00
Aerosil	0.00	0.00

2.3.2. Dependence of hydroxyl radical formation on type of particle, pH, ionic strength and buffer content

SRM 2975, diesel particulate matter, exhibited by far the highest rate of $\cdot\text{OH}$ production (R_{OH}) in the presence of NADPH, exceeding the next highest value (SRM 1632b) by over one order of magnitude (Figures. 2-9, 2-11). Values of R_{OH} decreased in the order, SRM 2975 \gg SRM 1632b $>$ SRM 1649 $>$ SRM 1648 $>$ SRM 2689. R_{OH} for Fly Ash (I) and (III) were near the detection limit, whereas those for Fly Ash (II), kaolinite and silica were indistinguishable from zero (Figure 2-9, inset).

Except for SRM 2975, R_{OH} was linearly related to particle concentration at constant [NADPH] (Figures. 2-9, 2-10). A 20-fold decrease in phosphate concentration decreased R_{OH} only modestly by factors of 2-3 (Table 2-3). Similarly, substantial changes in ionic strength had little effect on R_{OH} . The effect of pH on R_{OH} was much more variable with particle type, with R_{OH} increasing by 1.3-fold (SRM 2975) to greater than 13-fold (SRM 2689) with a decrease of pH from 8.5 to 4.8 (Table 2-3). The mobilization of metal content can be one of the reasons for increasing R_{OH} at lower pH.

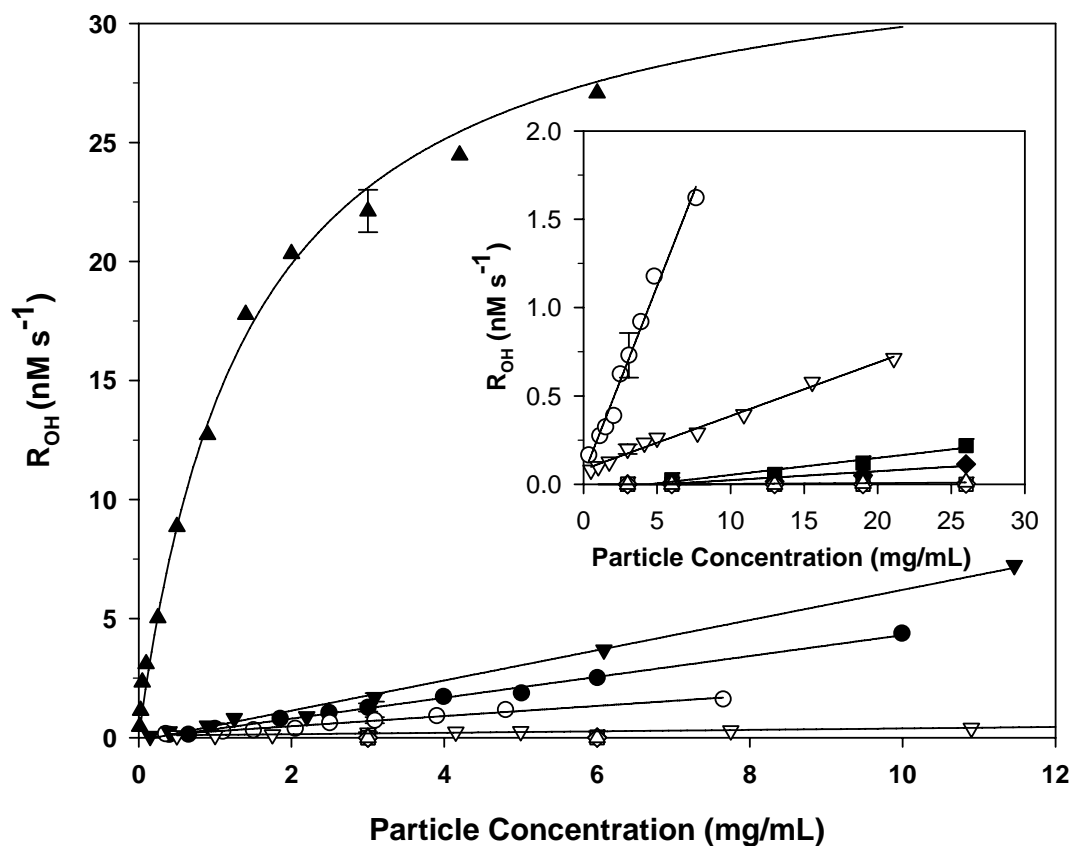


Figure 2-9. Dependence of R_{OH} on particle concentration for SRM 2975 (▲); SRM 1649 (●); SRM1648 (○); SRM 1632b (▼); SRM 2689 (▽); Fly Ash I (■); Fly Ash II (□); Fly Ash III (◆); Aerosil (◇); KGa-1b (Δ). Other solution conditions are as in Fig. 2-7 (aerobic condition). Error bars represent one standard deviation from the mean value ($n=3$).

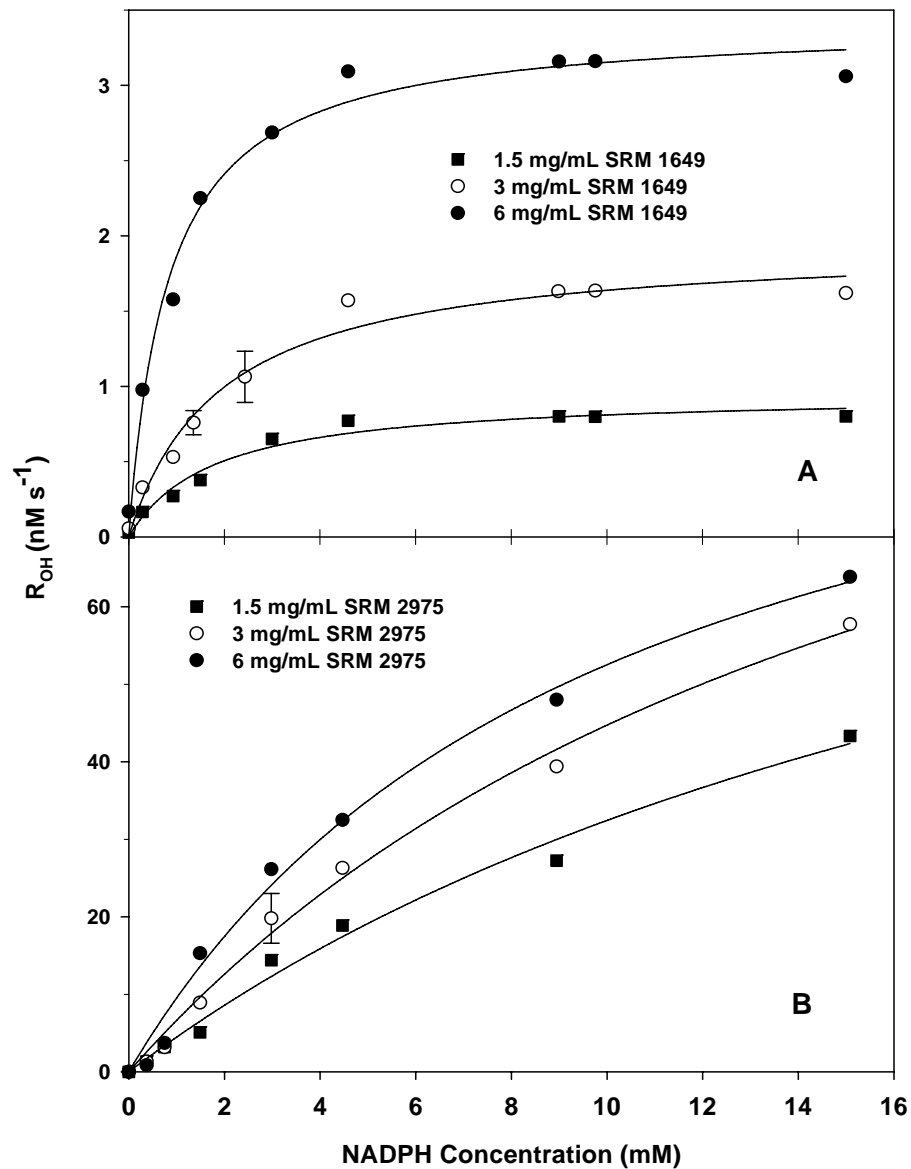


Figure 2-10. Dependence of R_{OH} on NADPH concentration for SRM 1649 (A) and SRM 2975 (B) at 1.5 mg/mL (■), 3 mg/mL (○) and 6 mg/mL (●) particle concentration. Other solution conditions are as in Fig. 2-7 (aerobic condition). Error bars represent one standard deviation from the mean value ($n=3$).

Table 2-3. Dependence of R_{OH} phosphate concentration, pH and ionic strength.

Buffered Solution, pH	rate of $\cdot OH$ formation ($nM s^{-1}$)		
	SRM 1649	SRM 2975	SRM 2685
100 mM phosphate buffer, 7.50	1.6	24	0.22
5 mM phosphate buffer, 7.50	0.63	8.7	0.084
0.9% NaCl & 5 mM phosphate buffer, 7.50	0.69	8.7	0.12
0.9% NaCl, 7.50	0.69	7.5	0.039
5 mM phosphate buffer, 4.84	1.9	11	0.24
5 mM phosphate buffer, 6.00	1.6	9.6	0.21
5 mM phosphate buffer, 6.79	1.4	8.7	0.15
5 mM phosphate buffer, 7.95	0.60	8.7	0.072
5 mM phosphate buffer, 8.45	0.29	8.7	0.018

2.3.3. Dependence of hydroxyl radical formation rate on NADPH

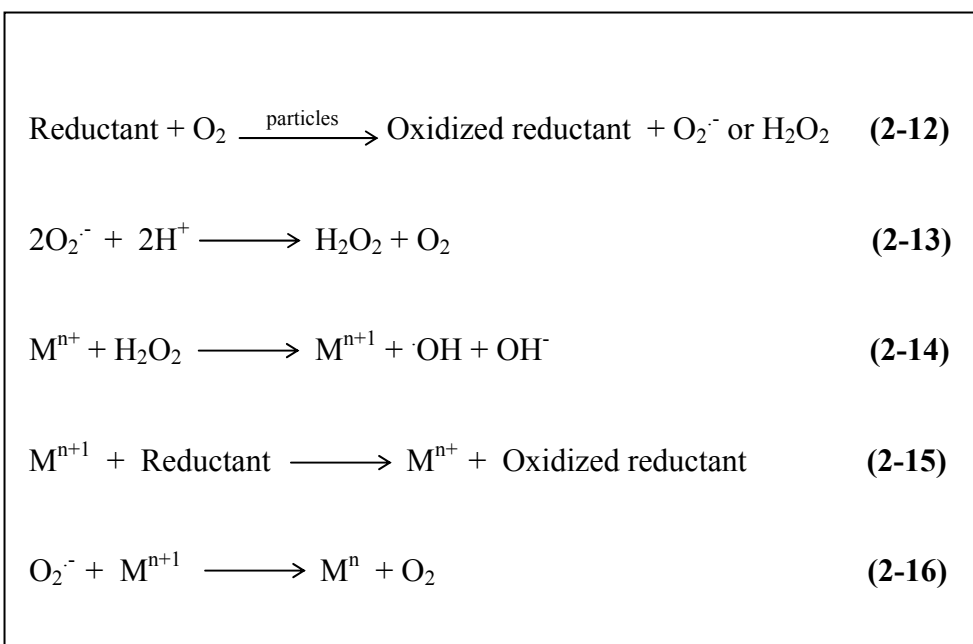
R_{OH} did not increase linearly with NADPH concentration, but instead exhibited evidence of saturation at high [NADPH] for both SRM 1649 and SRM 2975 (Figure 2-10), suggesting the involvement of surface-catalyzed reactions in the production of $\cdot OH$. The dependence of R_{OH} on [NADPH] could be fit to the form,

$$R_{OH} = \frac{R_{max} [NADPH]}{\beta + [NADPH]} \quad (2-11)$$

where R_{max} represents the maximal rate of $\cdot OH$ generation at saturating [NADPH] and β represents the [NADPH] at which $R_{OH} = \frac{1}{2} R_{max}$. For both SRM 1649 and 2975, the values of β were independent of particle concentration. At 1.5 mg/ml, SRM 2975 exhibited much higher values of R_{max} (106 nM s^{-1}) and β (23 mM) than did SRM 1649 ($R_{max} = 0.95 \text{ nM s}^{-1}$; $\beta = 1.8 \text{ mM}$).

2.3.4. The origin of hydroxyl radical

These results suggest that $\cdot\text{OH}$ can be generated catalytically by certain particles in the presence of O_2 and/or H_2O_2 and a significant pool of electron donors. A reasonable series of reactions for this process is provided below (Dellinger et al. 2001),



Scheme 2-2. Possible oxidation/ reduction reactions for particle constituents.

where “Reductant” is either NADPH or organic (and possibly inorganic) constituents of the particles, and M^{n+} and M^{n+1} represent reduced and oxidized metal species, respectively, provided by the particles.

Consistent with this set of reactions, the $\cdot\text{OH}$ formation was eliminated in all cases upon addition of catalase (1800 units/mL) to remove H_2O_2 (Figure 2-11, Rxn. 2-14). Further, the rate of $\cdot\text{OH}$ formation (R_{OH}) was approximately halved by the addition of SOD (3000 units/mL) to SRM 1649, 1648, 1632b, 2689, but was not affected by SOD addition to SRM 2975, consistent with the involvement of Rxn. 2-16 in most cases (Figure 2-11). Figure 2-12 shows the time course of integrated $\cdot\text{OH}$ formation by SRM 1649 and 2975 in the presence of CAT and SOD.

That trace metals are involved in the production of $\cdot\text{OH}$ (Rxns. 2-14, 2-15) was supported by the suppression of R_{OH} in the presence of DFX. This suppression was observed for all particles except SRM 1649 (Figure 2-11). Interestingly, addition of DTPA generally enhanced R_{OH} . Table 2-4 shows the stability constant at physiological pH for the complex of DFX and DTPA with biologically active metals (Dawson et al. 1986; Kiss et al. 1998, Anderegg et al. 2005). The origin of the contrasting behavior of these two metal chelators is discussed in section 2.4.

Table 2-4. Stability constants for metal complexes at physiological pH.

Name of chelator	Log stability constant								
	Mg^{+2}	Ca^{+2}	Mn^{+2}	Fe^{+2}	Co^{+2}	Ni^{+2}	Cu^{+2}	Zn^{+2}	Fe^{+3}
Diethylene-Triaminopenta-acetic acid (DTPA)	5.2	6.6	11.5	11.9	15.2	16.1	17.4	14.5	23.7
Deferoxmine DFX	23.9	22.4	-	25.9	21.3	19.7	24.0	20.4	41.4

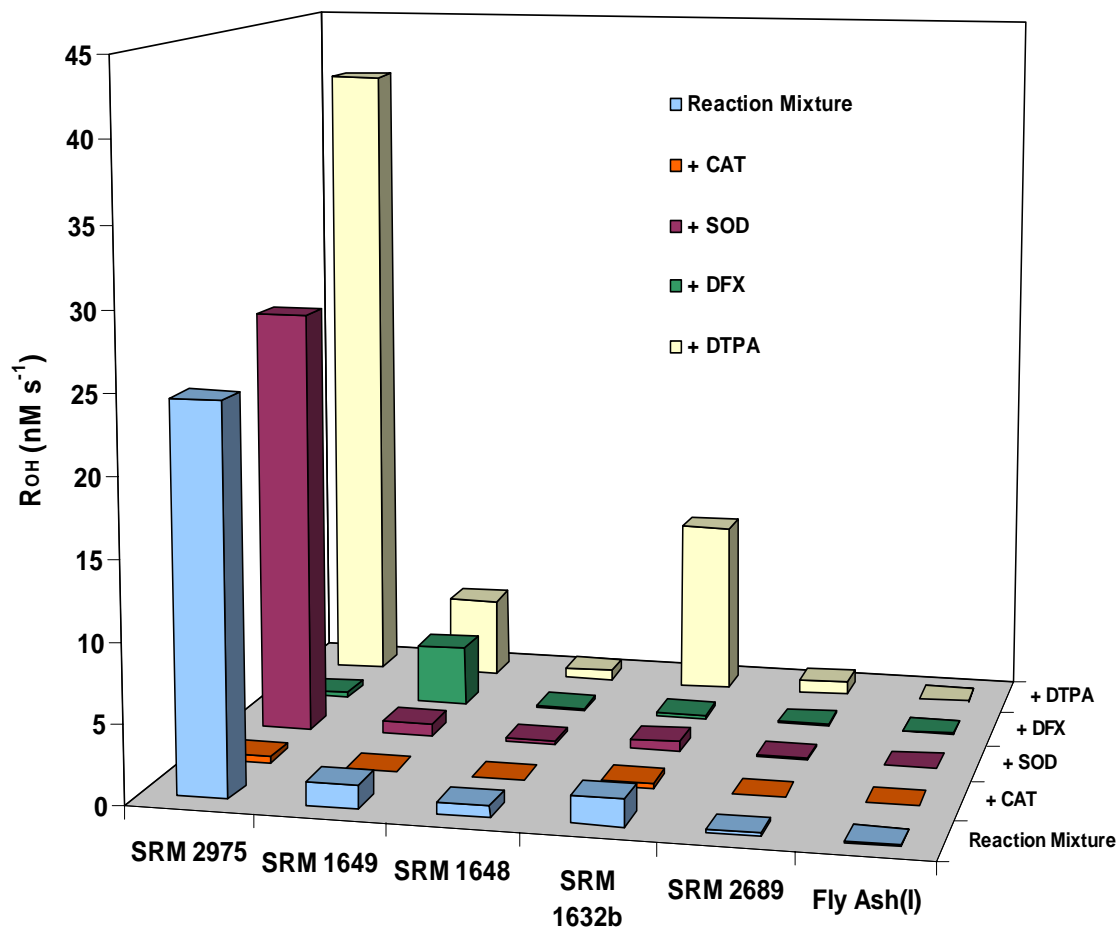


Figure 2-11. Production rate of $\cdot\text{OH}$ (R_{OH}) for airborne particles and with addition of CAT (1800 U/mL), SOD (3000 U/mL), DTPA (600 μM) and DFX (600 μM). Other solution conditions (reaction mixture) are as in Fig. 2-7 (aerobic condition).

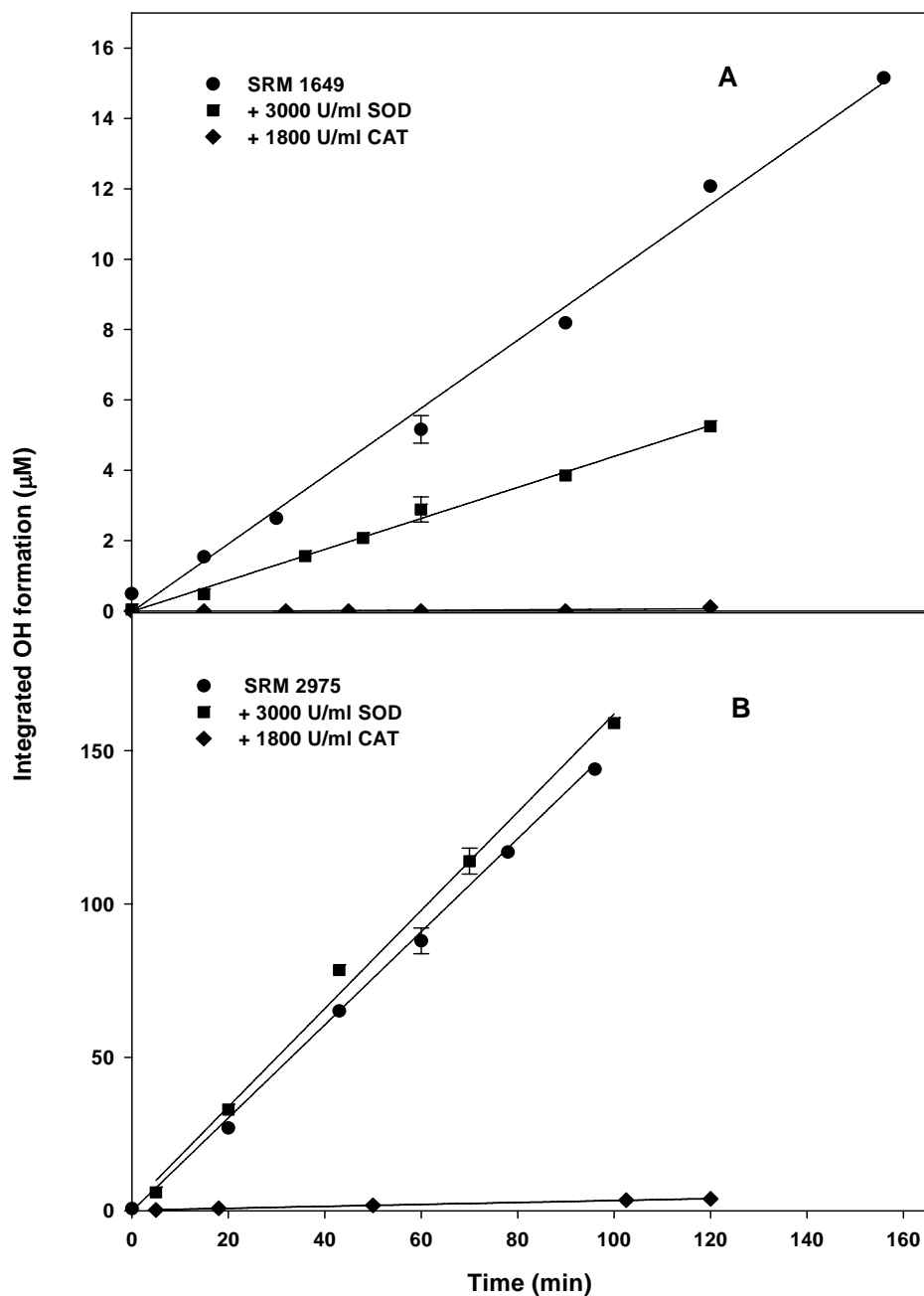


Figure 2-12. Time course for formation of hydroxyl radical by SRM 1649 (A) and SRM 2975 (B) (●), with addition of 3000 U/mL SOD (■), and with addition of 1800 U/mL CAT (◆). Other solution conditions are as in Fig. 2-7 (aerobic condition). Error bars represent one standard deviation from the mean value (n=3).

Because the data in Figure 2-10 imply that sorption and reaction of NADPH on particle surfaces may in part be required for $\cdot\text{OH}$ production, we tested whether the particles or the soluble components of the particles were primarily responsible for $\cdot\text{OH}$ production. SRM 1649 and SRM 2975 were first incubated for one hour in the 100 mM phosphate, pH=7.5 buffer; the particles were then separated from their soluble constituents by centrifugation at 14000 rpm for 4 min., with the supernatant then drawn off and passed through a 0.2 μm filter. Following resuspension of the particles in the original buffer, R_{OH} was measured for the resuspended particles, the supernatant and the original suspension. At 3 mM NADPH, approximately equal values of R_{OH} were obtained for the supernatant and resuspended particles of SRM 1649, whereas for SRM 2975 the suspended particles dominated R_{OH} , with much less $\cdot\text{OH}$ production observed in the supernatant (Figures 2-13, 2-14, 2-15, 2-16). 24 hours or even longer incubation in 100 mM phosphate buffer did not change R_{OH} for supernatant or resuspended particles (SRM 1649 or SRM 2975), but some degradation in $\cdot\text{OH}$ generation was observed as time passed (Figures 2-14, 2-15, 2-16). Interestingly, addition of DTPA during the incubation period enhanced R_{OH} in both the supernatant and resuspended fractions. Longer incubation times (up to two days) provided similar results (Figures 2-14, 2-15), suggesting that the solubilization/activation of particle components by DTPA occurs rapidly.

At higher [NADPH], R_{OH} for the resuspended particles again showed evidence of saturation, consistent with a surface reaction of NADPH, while in contrast, R_{OH} for the supernatants increased linearly with [NADPH] (Figure 2-13), as one would expect for a homogenous solution reaction. Addition of DTPA increased the β value of the

original suspension while enhancing R_{OH} in the supernatant (Figure 2-13c), suggesting partial suppression of surface interactions, but overall activation of both particle and supernatant phases. These results indicate that both homogeneous and heterogeneous reactions can contribute to the overall formation of $\cdot OH$ in these suspensions.

Figure 2-13. Dependence of R_{OH} on NADPH concentration for the supernatant (\circ), the resuspended particles (\blacktriangledown) and the original suspension (\bullet) of SRM 1649 (A), SRM 2975 (B) and SRM 1649 with 600 μM DTPA (C), following an hour incubation in pH=7.5, 100 mM phosphate buffer. Other solution conditions are as in Fig. 2-7 (aerobic condition). Error bars represent one standard deviation from the mean value (n=3).

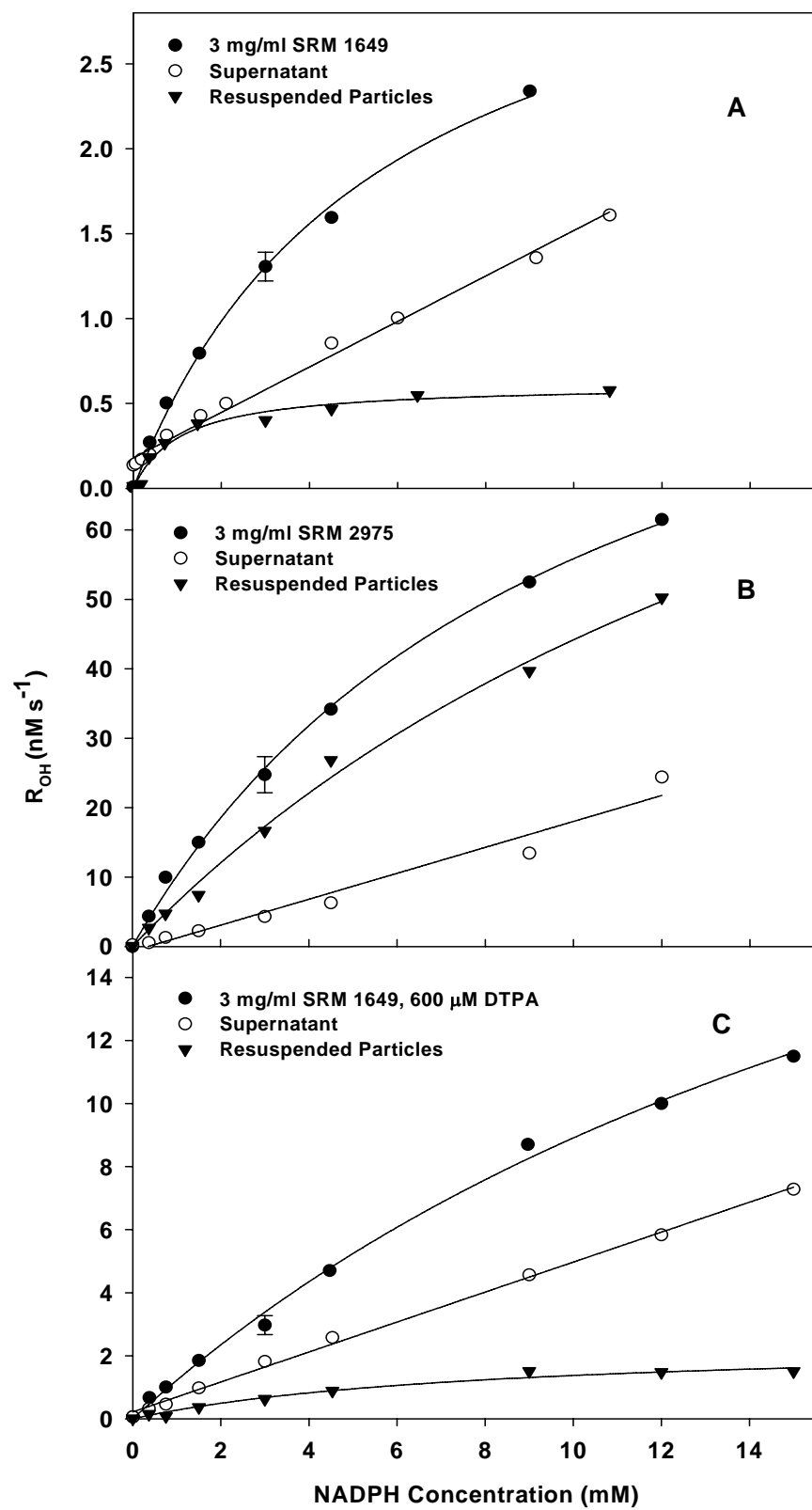


Figure 2-13

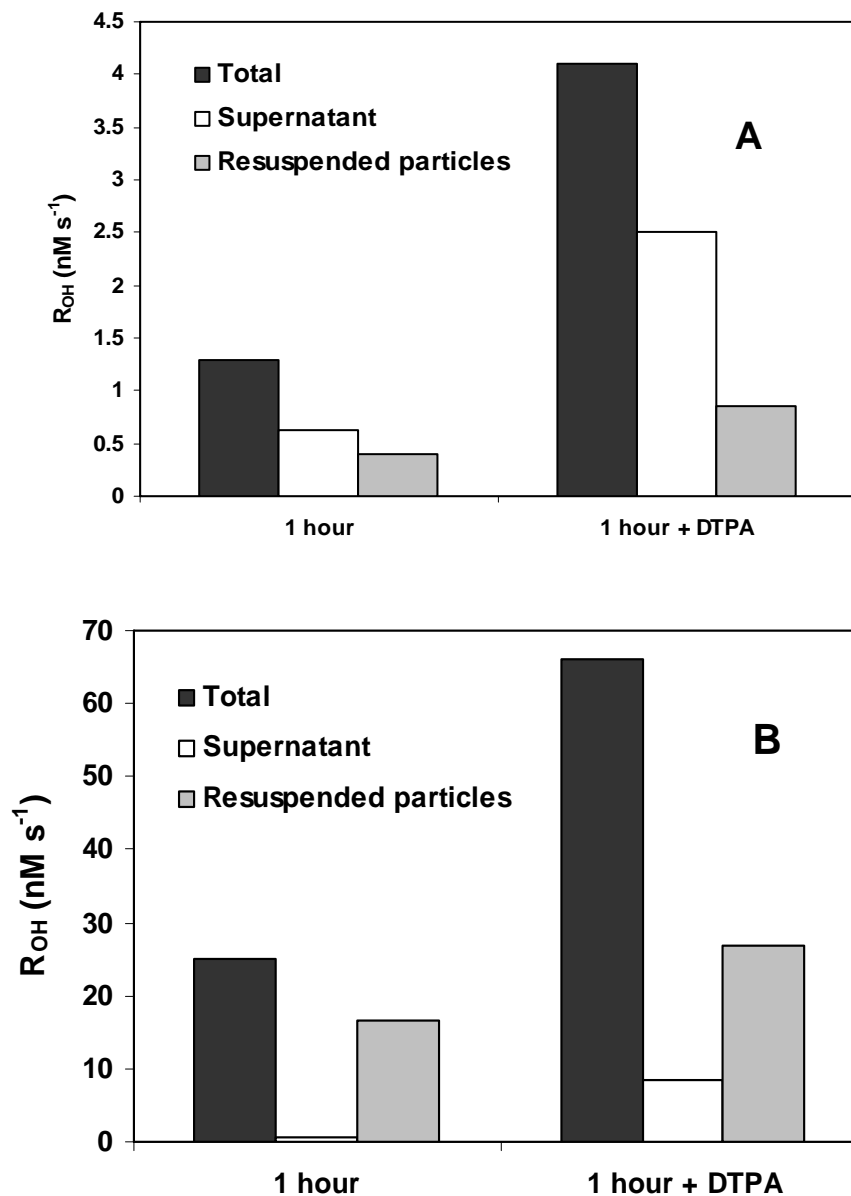


Figure 2-14. R_{OH} for the supernatant, the resuspended particles and original suspension of (A) **SRM 1649** and (B) **SRM 2975** following incubation for 1 hour in 100 mM phosphate buffer or 600 μ M DTPA in 100 mM phosphate buffer. R_{OH} was determined in the presence of 3 mM NADPH, 5% DMSO, 1500 μ M 3ap and 3 mg/ml SRM 1649 or SRM 2975 under aerobic condition.

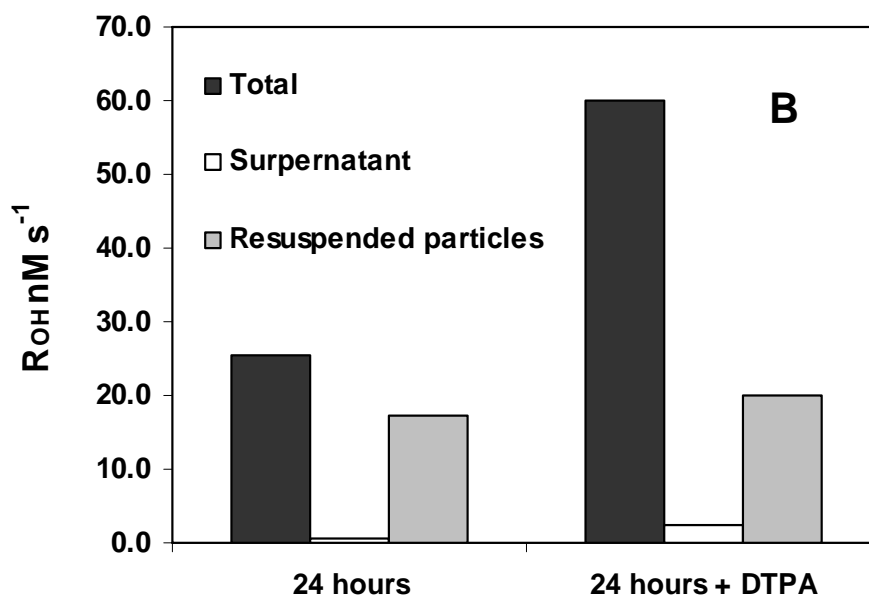
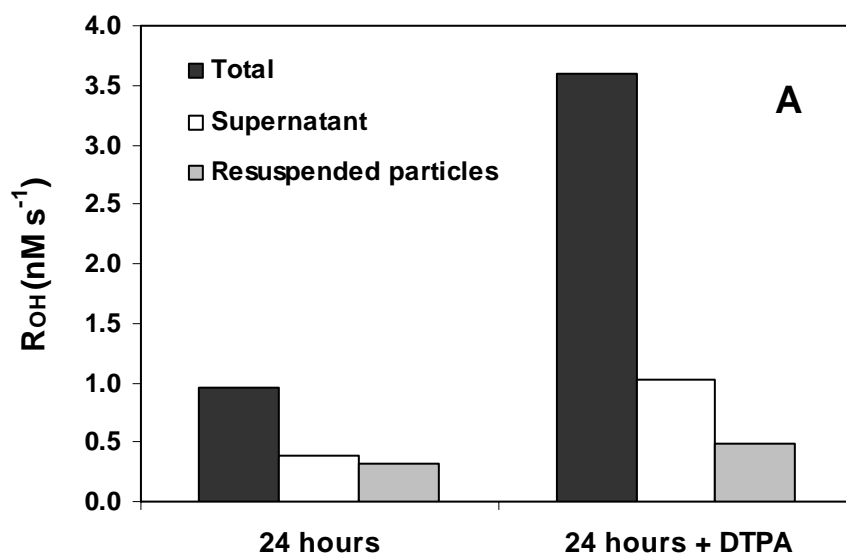


Figure 2-15. R_{OH} for the supernatant, the resuspended particles and original suspension of (A) **SRM 1649** and (B) **SRM 2975** following incubation for 24 hours in 100 mM phosphate buffer or 600 μM DTPA in 100 mM phosphate buffer. R_{OH} was determined in the presence of 3 mM NADPH, 5% DMSO, 1500 μM 3ap and 3 mg/ml SRM 1649 or SRM 2975 under aerobic condition.

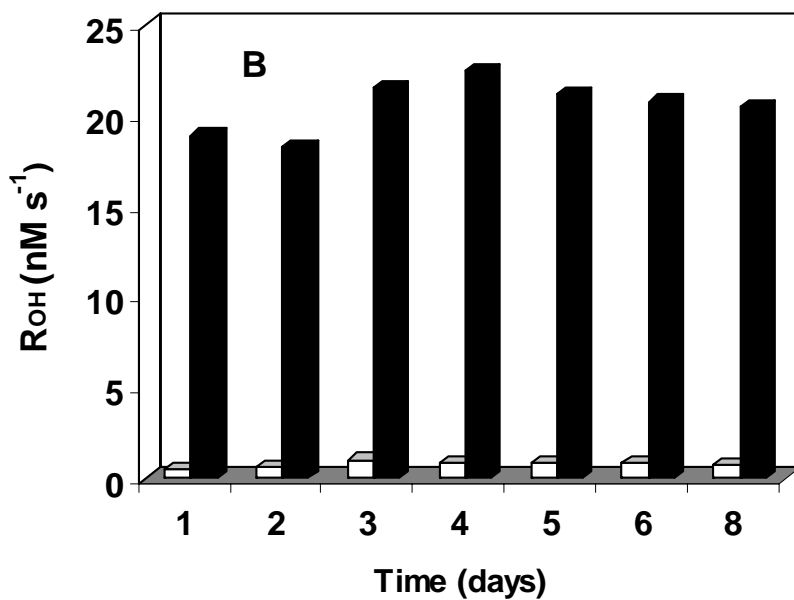
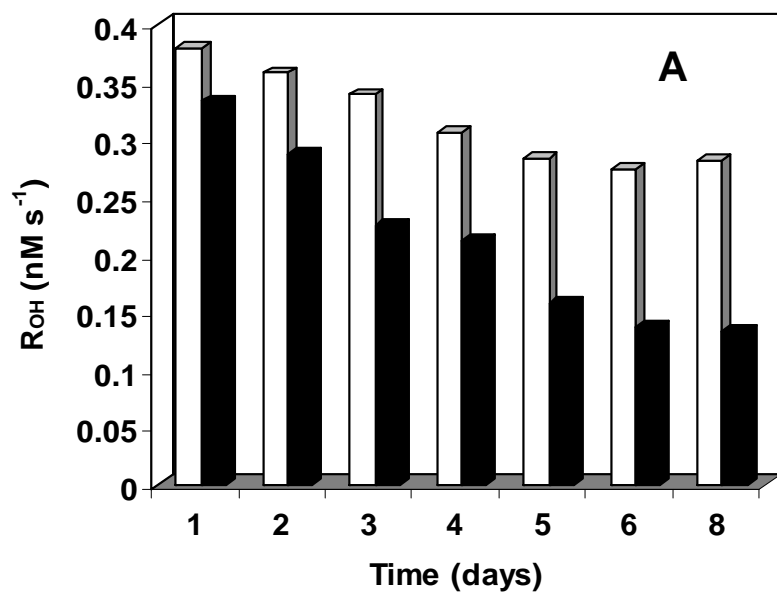


Figure 2-16. R_{OH} for the supernatant (\square) and the resuspended particles (\blacksquare) of (A) SRM 1649 and (B) SRM 2975 following incubation over days in 100 mM phosphate buffer. R_{OH} was determined in the presence of 3 mM NADPH, 5% DMSO, 1500 μ M 3ap and 3 mg/ml SRM 1649 or SRM 2975 under aerobic condition.

2.4. Discussion

These results can be largely understood within the mechanism of redox cycling originally proposed by Dellinger et al. (2001) and Squadrito et al.(2001) and supported by later work (Valavanidis et al. 2005; Valavanidis et al. 2006) (outlined in reactions 2-12 to 2-16). This mechanism, which is based on quinone redox cycling, is also thought to operate in some biological systems, and in fact, is analogous to that proposed for one mode of action of the quinone anti-cancer compounds such as diaziquone (eg. Li et al. 2000; Li et al. 1999, 12; Gutierrez 2000). In this mechanism, certain quinones and metal ions (principally Fe but other redox-active metals as well) act as catalysts to support the oxidation of organic compounds by O_2 (Rxn 2-12), and in this process, produce $\cdot OH$ (Rxn. 2-14). Thus, it is not surprising that insignificant amounts of $\cdot OH$ are produced by the pure mineral phases such as silica (aerosil) or kaolinite, because these particles either do not contain a catalyst (redox-active metal ion or quinone) or a pool of reduced organic (or inorganic) compounds that can serve as electron donors to O_2 or H_2O_2 . Addition of an electron donor (NADPH) to the silica and kaolinite did not increase R_{OH} in the presence of either air or H_2O_2 , also suggesting that these particles cannot catalyze the O_2 - or H_2O_2 -dependent oxidation of NADPH. The fly ashes exhibited similar behavior to these mineral phases, implying that they as well do not contain catalysts that can support the oxidation of NADPH by O_2 .

The very low R_{OH} observed for the other particles in the presence of air but absence of NADPH could be attributed to several factors: 1) a limited pool of electron donors available from the particles; 2) limited production of H_2O_2 ; 3) O_2 acting as a “sluggish” electron acceptor. For SRM 2975, the substantial increase in R_{OH} in the presence of H_2O_2 , either in the presence or absence of O_2 , suggests that electron donors are not limiting, but instead that H_2O_2 acts as a more direct and perhaps a more facile electron acceptor for $\cdot OH$ production (Figure 2-7A). In contrast, although SRM 1649 does show some increase in $\cdot OH$ production in the presence of H_2O_2 , this increase does not extend beyond ~ 50 min. (Figure 2-7B), suggesting a limiting pool of electron donors.

The contrasting effects of DFX and DTPA imply that metal ions play two distinct roles in $\cdot OH$ production. DFX is a strong and selective chelator of iron, and would be expected to suppress $\cdot OH$ formation through inhibition of the Fenton reaction (Rxn. 2-14) as is observed (Figure 2-11). In contrast, DTPA is capable of strongly chelating a broad spectrum of metal cations including iron. Although elevation of R_{OH} in the presence of DTPA might be attributed to enhanced metal mobilization (Smith and Aust 1997) and the ability of reduced metal-DTPA complexes to remain active as Fenton reagents (Welch et al. 2002; Miller et al. 1990), this explanation appears inconsistent with recent work that examined a well-defined redox-cycling system containing NADPH, diaziquone and iron (Li et al. 2000), in which DTPA significantly suppressed $\cdot OH$ production. An intriguing, alternative possibility is that DTPA enhances R_{OH} by chelating divalent metal cations that would normally stabilize *o*-semiquinone radicals via complexation (Felix and Sealy 1981).

These stabilized *o*-semiquinones would be expected to undergo less facile reaction with O_2 and $O_2^{\cdot -}$, thereby slowing the catalytic production of $O_2^{\cdot -}$ and H_2O_2 . If so, then the presence of redox-inactive metal cations such as Mg^{2+} , Ca^{2+} , Cd^{2+} and Zn^{2+} could also substantially influence $\cdot OH$ production rates in these particles. This would also suggest a key role for *o*-semiquinones in the redox cycling, consistent with the original proposal of Pryor and co-workers (Dellinger et al. 2001; Squadrito et al. 2001), as well as more recent EPR results (Valavanidis et al. 2005; Valavanidis et al. 2006).

In the presence of NADPH, the very high values of R_{OH} observed for diesel particulate matter and the lesser, but still high values observed for urban dust provide further support for the role of quinone redox cycling. Cho et al. 2004 reported recently that diesel particulate matter contained high levels of four quinones, while urban dust (SRM 1649) contained much smaller but significant levels of these same quinones, mirroring the trend in R_{OH} .

To our knowledge, these measurements have provided the first quantitative estimates of $\cdot OH$ formation for a wide range of airborne particulate matter. The method employed is relatively fast and highly-sensitive and should be widely applicable to the measurement of $\cdot OH$ formation in many of particle types, including nanoparticles. Rapid screening by fluorescence based approaches (Blough and Simpson 1988; Li et al. 1999a) may further prove possible.

Chapter 3: Impact of Airborne Particulate Matter on Cellular Toxicity

Abstract

Suspensions of human airway epithelial cells (BEAS-2b) and mouse epidermal cells (JB6) were employed to examine the effects of different airborne particles on cell survival and hydroxyl radical ($\cdot\text{OH}$) generation. The production of $\cdot\text{OH}$ in these cell systems was examined by a sensitive method which employed a fluorescamine-derivatized nitroxide probe. The airborne particles that were examined included urban dust (SRM 1649), diesel particulate matter (SRM 2975), coal fly ash (SRM 2689), Kaolinite (KGa-1b) and Aerosil (pure silica).

Although some $\cdot\text{OH}$ production was observed in the presence of these cell lines when exposed to diesel particulate matter and urban dust, rates of cell death did not correlate with the $\cdot\text{OH}$ production rate. Further, silica particles, which exhibited no evidence of $\cdot\text{OH}$ production, produced the most rapid cell death. These results suggest that the $\cdot\text{OH}$ production is not the primary factor controlling cell death following short term exposure to these particles.

On the other hand, both cell death and hydroxyl radical formation were dramatically enhanced when an external biological reductant, NADPH, was added to a suspension of cells and urban dust. In this situation, the high flux of $\cdot\text{OH}$ is the likely factor causing cell death.

3.1. Introduction

Lung epithelial cells are exposed to a variety of stresses such as bacteria, viruses, inorganic particles (asbestos, silica), air pollution toxins (NO₂, N₂O₃, O₃) and airborne particulate matter. It has been reported (Andersson et al. 1990; Andersson et al. 1997; Pope III et al. 2002; Brook et al. 2004; Somers et al. 2004) that airborne particulate matter contributes to several lung diseases, including pulmonary fibrosis, acute respiratory diseases and lung cancer. A variety of studies have been conducted to understand the mechanisms by which particulate matter (PM) interacts with lung tissue (MacNee and Donaldson 2003; Agopyan et al. 2003; Dellinger et al. 2001). However, the heterogeneity in PM composition makes it difficult to identify a single mechanism to explain the toxicity of airborne particulate matter. Production of reactive oxygen species (ROS) by airborne particles has been suggested to be one of the possible mechanisms causing the adverse health effects (Brown et al. 1996; Heunks et al. 2000; Li et al. 2002; Tao et al. 2003).

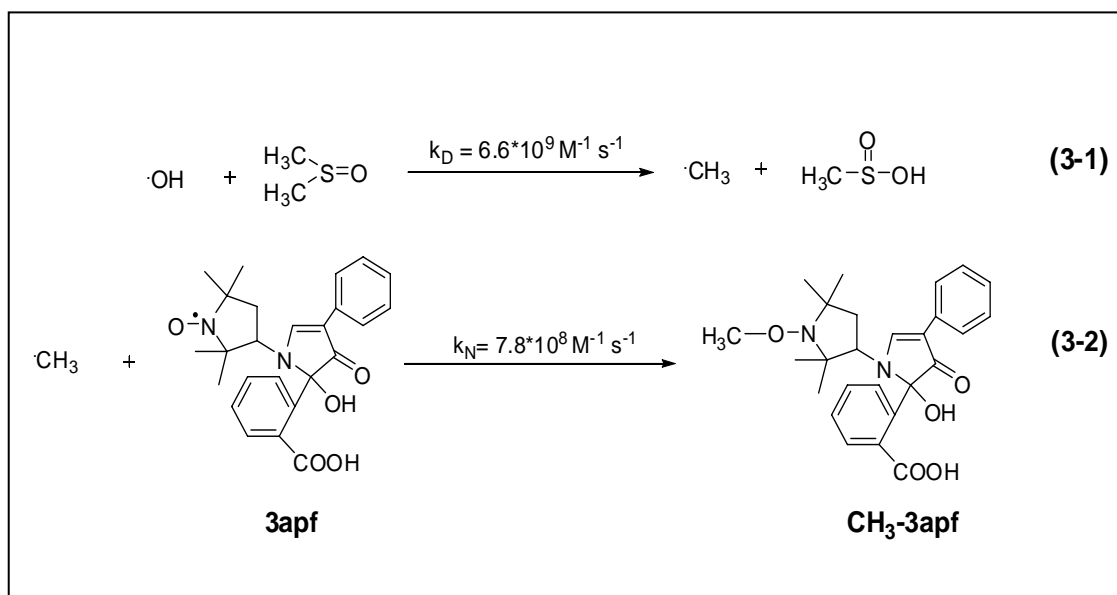
Most past efforts to detect ROS generated by airborne particles, particularly the hydroxyl radical ($\cdot\text{OH}$), have employed spin trapping with electron spin resonance detection (ESR; Briedé et al. 2005; Schins et al. 2002; Kadiiska et al. 1997; Ding et al. 2001; Shi et al. 2003a) and only few of these studies have examined the generation of $\cdot\text{OH}$ in cell systems. However, spin trapping with ESR detection can not provide quantitative estimates of the rate of $\cdot\text{OH}$ production (Kieber and Blough 1990b; Pou et al. 1994; Finkestein et al. 1980). In addition to spin trapping and ESR detection, formation of 8-hydroxy-2' deoxyguanosine (8-oxo-dG) or DNA strand breakage have

been employed as markers for OH production (Li et al. 2003; Prahalad et al. 2001; Karlsson et al. 2005, Aljandali et al. 2001). These two methods can not be readily employed to measure $\cdot\text{OH}$ production. Guanine is oxidized during the sample preparation while DNA strand breaks require repeated attack of $\cdot\text{OH}$ in the same location (Xu et al. 1999; Shi et al. 2003b).

Only a few studies have examined the toxicity of airborne particulate matter on cells and its possible relationship with hydroxyl radical production (Hiura et al. 1999; Li et al. 2002; Hirano et al. 2003, Upadhyay et al. 2003). Existing studies have usually employed non-specific techniques such as a decline in GSH/GSSG ratio, increase in IL-8 or a decrease in cell death in the presence of radical scavengers to determine ROS production.

Here, we examine the effects of several types of airborne particles on the survival of human airway epithelial cells (BEAS-2b) or mouse epidermal cells, as well as its relationship to $\cdot\text{OH}$ generation. A highly sensitive technique was employed to quantify $\cdot\text{OH}$ produced by several airborne particles in the presence of two cell lines. In this technique, $\cdot\text{OH}$ reacts with DMSO to produce a methyl radical. The methyl radical is then trapped with a fluorescamine-derivatized nitroxide, 3apf, to produce the stable *O*-methyl-hydroxylamine product (Scheme 3-1). The product is separated by reversed phase liquid chromatography and detected fluorometrically (Kieber and Blough, 1990b; Johnson et al. 1996; Vaughan and Blough, 1998; Li et al. 1999a; Li et al. 1999b; Li et al. 2000). In this work, effect of airborne particles on the death of BEAS-2b and JB6 cell was first examined. Our results suggest that the $\cdot\text{OH}$

production is not the primary factor controlling cell death in the presence of these particles.



Scheme 3-1. ·OH trapping method; (Li et al. 1997; Li et al. 1999b)

3.2. Experimental section

3.2.1. Materials

The reduced form of β -nicotinamide adenine dinucleotide phosphate (NADPH), fluorescamine, catalase (CAT) and superoxide dismutase (SOD) were purchased from Sigma. Dimethyl sulfoxide (DMSO) (99.9%), potassium dihydrogen phosphate (99.99%), sodium chloride (99.999%), hydrochloric acid (99.999%), boric acid, and acetonitrile were purchased from Aldrich. 3-Amino-2,2,5,5-tetramethyl-1-pyrrolidinyloxy (3ap) and 3-carbamoxyl peroxide (3cp) was purchased from Acros. Hydrogen peroxide was purchased from Fisher. Acetic acid and methanol (HPLC grade) were purchased from J.T.Baker. AZQ was provided by Drug Synthesis & Chemistry Branch, Developmental Therapeutics Program, Division of Cancer Treatment and Diagnosis, National Cancer Institute, Bethesda, MD. Ultra High Pure (UHP) grade nitrogen was obtained from Airgas. Keratinocyte basal medium (KBM) and additives insulin, gentamicin sulfate and amphotericin (GA), bovine pituitary extract (BPE), epidermal growth factor (rhEGF) and hydrocortisone were purchased from Clonetics. Cell culture medium [Earl's modified essential medium (EMEM)], L-glutamine, fetal calf serum (FCS), penicillin/streptomycin and trypsin-EDTA were purchased from Gibco. All chemicals were used as received. A Millipore Milli-Q system provided water for all experiments.

Phosphate-buffered saline (PBS) was prepared by dissolving 6.7 mM KH_2PO_4 and 0.9% (w/w) NaCl in Milli-Q water, the pH of the buffer solution was

adjusted to 7.4 using concentrated sodium hydroxide solution. The buffer was then autoclaved and stored at 4°C.

3.2.2. Particle source

Standard reference materials urban dust (SRM 1649), diesel particulate matter (SRM 2975), coal fly ash (SRM 2689) were obtained from National Institute of Standard and Technology, Gaithersberg, MD. The Clay standard kaolinite (KGa-1b) and Aerosil were received from the Clay Mineral Society and the Degussa Corporation, respectively. All airborne particulate matter was used without pretreatment.

3.2.3. Apparatus

The UV-Vis spectrophotometers, balance, pH meter and HPLC employed in these experiments are described in chapter 2. Chromatographic conditions were identical to those used in chapter 2 (section 2.2.3). A Bruker/IBM ER 200D-SRC ESR spectrometer was employed in all ESR measurements. Samples were drawn into 50 µL capillary tubes which then sealed at the top and bottom, and placed within standard 3 mm i.d. quartz ESR tubes. Standard instrument settings were as follows: frequency 9.90 GHz; microwave power 10 mW; modulation amplitude, 0.952 G; sweep width, 80 G; time constant, 40.96 ms; and scan time, 30 s.

To obtain spin concentration of 3apf, 3-carbamoyl-proxyl (3cp) was used to provide a calibration curve. A 10 mM 3cp stock solution was prepared in water with exact concentration of 3cp stock which was measured by UV-Vis absorption (the extinction coefficient of 3cp at $\epsilon_{326}=2850 \text{ M}^{-1} \text{ cm}^{-1}$; Gan 2004). After a serial dilution of 3cp solution, their ESR peak area obtained by double integration. Based on this calibration curve, spin concentration of 3apf was then obtained.

3.2.4. Cell culture

3.2.4.1. Preparation of culture medium for lung epithelial cells (BEAS-2b)

Human epithelial lung cells (BEAS-2b) were received from Dr. Peter L. Gutierrez and were grown in continuous culture in keratinocyte basal medium (KBM) supplemented with insulin, gentamicin sulfate, amphotericin, bovine pituitary extract, epidermal growth factor and hydrocortisone. The complete media was called keratinocyte growth medium (KGM). Cell viability was determined by trypan blue exclusion, whereas cell numbers were determined with a hemacytometer.

3.2.4.2. Preparation of culture medium for mouse epidermal cells (JB6)

Mouse epidermal cells (JB6) were also received from Dr. Peter L. Gutierrez and were grown in continuous culture in Earl's modified essential medium (EMEM) supplemented with 10% fetal calf serum, 2 mM L-Glutamine, 50 U/ml penicillin and 50 $\mu\text{g/ml}$ streptomycin.

3.2.4.3. Maintenance of cell culture for BEAS-2b cells

Cells were incubated in T-75 flasks at 37°C in a humidified atmosphere of 5% CO₂ in air, and examined every 2-3 days to determine whether they needed subpassage or media change.

Cell cultures at 80-100% confluent density were harvested by first aspirating off the media and washing the cells with 10 mL of PBS. The aspirated growth media (old media) was kept for the next step. 4-5 mL trypsin EDTA solution was then added to the flask, which was incubated at 37°C for 5 minutes. When approximately 80-90% of the cells were detached (which can be facilitated by “tapping” the flask), 8-10 mL old media was added to the flask to neutralize the proteolytic activity of the trypsin solution., and then the nonadherent cells transferred to the sterile tube. The cells was centrifuged at 1200 rpm for 10 minutes. The supernatant was aspirated off and 10 mL KGM was added to the tube. Known amounts of the suspended cells were transferred to new T-75 flasks, and total volume was brought up to 12-14 mL with fresh media (KGM). The newly transferred cells were then incubated at 37°C and the media was changed every 3 days.

3.2.4.4. Maintenance of cell culture for JB6 cells

Cells were incubated in T-75 flasks at 37°C in a humidified atmosphere of 5% CO₂ in air, and examined every 2-3 days to determine whether they needed subpassage or media change.

Cell cultures at 80-100% confluent density were harvested by first aspirating off the media and washing the cells with 10 mL of PBS. 2 mL trypsin EDTA solution was then added to the flask, which was incubated at room temperature for 4 minutes. When approximately 80-90% of the cells were detached (which can be facilitated by “tapping” the flask), 4 mL of growth medium was added to the flask to neutralize the proteolytic activity of the trypsin solution. A known quantity of the suspended cells were transferred to new T-75 flasks, and total volume was brought up to 10 mL with fresh medium (EMEM). The newly transferred cells were then incubated at 37°C, with the media changed every 3 days.

3.2.4.5. Preparation and counting cell suspension

A hemocytometer was used to count the viable cells in suspension after being mixed with trypan blue solution. A serial dilution of the cell suspension was made in either growth media or PBS. The hemocytometer consisted of several 1 mm squares divided into smaller squares. One of the 1 mm squares represented a volume of 0.1 cm³ (or 1 × 10⁻⁴ mL). Using the 20X objective, the number of cells was counted in a 1mm square area. If more than a single 1-mm square area was counted, the results were averaged to calculate the concentration of cells. The average number of cells (n) present in 0.1 mm³ (or 1 × 10⁻⁴ mL) area gave a concentration of n × 10⁻⁴ cells/mL. Since the cell suspension was diluted 1:1 with the trypan blue solution, then the number of cells in the original cell suspension was calculated by 2n × 10⁻⁴ cells/mL.

3.2.4.6. Dye exclusion test for the viability of cells

The dye exclusion test was used to determine the number of viable cells present in a cell suspension. It is based on the principle that live cells possess intact cell membranes that exclude certain dyes, such as trypan blue, whereas dead cells do not. In this test, a cell suspension was simply mixed with equal volume of trypan blue solution (10-50 μ L), with a low magnification microscope (20X) then used to visually determine whether cells take up or exclude dye. Viable cells will have a clear cytoplasm whereas nonviable cells will have a blue cytoplasm. The percentage of viable cells was calculated as follows:

$$\text{Viable cells (\%)} = \frac{\text{total number of viable cells per mL of aliquot}}{\text{total number of cells per mL of aliquot}} \times 100$$

3.2.4.7. Preparation of the BEAS-2b and JB6 cells for experiments

Either BEAS-2b or JB6 cells (~80-90% confluent density) were harvested by aspirating off the growth medium and washing the cells with 10 mL of 37°C PBS. BEAS-2b was incubated at 37°C with 4-5 mL trypsin-EDTA solution for 5 minutes and 2 mL trypsin solution was added to JB6 cells, followed by incubation at room temperature for 5 minutes. After cells was detached from the flask surface, 8-10 mL of used growth medium (medium aspirated off the cell culture flasks containing cells; KGM) to the BEAS-2b suspension and growth medium (EMEM) to the JB6

suspension. The cells were then centrifuged for 10 minutes at (1200 rpm for BEAS-2b and ~1200 rpm for JB6, using table ICE clinical centrifuge), the supernatant decanted and the pellet resuspended in 10 mL PBS. The cells were washed with PBS, and then suspended in an appropriate volume of PBS for the experiments.

3.2.5. Toxicological studies

In this study, we used two different methods to determine the toxicity of airborne particulate matter on lung epithelial cells (BEAS-2b) and mouse epidermal cells (JB6). In the following sections, these two methods are described.

3.2.5.1. Toxicological method I

In the first method, equal concentration of BEAS-2b cells, attached to T₂₅ flasks, was exposed to different concentration of particles (Urban Dust, Diesel Particulate Matter and Aerosil) in PBS for 2 hours while they were incubating at 37°C. After the incubation time, the particles were drawn out and the cells were washed with PBS. The cells were then fed with keratinocyte media for 12 days. After 12 days, the viable cells were counted with trypan blue exclusion. The percentage of viable cells was calculated based on the control which was incubated with PBS for 2 hours before addition of keratinocyte media for 12 days. The precision of the method was determined from the reproducibility of three measurements of viable cells for a

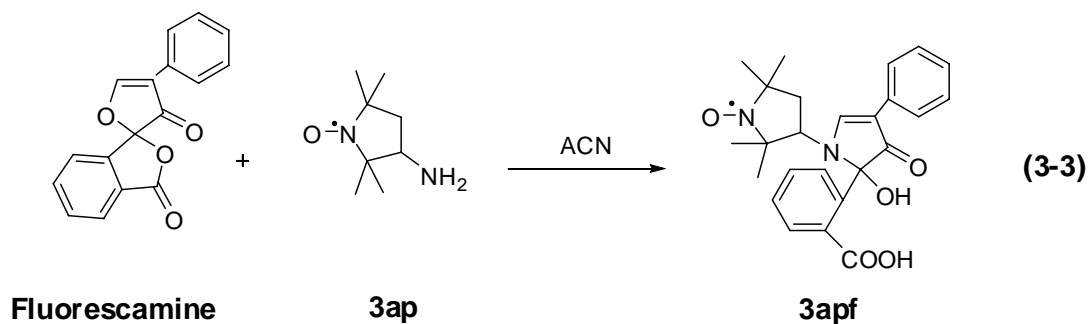
given experimental condition. The maximum %RSD was 52 %. Error bars reported in the figures represent \pm one standard deviation.

3.2.5.2. Toxicological method II

To investigate further the toxicity of airborne particles, additional experiments were performed in PBS or suspension of particles in PBS, using not only BEAS-2b cells, but the mouse epidermal cell line JB6. In this experiment, either 0.1 or 1 mg/mL Urban Dust (SRM 1649, UD), Diesel Particulate Matter (SRM 2975, DPM), Coal Fly Ash (SRM 2689, CFA), Kaolinite (KGa-1b) or Aerosil (AS) was added to suspension of 2×10^6 cells/mL in PBS. Cell viability was assessed every 30 minutes by the trypan blue exclusion method over a course of 3.5 hours. The percentage of viable cells in PBS was employed as the control for this experiment. The precision of the method was determined from the reproducibility of three measurements of viable cells for a given experimental condition in the same day as well as for the experimental condition over multiple days. The maximum %RSD was 15 %, Error bars reported in the figures represent \pm one standard deviation.

3.2.6. Synthesis of 3apf

3apf was synthesized by a one-step reaction of 3ap with fluorescamine in acetonitrile (rxn. 3.3).



123.9 mg of fluorescamine was dissolved in 3 mL of dry ACN. 70 mg 3ap was dissolved in 3 mL of dry acetonitrile and then added dropwise with stirring to the solution of fluorescamine (after adding each 4-5 droplet of 3ap aliquot, the fluorescamine solution was vortexed for 1 minute.). After adding all 3ap to fluorescamine solution, the total volume of solution was reduced to 0.5 mL by flushing with dry nitrogen. The final solution was stored at -20 °C for 48 hours, till the bright yellow precipitate of 3apf was produced. The supernatant was decanted, and the precipitate was rinsed three times with total of 9 mL of ethyl ether and then dried with nitrogen. The yellow product was stored in the dark at -20 °C. Analysis by HPLC (mobile phase containing 55% acetate buffer pH = 4.0, and 45% methanol) showed approximately 97% purity for 3apf. ESR spectra showed an intense three-line spectrum with $A_N = 16.0$ G, and a 3apf spin concentration was measured by comparing to 3cp standard calibration curve (described in section 3.2.3).

3.2.7. Kinetics of the probe bioreduction

Different concentrations of BEAS-2b ($0.99\text{-}33 \times 10^6$ cells/mL) were suspended in PBS containing 500 μM 3apf and 50 mM DMSO (0.35%) and incubated at 37 °C. Aliquots of the samples were drawn into 50 μL capillaries after appropriate incubation periods, and placed within standard 3 mm i.d. quartz ESR tubes. Incubation times were measured from the addition of 3apf to the start of ESR data collection. An average of 16 ESR spectra scans requiring 8 min was recorded on a Bruker/IBM 200D-SRC ESR spectrometer for each of these aliquots. Standard instrument settings were as follows: frequency 9.90 GHz; microwave power 10 mW; modulation amplitude, 0.952 G; sweep width, 80 G; time constant, 40.96 ms; and scan time, 30 s. As shown in Figure 3-1, the bioreduction of 3apf is negligible for 2.0×10^6 cells/mL of BEAS-2b. Based on bioreduction of 3apf by JB6, reported previously (Li et al. 1999b), 2.0×10^6 cells/mL is an appropriate concentration to be used in these experiments.

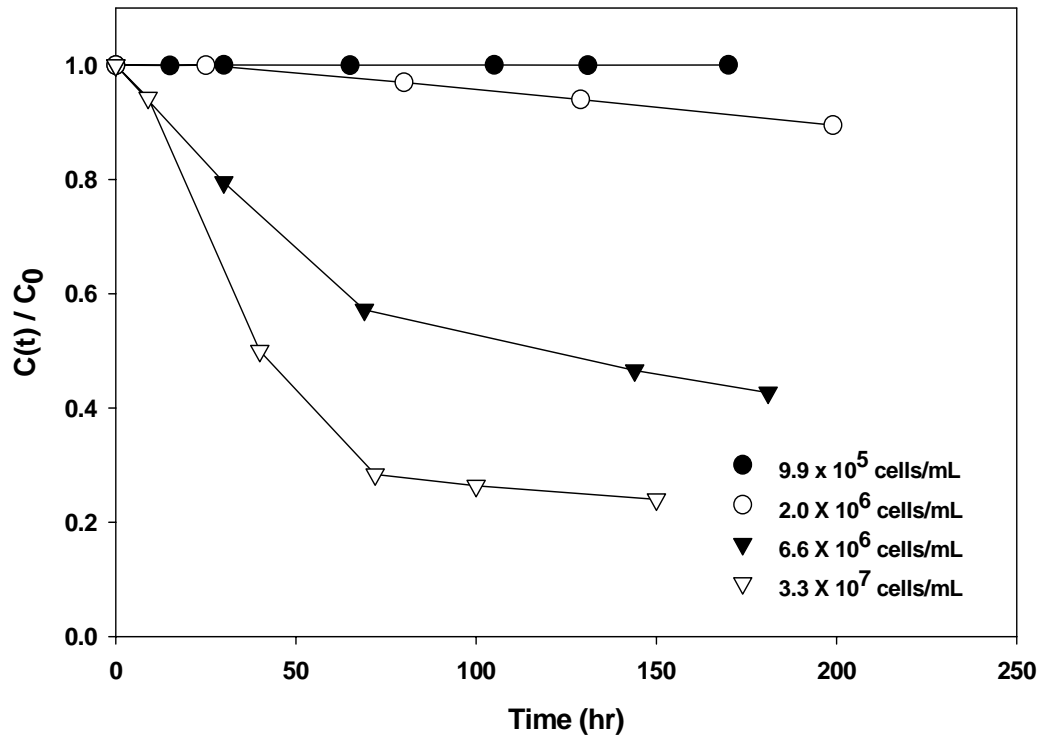


Figure 3-1. Kinetics of the bioreduction of 3apf by BEAS-2b cells ($0.99 - 33 \times 10^6$ cells/mL). Cells were suspended in PBS containing $500 \mu\text{M}$ 3apf and 0.05 M DMSO. Time courses for reduction. $C(t)/C_0$ represents the fraction of the original ESR signal amplitude remaining at time t .

3.2.8. Hydroxyl radical determination

$500 \mu\text{M}$ 3apf and 0.05 M DMSO were added to the cell suspensions (2×10^6 cells/mL) in PBS. The reaction was initiated by adding a suspension of particles in PBS to a final volume of 1 mL . The mixture was incubated at 37°C in a humidified atmosphere of $5\% \text{ CO}_2$. Reactions were terminated by centrifuging the cell and particle suspension for 4 min at 3000 rpm (model 5415c Ependorf centrifuge). The

supernatant was analyzed by HPLC. Incubation times were measured from the addition of particles until the injection of supernatant onto the HPLC system. Viability of cells was tested by trypan blue exclusion after each injection.

3.2.9. Hydroxyl radical detection and quantification

The method for detection and quantification of $\cdot\text{OH}$ in biological systems was previously described in our laboratory (Li et al. 1999a; Li et al. 1997). A detailed description of technique for the preparation of Me-3apf standard was explained in chapter 2. This method was employed to determine quantitatively the formation of hydroxyl radical.

The conditions for detecting and quantifying $\cdot\text{OH}$ with 3apf in the presence of JB6 cells were previously determined (Li et al. 1999b), but it was necessary to establish whether these conditions were compatible with BEAS-2b cells. Therefore, we focused on experiments that examined the dependence of Me-3apf yield on DMSO and 3apf concentration (see section 3.3.4).

3.2.10. Precision, accuracy and detection limit (D.L.)

The precision of the first and second toxicological tests was determined from the reproducibility of multiple viable cell counting (≥ 3) for a given experimental condition. The maximum %RSD was 52 % and 15 % for first and second tests, respectively, which includes the reproducibility of the measurements. Error bars reported in the figures represent \pm one standard deviation.

The precision of the method for measuring $\cdot\text{OH}$ produced by airborne particles in the presence of cells was determined from the reproducibility of multiple HPLC injections (≥ 3) for a given experimental condition over multiple days. The maximum %RSD was 5 %, which includes the reproducibility of the measurements from day to day. Error bars reported in the figures represent \pm one standard deviation.

The accuracy of the method to measuring $\cdot\text{OH}$ depends on accuracy of the molar extinction coefficient for $\text{CH}_3\text{-3apf}$ because the peak area of chromatograms was converted to concentration of $\text{CH}_3\text{-3apf}$ obtained by UV-Vis method as explained in sections 2.2.5.1 and 2.2.5.5. Moreover, the accuracy of the method mainly depends on the accuracy of a coefficient which was used to convert Me-3apf concentration in aerated samples to integrated $\cdot\text{OH}$ formation through multiplication by a factor of 3.2 ± 0.2 and 2.9 ± 0.36 obtained at $[\text{3apf}]=500 \mu\text{M}$ and $[\text{O}_2]=250 \mu\text{M}$ in the presence of BEAS-2b and JB6 cells, respectively.

In these experiments, using 0.05 M DMSO is another important factor which has a large effect on accuracy. Figure 3-5 showed that $\cdot\text{OH}$ production at high concentration of DMSO is approximately 52% higher than $\cdot\text{OH}$ production at 0.05 M

DMSO. A factor was used to adjust ·OH production in the presence of 0.05 M DMSO to ·OH production at high enough concentration of DMSO, which provided a saturation level. The accuracy of method depends on the accuracy of the factor.

Defining the detection limit as twice the standard deviation of the blank (500 μ M 3ap, 0.05 M DMSO, 2×10^6 cells/mL; $n \geq 8$), values of 9 and 8 nM were estimated for CH₃-3apf (50 μ L injection volume) for samples containing BEAS-2b and JB6 cells, respectively. These values are similar in magnitude to the detection limits previously reported for this method when applied to other systems (Li et al. 1997; Li et al. 1999b).

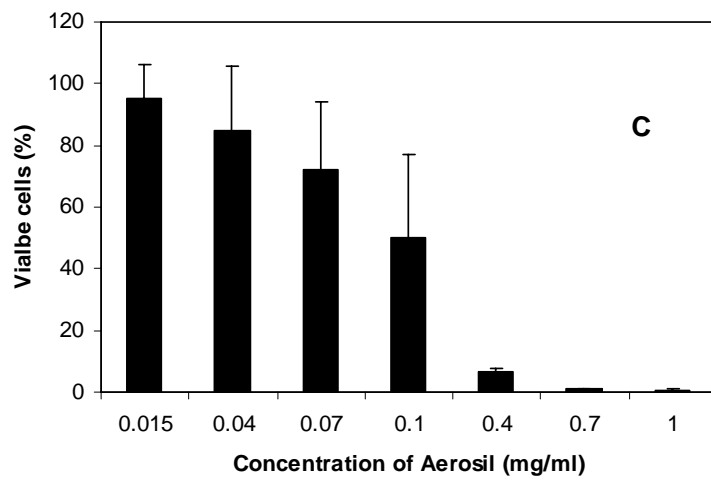
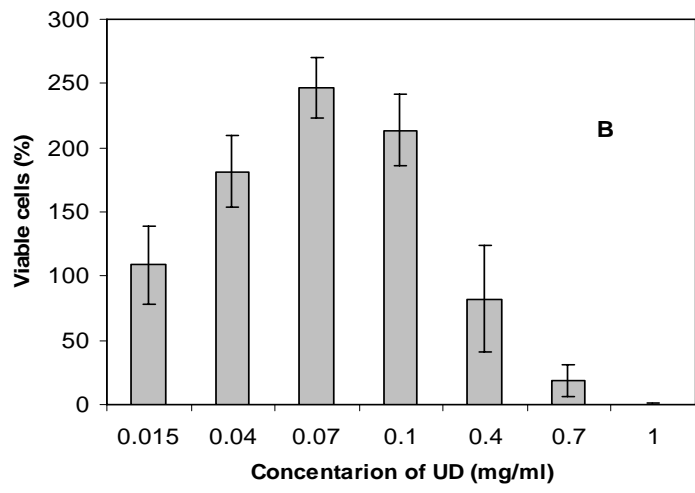
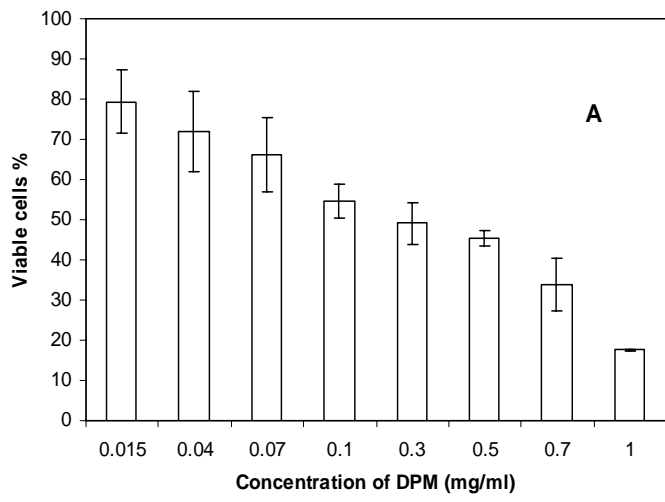
3.3. Results

3.3.1. Toxicity of diesel particulate matter, urban dust and Aerosil

The toxicity of particles to lung epithelial cells was investigated first by exposing BEAS-2b cells to a suspension of particles in PBS for 2 hours and subsequently growing the cells in the culture media (for method I). Figures 3-2 A-C show the viability of BEAS-2b cells following exposure to DPM, UD and Aerosil, respectively. Viability of BEAS-2b cells decreased from 80% to 20% when the concentration of DPM increased from 0.015 to 1.0 mg. UD enhanced cell growth up to 0.07 mg/mL, but decreases in cell viability were observed from 0.1 mg/mL through 0.7 mg/mL, with no viable cells detected at 1 mg/mL. In the presence of Aerosil,

there was a similar decrease to DPM between 0.015 and 0.1 mg/mL and substantial reductions were observed at concentrations higher than 0.1 mg/mL. This resulted in very low cell viability at 0.4 mg/mL to total cell death at 1 mg/mL. The rate of cell death was much faster in the presence of Aerosil than two other tested particles.

Figure 3-2. Graphs A, B and C illustrating BEAS-2b cells growth treated with different concentration of SRM 2975 (DPM), SRM 1649 (UD) and Aerosil for 2 hours, respectively. Error bars represent one standard deviation from the mean value (n=3).



A second test (method II) was performed to investigate further the toxicity of airborne particles, using not only BEAS-2b cells, but the mouse epidermal cell line JB6. In this test, 2×10^6 cells/mL of BEAS-2b or JB6 were suspended in PBS alone, or in 1 mg/mL or 0.1 mg/mL of the three airborne particles used above (DPM, UD, Aerosil), as well as CFA and Kaolinite. Cell viability was assessed every 30 minutes by the trypan blue exclusion method over the course of 3.5 hours (Figure 3-3, 3-4).

In the course of 3.5 hours, viability of BEAS-2b cells decreased to 42% when the cells were kept in PBS. 5% BEAS-2b cells were viable in the presence of 1 mg/mL Aerosil while viability of the cells exposed to 1 mg/mL DPM decreased to 30%. The cell viability was also decreased to 30% and 56% when they were incubated with 1 mg/mL of CFA and Kaolinite, respectively. In contrast 100% of BEAS-2b was viable after 3.5 hours incubation with 1 mg/mL UD (Figure 3-3-A). Figure 3-3-B clearly shows that UD kept BEAS-2b viable during the course of 3.5 hours while Aerosil was the most toxic particle and dramatically killed the cells. Chang et al. 2007 also reported that cell membrane is damaged at high dosages of silica. The rest of the particles did not show an obvious toxicity to the cells comparing to PBS.

Viability of JB6 was also tested with exposing to 1 mg/mL of each particles, as well as PBS. After a course of 3.5 hours, 100% of JB6 cells were viable, while cell viability was decreased to 30%, 43%, 55% and 56% when the cells were incubated with 1 mg/mL of DPM, Aerosil, CFA and Kaolinite, respectively. On the other hand, 100% of the cells were viable when they were exposed to 1 mg/mL UD (Figure 3-3-C). Figure 3-3-D shows that UD kept JB6 viable during the course of 3.5 hours while

DPM was the most toxic particle and killed the cells faster than the other particles. Viability of JB6 cells showed same decreasing pattern when the cells were incubated with 1 mg/mL of CFA, Kaolinite and Aerosil.

We also examined the viability of both BEAS-2b and JB6 cells in the presence of 0.1 mg/mL of the each suspended particles mentioned above. Either PBS or 0.1 mg/mL suspension of the particles in PBS caused approximately 30-50% cell death for BEAS-2b cells over the course of 3.5 hours (Figure 3-4-A) and they did not cause any toxicity to the cells (Figure 3-4-B). Neither PBS nor 0.1 mg/mL suspension of the particles in PBS caused cell death for JB6 cells (Figure 3-4-C & D).

There are some differences between the observed toxicity for the first (Figure 3-2) and second (Figure 3-3, 3-4) toxicological experiments because it is more possible to generate toxic species (such as $\cdot\text{OH}$) in the presence of culture medium. In the case of DPM, viability of cells was decreased linearly in both first and second experiment, but the cell death was faster in the first experiment which is consistent with increase in hydroxyl radical production and cell toxicity in the presence of media. In the case of Aerosil, viability of BEAS-2b cells was decreased rapidly when the cells kept in PBS or medium.

In general, these toxicology experiments showed that BEAS-2b cells are very sensitive to their environment. They were killed with a relatively high rate at 1 mg/mL of diesel particulate matter, coal fly ash, kaolinite and Aerosil. In contrast, JB6 cells showed less sensitivity to the toxic environment.

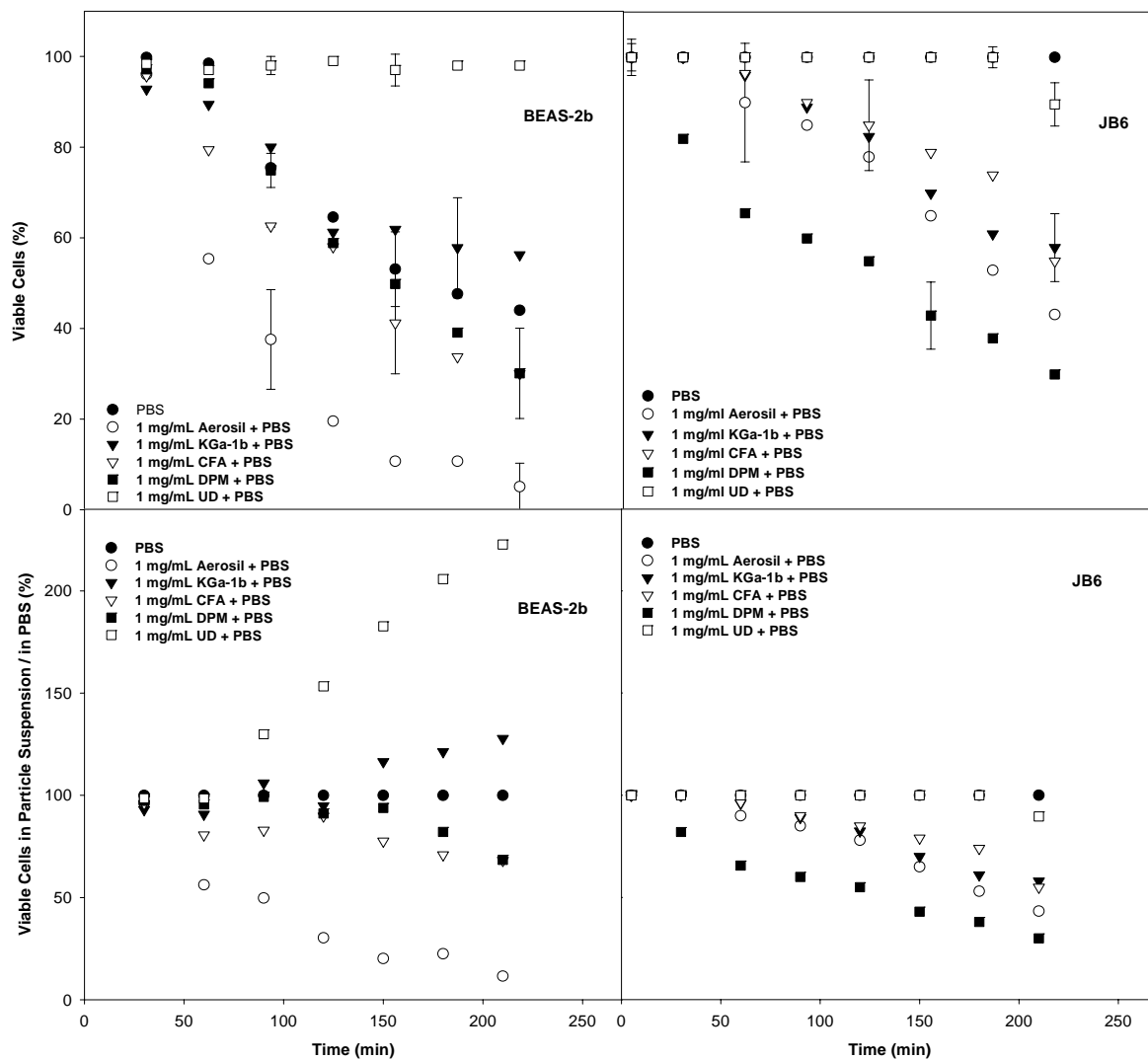


Figure 3-3. Time course for viability of BEAS-2b and JB6 cells in PBS (●); in PBS and suspension of 1 mg/mL Aerosil (○); KGa-1b (▼); SRM 2689 (CFA) (▽); SRM 2975 (DPM) (■); SRM 1649 (UD) (□). Error bars represent one standard deviation from the mean value (n=3). The lower graphs represent time course for percentage of viable cells in each particle suspension to viable cells in PBS.

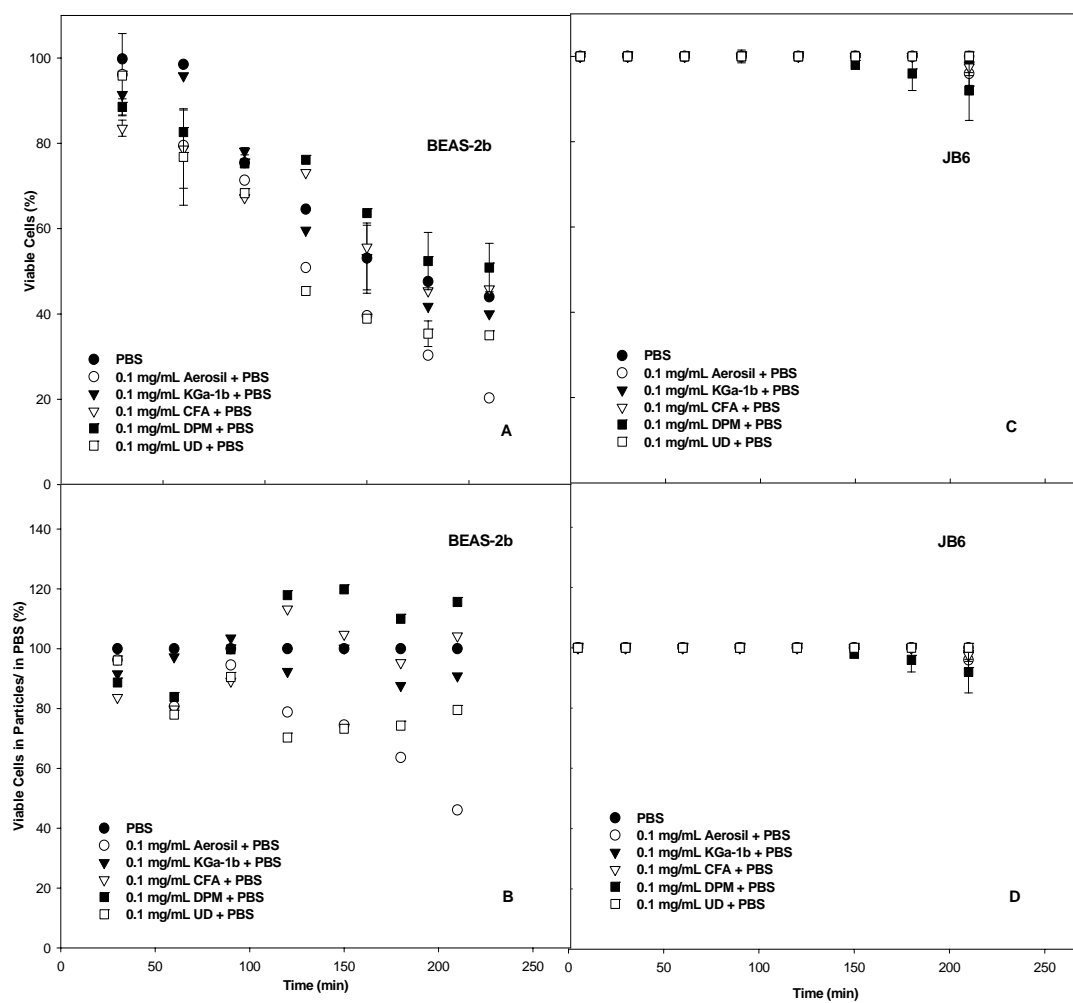


Figure 3-4. Time course for viability of BEAS-2b and JB6 cells in PBS (●); in PBS and suspension of **0.1 mg/mL** Aerosil (○); KGa-1b (▼); SRM 2689 (CFA) (▽); SRM 2975 (DPM) (■); SRM 1649 (UD) (□). Error bars represent one standard deviation from the mean value (n=3). The lower graphs represent time course for percentage of viable cells in each particle suspension to viable cells in PBS.

3.3.2. Effect of DMSO concentration on cell viability

Since DMSO is required to react with ·OH in the reaction mixture, it was necessary to find the exact concentration of DMSO under which cells would remain viable. To establish this condition, BEAS-2b cells (2×10^6 cells/mL) were suspended in different concentrations of DMSO in PBS (Table 3-1). The percentage of viable cells in the presence of 0.05 M DMSO was same as PBS, but this percentage rapidly decreased at higher concentration of DMSO.

Based on these results and DMSO dependence (see section 3.3.4), 0.05 M DMSO and 500 μ M 3apf were selected as the optimum condition to maintain cell viability in the nitroxide studies.

Table 3-1. Viability of BEAS-2b cells in the presence of different concentration of DMSO. Error bars represent one standard deviation from the mean value (n=3).

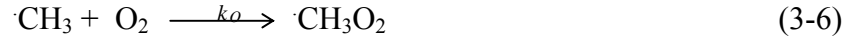
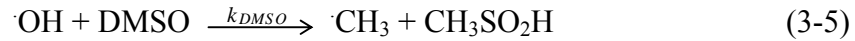
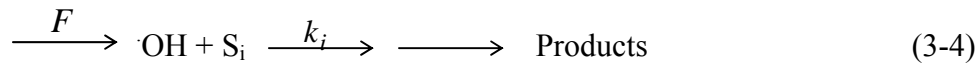
Concentration of DMSO	Time (min)	Viable Cell
PBS	120	64.5% \pm 1.4
PBS, 0.025 M DMSO	120	63.2% \pm 3.4
PBS, 0.036 M DMSO	120	64.4% \pm 4.5
PBS, 0.05 M DMSO	120	60.2% \pm 2.9
PBS, 0.1 M DMSO	120	45.3% \pm 4.8
PBS, 0.7 M DMSO	120	11.3% \pm 6.0

3.3.3. Results of bioreduction of 3apf

There is ample evidence that cells and tissues can reduce most types of nitroxides to their corresponding hydroxylamines. The rate of bioreduction varies with the structure of the nitroxide, cell permeability, and type and physiological state of the cells. In our studies, a nitroxide (3apf) was the molecular probe used to analyze the production of $\cdot\text{OH}$. Thus, it was necessary to examine the kinetics of probe bioreduction for establishing the appropriate conditions for $\cdot\text{OH}$ measurements quantitatively. Swartz and co-workers (Kocherginsky and Swartz, 1995) reported that pyrrolidinyl nitroxides have higher resistance to bioreduction than piperidinyl nitroxides because the six member ring nitroxides, (piperidines), can undergo conformational changes that make the reaction sites more approachable for reduction. As examined previously by Li et al. (Li et al. 1999b), bioreduction of 3apf, a pyrrolidinyl nitroxide, in the presence of mouse epidermal cells (JB6) had a first-order decay kinetics at higher cell densities, and exhibited very slow reduction at cell densities between $2 - 4.5 \times 10^6$ cells/mL. To work with lung epithelial cells (BEAS-2b), we examined the bioreduction of 3apf to find the best cell density to measure $\cdot\text{OH}$ quantitatively. The nitroxide 3apf, showed a faster bioreduction with BEAS-2b comparing to JB6 cells. The appropriate cell density used in these experiments was 2.0×10^6 cells/mL, in which only $\sim 10\%$ of 3apf was lost over the course of 3.5 hours (Figure 3-1).

3.3.4. Dependence of Me-3apf and $\cdot\text{OH}$ production on DMSO and 3apf concentration

To establish the condition for determining hydroxyl radical quantitatively, the dependence of formation rate of Me-3apf on the concentration of DMSO and 3apf was first examined. Hydroxyl radical competitively reacts with DMSO and other solution constituents (S_i ; Rxns. 3-4 and 3-5). Methyl radical, also, will react with oxygen in competition with its reaction with 3apf (Rxns. 3-6 and 3-7).



At steady-state condition, equation (3-8) shows the initial rate of $\text{CH}_3\text{-3apf}$ formation:

$$R = \left(\frac{d[\text{CH}_3\text{-3apf}]}{dt} \right) = \frac{F \cdot k_N [\text{3apf}] k_{\text{DMSO}} [\text{DMSO}]}{(K_O[\text{O}_2] + k_N[\text{3apf}]) \left(\sum_i k_i[\text{S}_i] + k_{\text{DMSO}}[\text{DMSO}] \right)} \quad (3-8)$$

To determine the concentration of DMSO needed for quantitative analysis of hydroxyl radical, the concentration of 3apf and O_2 were held constant and the dependence of rate of $\text{CH}_3\text{-3apf}$ on DMSO concentration (R) was obtained (Figure 3-

5). Under these conditions, equation (3-8) can be considered as a hyperbolic dependence R on [DMSO] (equation 3-9),

$$R = \frac{k_{DMSO} [DMSO] \cdot C \cdot F}{\sum_i k_i [S_i] + k_{DMSO} [DMSO]} \quad (3-9)$$

where $C = [k_N[3apf]/(k_N[3apf] + k_O[O_2])]$ is a constant (Vaughan and Blough, 1998; Li et al. 2000; Li et al. 1997; Li et al. 1999a Li et al. 1999b). This equation predicts a hyperbolic dependence of R on [DMSO]. It means that at sufficiently high [DMSO] such that $k_{DMSO} [DMSO] \gg \sum k_i [S_i]$, the formation rate of Me-3apf was independent of [DMSO], and quantitative reaction will be achieved.

Figures 3-5-A and 3-5-B show the formation rate of Me-3apf versus DMSO concentrations. In the presence of JB6, the difference between CH₃-3apf formation rate at 50 mM DMSO and its saturation rate was 53.2%. For BEAS-2b cells, this difference was 52.5%. Here, we used a correction factor to report exact ·OH concentration in a condition which is independent of DMSO concentration.

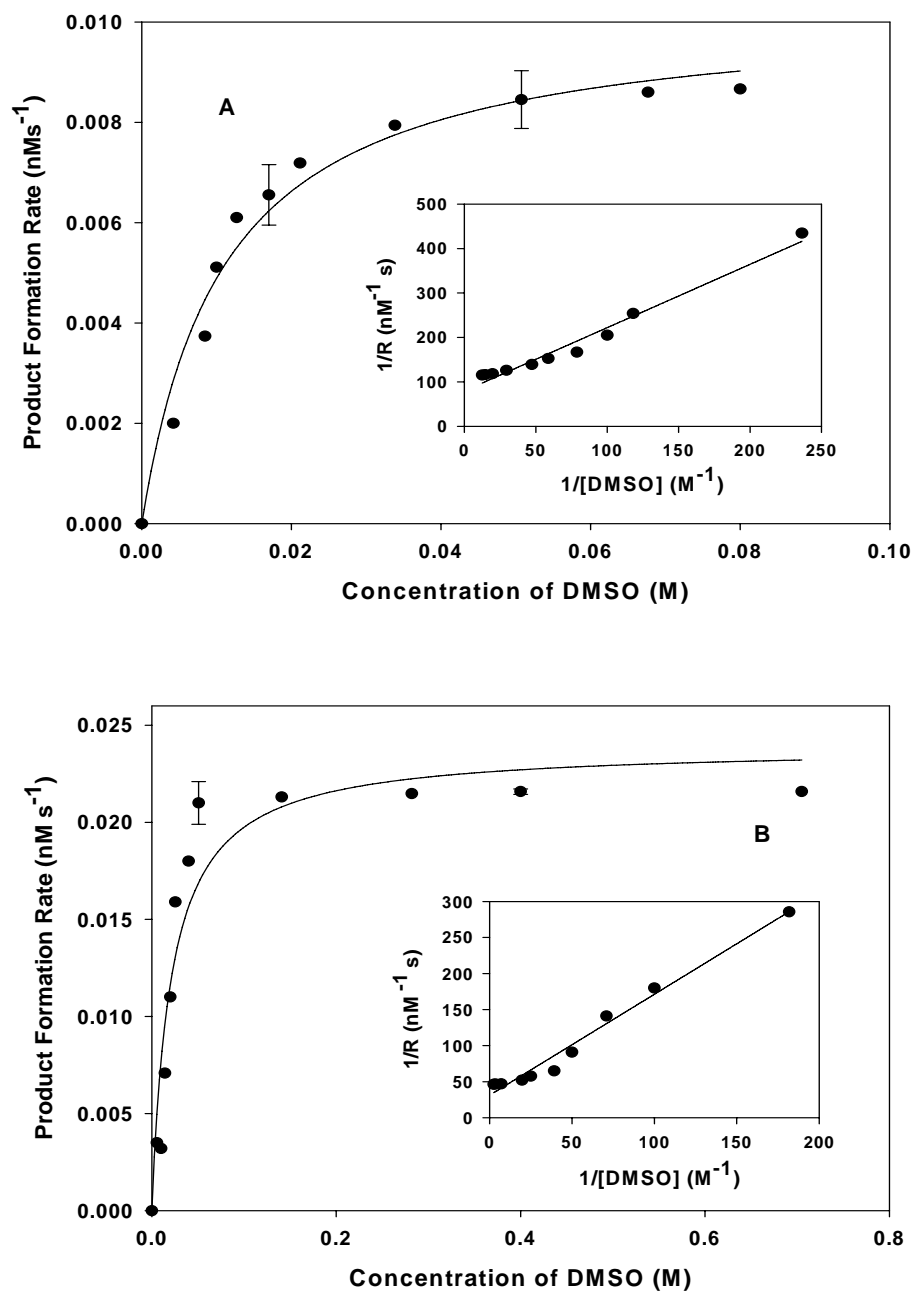
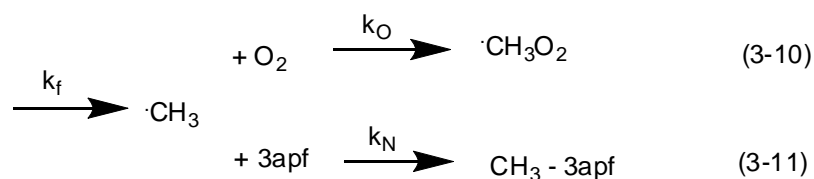


Figure 3-5. Dependence of the product formation rate on DMSO concentration in the reaction mixture containing 1 mg/ml SRM 1649 (UD) and 500 μ M 3apf in the presence of 2×10^6 cells/mL **BEAS-2b** (A) and **JB6** (B) reacting over two hours. Inset is the linearized form of the data. Error bars represent one standard deviation from the mean value (n=3).

The dependence of the formation rate of Me-3apf on the concentration of 3apf was then determined to define the condition that are appropriate for quantifying the formation of methyl radical and consequently hydroxyl radical. Since dioxygen competes with 3apf for methyl radical, it is necessary to define the condition that provides quantitative measurement of methyl radical.



If DMSO concentration is sufficient, the initial rate of product Me-3apf formation at steady state is given by the expression

$$R = \left(\frac{d[\text{CH}_3-3\text{apf}]}{dt} \right) = \frac{k_f k_N [3\text{apf}]}{k_O [\text{O}_2] + k_N [3\text{apf}]} = \frac{k_f [3\text{apf}]}{k_f S + [3\text{apf}]} \quad (3-12)$$

where k_f is the $\cdot\text{OH}$ formation rate and $S = (k_O [\text{O}_2]) / (k_f k_N)$. k_f and $k_f S$ were obtained from a nonlinear least-square fit to hyperbolic curve (Figure 3-6). Assuming an $[\text{O}_2] = 250 \mu\text{M}$, k_f and $k_f S$ from Figure 3-6 can be substituted into above equation to calculate k_O/k_N , which are the rate constant for the reaction of the methyl radical with O_2 and 3ap, respectively. This value, 4.4 ± 0.4 , 3.8 ± 0.5 , 3.6 ± 0.4 obtained from BEAS-2b, JB6 cells suspensions and absence of the cells respectively, is in a reasonable agreement with the result reported previously (Li et al. 1999b; Kumagai et al. 1997). Since this experiment indicates that O_2 is the only major competitor for

methyl radical, a rearranged form of eq. 3-12, eq. 3-13 should be used to calculate k_f under conditions in which methyl radical and 3apf don't react quantitatively.

$$k_f = R \left(1 + \frac{k_{ol}[O_2]}{k_N[3apf]} \right) = R \left(1 + \frac{k_f S}{[3apf]} \right) \quad (3-13)$$

In both cases of BEAS-2b and JB6 cells, 500 μ M 3apf was used. k_f is defined as $k_f = (3.2 \pm (0.20))R$ and $k_f = (2.9 \pm (0.36))R$, respectively. Based on these results, Me-3apf concentration in aerated samples was converted to integrated \cdot OH formation through multiplication by a factor of 3.2 ± 0.20 and 2.9 ± 0.36 for 500 μ M 3apf (Vaughan and Blough, 1998; Li et al. 2000; Li et al. 1997; Li et al. 1999a Li et al. 1999b) in the presence of BEAS-2b and JB6 cells, respectively. This concentration was employed in all subsequent analyses.

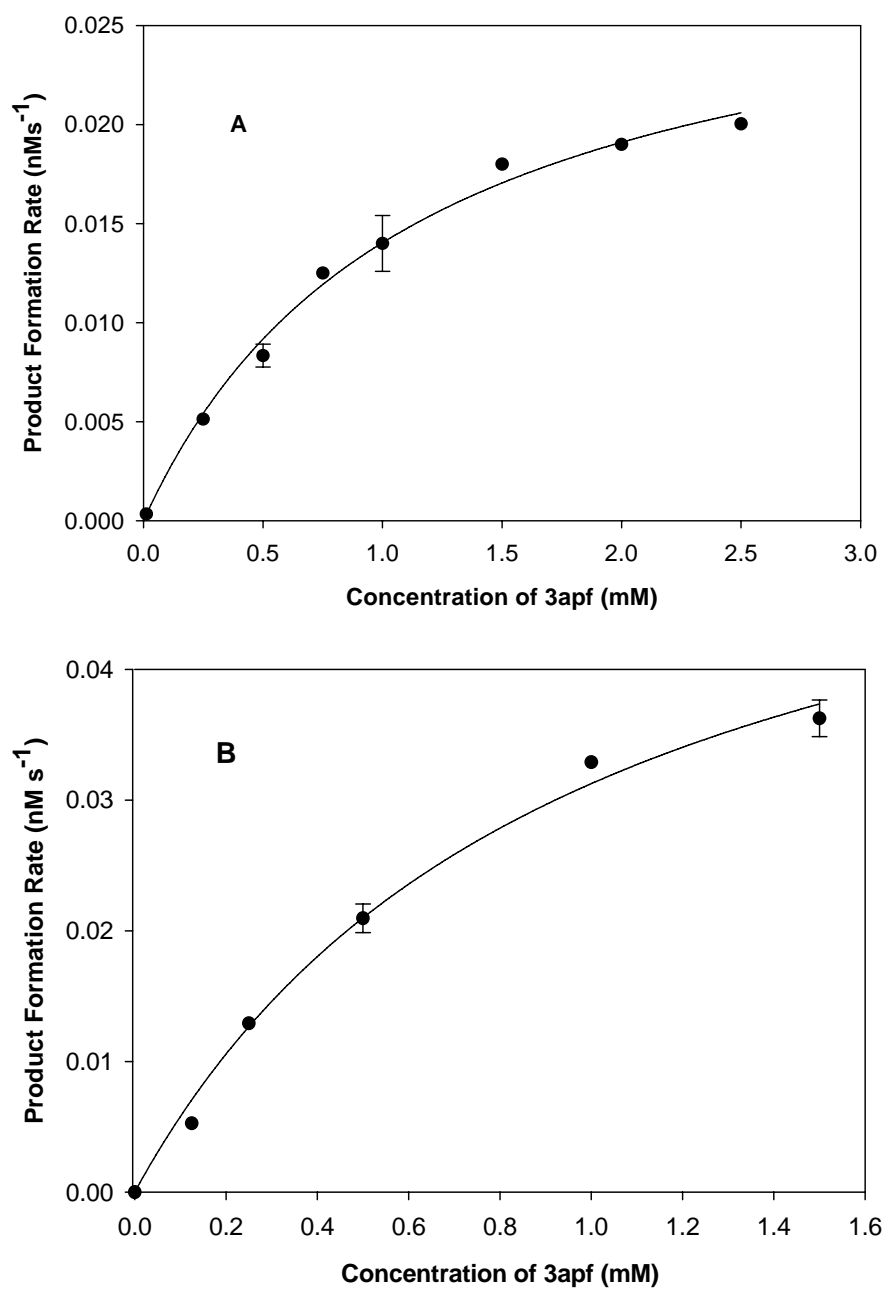


Figure 3-6. Dependence of Me-3apf formation on the concentration of 3apf in the standard reaction mixture containing 1 mg/ml SRM 1649 (UD), 0.05 M DMSO 500 μ M 3apf and 2×10^6 cells/mL of **BEAS-2b** (A) and **JB6** (B) reacting over two hours. Error bars represent one standard deviation from the mean value (n=3).

3.3.5. Determination of hydroxyl radical production

As determined from the formation of Me-3apf (see Scheme 3-1), hydroxyl radical production was not detected in the suspension of either BEAS-2b or JB6 cells over the course of 3.5 hours when the airborne particles were not present. However, addition of 1 mg/mL UD to either BEAS-2b or JB6 cells suspension produced a measurable level of $\cdot\text{OH}$ (Table 3-2; Figure 3-7). The $\cdot\text{OH}$ generation was increased linearly over the course of 3.5 hours in which 100% of these cell lines were viable. The rate of $\cdot\text{OH}$ production for JB6 was approximately two times higher than that of BEAS-2b cells. On the other hand, UD produced only very low level of $\cdot\text{OH}$ in the absence of these cell lines over the first 90 min and almost none thereafter (Figure 3-7). These results suggest that $\cdot\text{OH}$ is generated by urban dust in the presence of cells.

Table 3-2. Rates* of ·OH formation by different particles in the presence of BEAS-2b and JB6 cells.

Particles Type & Concentration (mg/mL)	Particles** (No Cells)	Rate of ·OH formation (nM s ⁻¹) x10 ³	
		BEAS-2b (2x10 ⁶ Cells/mL)	JB6 (2x10 ⁶ Cells/mL)
Diesel Particulate Matter (SRM 2975), 0.1	0*	6.8 ± 0.4	8.5 ± 0.2
Diesel Particulate Matter (SRM 2975), 1.0	0*	10.6 ± 0.2	16.0 ± 0.4
Urban Dust (SRM 1649), 0.5	6.5 ± 3.0	9.7 ± 0.4	21.2 ± 0.6
Urban Dust (SRM 1649), 1.0	15.4 ± 2.1	19.4 ± 0.6	40.7 ± 0.4
Urban Dust (SRM 1649), 2.0	29.1 ± 0.6	31.7 ± 1.7	72.8 ± 0.4
Coal Fly Ash (SRM 2689), 0.1	0*	0*	0*
Coal Fly Ash (SRM 2689), 1.0	0*	0*	0*
Kaolinite (KGa-1b), 0.1	0*	0*	0*
Kaolinite (KGa-1b), 1.0	0*	0*	0*
Silica(Aerosil), 0.1	0*	0*	0*
Silica(Aerosil), 1.0	0*	0*	0*

* is $\leq 3 \times 10^{-3}$ nM s⁻¹ which is equal or below detection limit.

** The rates were obtained prior to 90 minutes. ·OH formation was leveled off after 90 minutes.

♣ Rates of ·OH formation were obtained from the slope of plots of integrated ·OH formation versus time over the first 90 minutes (minimally 3 time points)

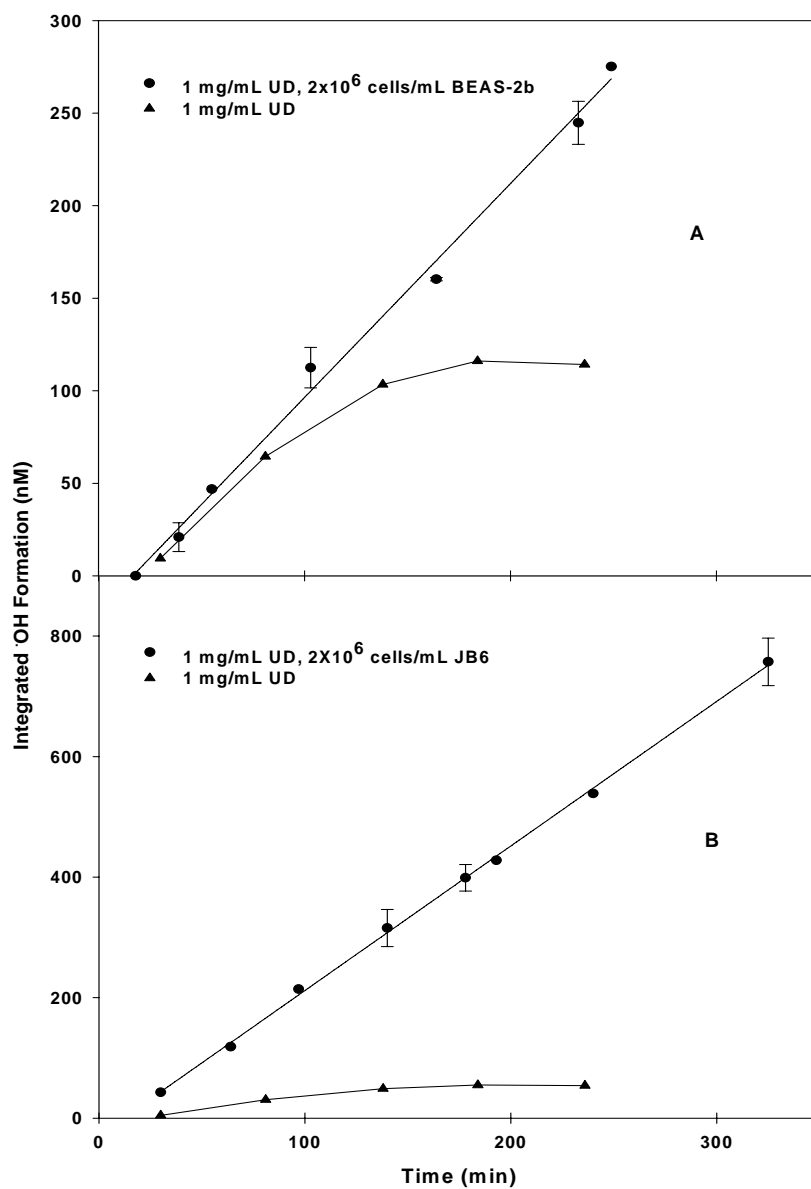


Figure 3-7. Time course for formation of $\cdot\text{OH}$ in suspension **BEAS-2b** (A) or **JB6** (B) cells treated with 1 mg/mL SRM 1649 (UD); in reaction mixture. The reaction mixture contained 0.05 M DMSO, 500 μM 3apf, particles and 2×10^6 BEAS-2b or JB6 cells/mL in 6.7 mM phosphate buffer pH 7.4. (\blacktriangle) represents blank including 1 mg/mL UD. Blank included just cells barely stand at detection limit (~ 9 nM). Error bars represent one standard deviation from the mean value ($n=3$).

At 1 mg/mL UD, $\cdot\text{OH}$ production rates increased linearly with increase in cell density for both BEAS-2b and JB6 cells (Figure 3-8). The $\cdot\text{OH}$ formation also was linear with different concentrations of Urban Dust when 2.0×10^6 cells/mL of both cell lines were present (Figure 3-9). The formation rates in the presence of 0.5, 1 and 2 mg/mL UD in the presence of either BEAS-2b or JB6 cells were reported in Table 3-2. Some hydroxyl radical production was observed in the presence of UD and BEAS-2b or JB6 cells over the course of 5.5 hours, but no cell death was observed during this period because short time exposure to urban dust stabilizes the cells. Figure 3-10 shows that cell death is independent of $\cdot\text{OH}$ formation rate over short time exposure.

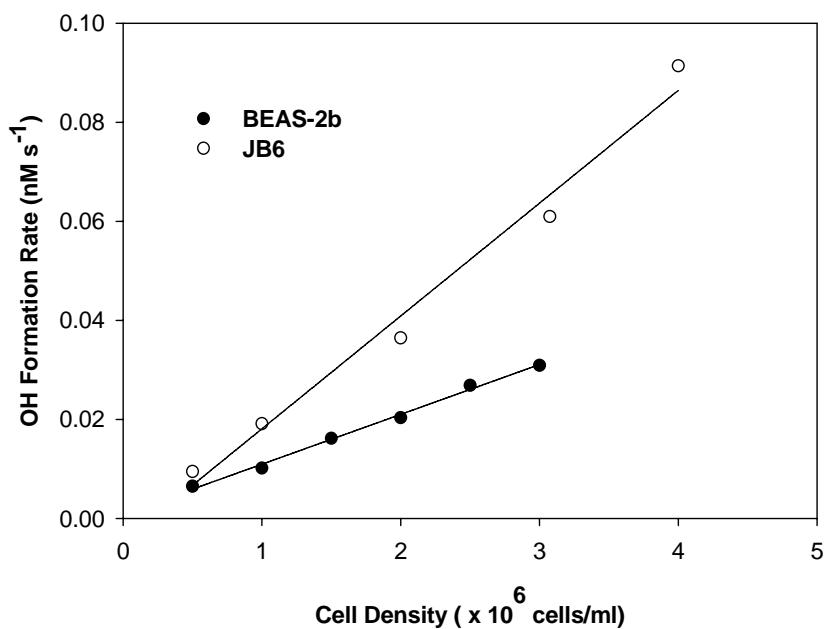


Figure 3-8. Dependence of $\cdot\text{OH}$ formation rates on cell density. The reaction mixture contained BEAS-2b or JB6 cells suspended in PBS, 1 mg/ml SRM 1649 (UD), 500 μM 3apf and 0.05 M DMSO.

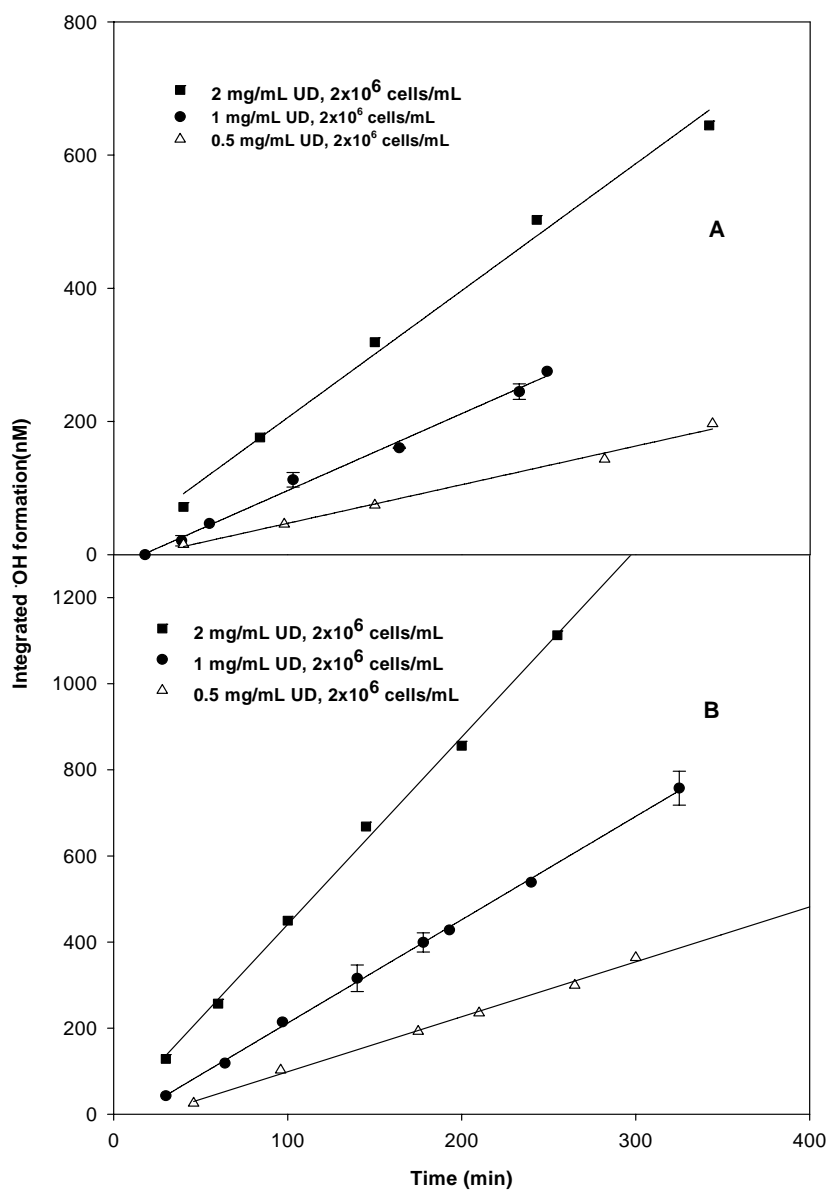


Figure 3-9. Time course for formation OH in suspension **BEAS-2b** (A) or **JB6** (B) cells treated with 0.5, 1, 2 mg/ml SRM 1649 (UD); in reaction mixture. The reaction mixture contained 0.05 M DMSO, 500 μ M 3apf, particles and 2×10^6 BEAS-2b or JB6 cells/ml in 6.7 mM phosphate buffer pH 7.4. Error bars represent one standard deviation from the mean value (n=3).

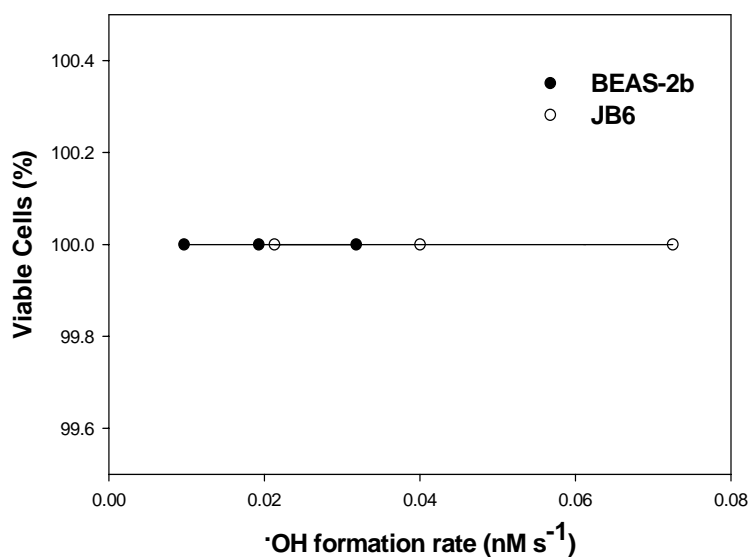


Figure 3-10. Dependence of cell viability on $\cdot\text{OH}$ formation rate generated with urban dust at different concentrations.

Exposing to either JB6 or BEAS-2b cells, 0.1 mg/mL DPM increased $\cdot\text{OH}$ formation linearly over the course of 3.5 hours. In this condition, the $\cdot\text{OH}$ production rate in the presence of BEAS-2b and JB6 was 6.8 ± 0.4 , 8.5 ± 0.2 , respectively, whereas, in the absence of cell lines $\cdot\text{OH}$ production was not observed (Table 3-2; Figure 3-10). The production of $\cdot\text{OH}$ did not increase linearly with increase in DPM concentration (Table 3-2) because 1 mg/mL of this particle cause 70% cell death for both BEAS-2b and JB6 over the course of 3.5 hours.

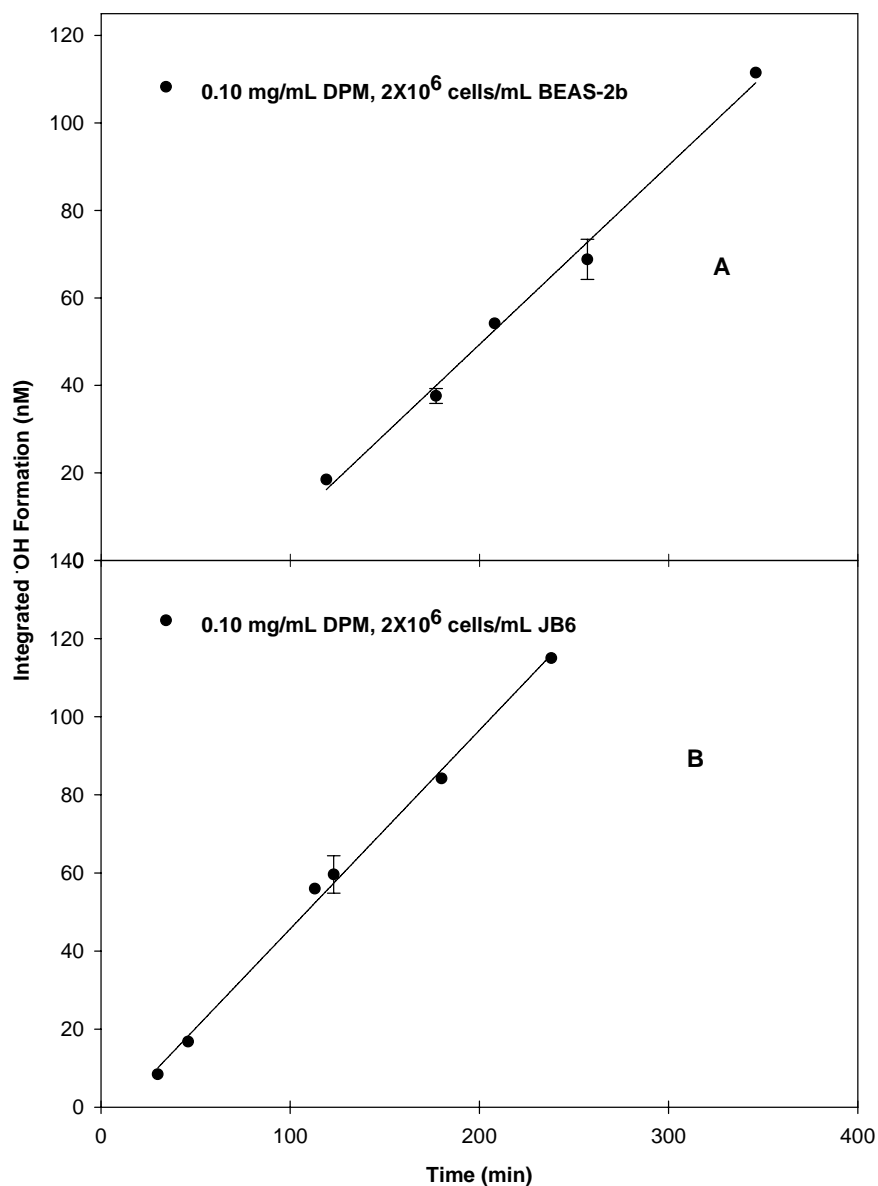


Figure 3-11. Time course for formation OH in suspension of **BEAS-2b** (A) or **JB6** (B) cells treated with 0.1 mg/mL SRM 2975 (DPM); in reaction mixture. Reaction mixture contained 0.05 M DMSO, 500 μ M 3apf, particles and 2×10^6 BEAS-2b or JB6 cells/mL in 6.7 mM phosphate buffer pH 7.4. Blanks included just cells or particles barely stand at detection limit (~ 9 nM). Error bars represent one standard deviation from the mean value (n=3).

In the presence of 0.1 or 1 mg/mL of CFA, Kaolinite and Aerosil, little or no $\cdot\text{OH}$, was produced by the BEAS-2b or JB6 cells (Table 3-2). Although Aerosil did not produce any $\cdot\text{OH}$, it was the most toxic particles and killed BEAS-2b cells very quickly (Figure 3-3, 3-4).

Our studies show that Aerosil, kaolinite and Coal Fly Ash did not generate $\cdot\text{OH}$. Some studies have shown that inhalation of these particles results in adverse health effect. The possible mechanism behind such effects can be explained by overloading the lung with poorly soluble particles, which results in less alveolar clearance and more chronic inflammation.

3.3.5. Cell Viability and $\cdot\text{OH}$ production in the presence of external biological reductant

Adding 1 mM of the biological reductant, NADPH, after 90 minutes exposure of 2×10^6 cells/mL BEAS-2b and JB6 to 1 mg/mL urban dust, dramatically enhanced production of $\cdot\text{OH}$ (Figure 3-11). In the presence of 1 mM NADPH, the rate of $\cdot\text{OH}$ production for BEAS-2b cells was 78 ± 1.2 and for JB6 cells was 95 ± 0.8 . This high flux of hydroxyl radical production correlated with an increase of cell death (Figure 3-12-A, B). Furthermore, adding 0.1 M DMSO, as a radical scavenger, protected the cells from death (Figure 3-12-A, B). Therefore, in the presence of an added reductant, the particles can produce $\cdot\text{OH}$ at a sufficient rate to kill the cells.

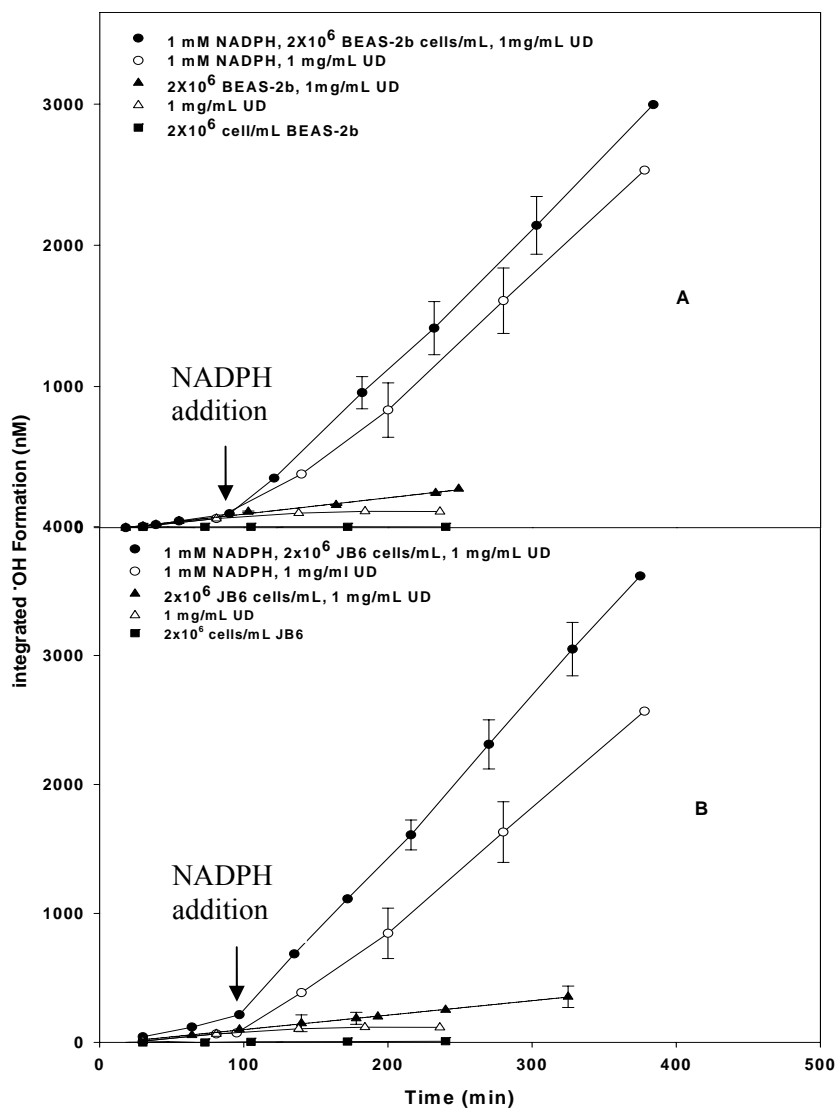


Figure 3-12. Time course for $\cdot\text{OH}$ formation in a cell suspension **BEAS-2b** (A) or **JB6** (B) containing 1 mg/mL SRM 1649 (UD) in the absence and presence of 1 mM NADPH in reaction mixture. Reaction mixture contained 0.05 M DMSO, 500 μM 3apf, particles and 2×10^6 cells/mL BEAS-2b or JB6 cells/mL in 6.7 mM phosphate buffer pH 7.4. Error bars represent one standard deviation from the mean value ($n=3$).

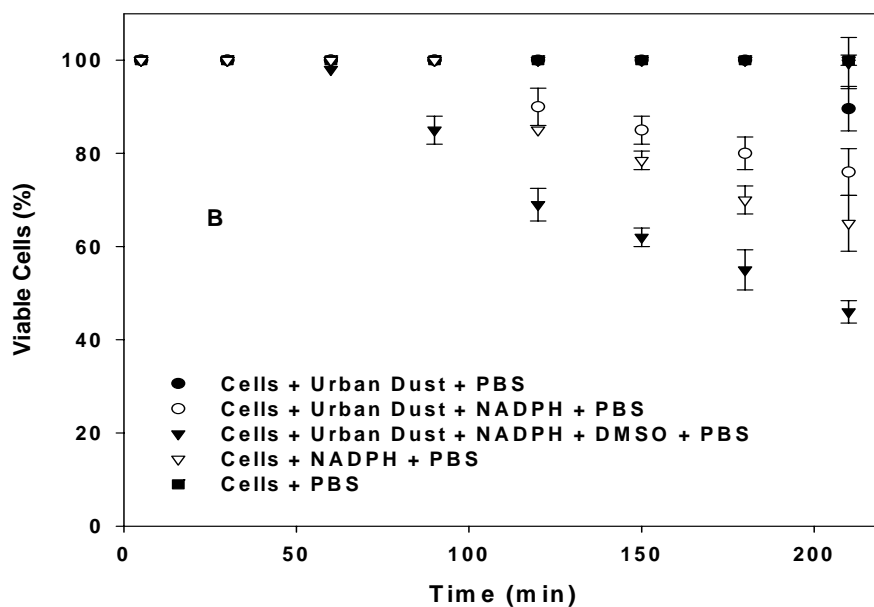
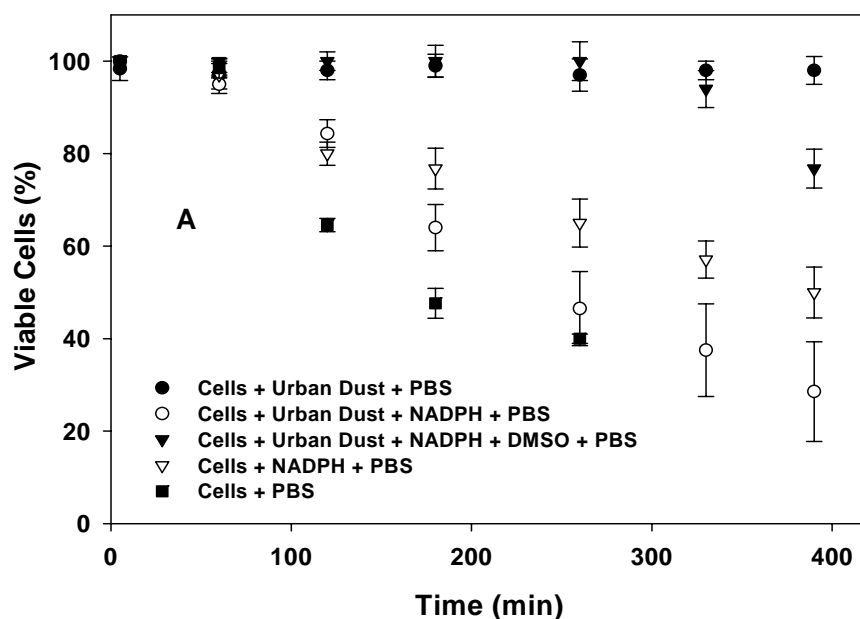


Figure 3-13. Time course for viability of **BEAS-2b** (A) or **JB6** (B) cells in PBS and 1 mg/mL SRM 1649 (UD) (●); PBS, 1 mg/mL SRM 1649 (UD) and 1 mM NADPH (○); added 0.1 mM DMSO (▼); PBS and 1 mM NADPH (▽); PBS (■). Error bars represent one standard deviation from the mean value (n=3). (at 100% viable cells, symbols ●, ▼ and ■ are overlapped.)

3.4. Discussion

According to the results obtained by method I and II (toxicological experiments), urban dust did not cause cell death for BEAS-2b and JB6 cells while $\cdot\text{OH}$ was generating at a very slow rate. In method I, BEAS-2b was proliferated when the concentration of urban dust increased from 0.015 to 0.07 mg/mL. At higher concentration of urban dust (more than 0.07 mg/mL), the viability of BEAS-2b cells decreased. The possible explanation for this proliferation effect is presence of substance that supports growth or low level of H_2O_2 (Doroshov 2006).

In method II, both BEAS-2b and JB6 cells were 100% viable over the course of 3.5 hours when the cells were exposed to 1 mg/mL of UD. On the other hand, in method I, most of the BEAS-2b cells were killed by exposing to 1 mg/mL UD. Here, there is a difference in the rate of cell death between two toxicological experiments. The cell death is faster when the cells were kept in media for long term (method I) comparing to PBS for short term (method II) because higher $\cdot\text{OH}$ can possibly be produced. Adding external biological reductant also accelerated $\cdot\text{OH}$ generation and cell death, thus showing that high rates of $\cdot\text{OH}$ generation, when present, can cause cell death.

The toxicological experiments also showed that DPM was very toxic to these cells. However, little or no $\cdot\text{OH}$ was detected in the presence of cells exposed to high concentration of DPM was detected, but using low concentration of DPM produced a little $\cdot\text{OH}$ generation. On the other hand, Kaolinite and Coal Fly Ash, which contained very low concentration of organic compounds or transition metals, produced little or no $\cdot\text{OH}$ generation in the presence of cells.

A number of studies have investigated the relationship of pulmonary silica burden and silicosis (Mossman et al. 1998). Some the studies claimed that $\cdot\text{OH}$ is the cause of tissue damage associated with silicosis (Vallyathan et al. 1988; Dalal et al. 1990; Ding et al. 2001). These studies have shown that only freshly fractured silica induce $\cdot\text{OH}$ generation as well as AP-1 and NF- κ B activation (Shukla et al. 2001; Kang et al. 2000). They reported that mechanical crushing of crystalline silica produce a significant concentration of silica-based radicals which react with a variety of chemical species in the atmosphere including trace amounts of water vapor to generate $\cdot\text{OH}$. In these studies, generation of $\cdot\text{OH}$ was determined with spin trapping and ESR detection. There are some shortcomings in that work. First, using ESR detection has numerous limitations and is not quantitative for $\cdot\text{OH}$ measurement (see section 1.5.1). Second, proposed mechanism for generating $\cdot\text{OH}$ by silica particle is not clear because it was assumed that freshly fractured silica provides silicon based radicals upon cleavage of silicon crystals and the silicon radicals then react with water to produce $\cdot\text{OH}$. They also reported that no $\cdot\text{OH}$ was produced in the presence of aged silica (Vallyathan et al. 1988; Dalal et al. 1990; Ding et al. 2001).

Our results show that Aerosil (pure silica) extensively caused cell death but $\cdot\text{OH}$ was not detected in this system. Therefore, the results indicate that $\cdot\text{OH}$ is not responsible for toxicity of silica and other possible mechanisms may be involved.

In conclusion, our results suggest that $\cdot\text{OH}$ production is not a primary factor producing cell death in the presence of these particles, because production rates of $\cdot\text{OH}$ is not great enough to compete with other lethal mechanism (Figure 3-12). This conclusion is supported by dramatic cell death in the presence of much higher

production of $\cdot\text{OH}$. For example, 100% of cells were viable when they were exposed to urban dust whereas cell death significantly increased when NADPH was externally added to the system. The $\cdot\text{OH}$ formation rate for the suspension of cells and urban dust was $78 - 95 \text{ nM s}^{-1}$ when NADPH was present while it was $6.8 - 9.2 \text{ nM s}^{-1}$ in the absence of added NADPH. Furthermore, adding DMSO, as a radical scavenger, to this system protected the cells from death. These results indicate that larger $\cdot\text{OH}$ production rates are necessary to cause rapid cell death. Therefore, a very low concentration of $\cdot\text{OH}$ produced by these particles does not cause lethality and cell death.

Chapter 4: Conclusion and Future Work

4.1. Conclusion

The objective of this work was to determine generated $\cdot\text{OH}$ by particulate matter (PM) with a sensitive method which was previously developed by Blough and co-workers (Blough and Simpson 1988; Li et al. 1997; Li et al. 1999a; Kieber and Blough 1990a; Kieber and Blough 1990b; Vaughan and Blough 1998; Thomas-Smith and Blough 2001; Li et al. 1999b; Petigara et al. 2002). In this work, the research was conducted to (i) determine of $\cdot\text{OH}$ produced by different PMs in the absence and presence of biological reductants (ii) investigate the mechanism(s) for hydroxyl radical generation by PMs (iii) examine on the effects of PM on viability of human lung epithelial cells (BEAS-2b) and mouse epidermal cells (JB6) and the correlation to production of hydroxyl radical in these systems.

In this research, a highly sensitive fluorescence-based method was employed to measure hydroxyl radical production by particulate matter. Some other studies have been done to detect $\cdot\text{OH}$ generated by PM (Jung et al. 2006; Briedé et al. 2005; Valavanidis et al. 2005; Antonini et al. 2004; Karlsson et al. 2005; Shi et al. 2003b; Prahalad et al. 2001), but this technique is the first quantitative technique to measure $\cdot\text{OH}$ and it is a highly sensitive and rapid method for potentially screening hydroxyl radical formation rate (R_{OH}) produced by different particles. The rate of $\cdot\text{OH}$ production for 3 mg/mL of these particles varied from 23 nM s^{-1} for diesel particulate matter (SRM 2975) to 0.20 nM s^{-1} for coal fly ash (SRM 2689) in the presence of biological reductant, NADPH. Diesel particulate matter produced the highest rate of

$\cdot\text{OH}$ formation in the presence of NADPH, and no production of $\cdot\text{OH}$ was observed for pure silica particles and very little for kaolinite while Vallyathan et al. (1988) reported generation of $\cdot\text{OH}$ by pure silica.

This technique was also employed to investigate on mechanism(s) of hydroxyl radical production from a broad spectrum of airborne particles in the absence and presence of a biological electron donor (NADPH). Our results are consistent with the redox cycling scheme (1-2) proposed by Pryor and his co-workers. Based on the results, the presence of oxygen and hydrogen peroxide are necessary factors to produce $\cdot\text{OH}$ because elimination of oxygen or hydrogen peroxide suppressed the $\cdot\text{OH}$ generation. The presence of metal ions is also another important factor in production of $\cdot\text{OH}$ by particulate matter since the $\cdot\text{OH}$ generation was suppressed in the presence of a strong metal chelator, deferoxmine. Partial inhibition of $\cdot\text{OH}$ production by superoxide dismutase indicates that superoxide is involving in the $\cdot\text{OH}$ production process.

Other studies on soluble and insoluble portions of airborne particles showed that both portions are responsible for $\cdot\text{OH}$ production. In the case of diesel particulate matter, $\cdot\text{OH}$ production was dominated by insoluble portion, but both soluble and insoluble portion of urban dust had an equal value for $\cdot\text{OH}$ generation. Therefore, both homogenous and heterogeneous reactions are responsible for $\cdot\text{OH}$ production by airborne particles. Furthermore, our results support the evidence of surface-catalyzed reaction for $\cdot\text{OH}$ production by airborne particles with observing a saturation effect at higher concentration of NADPH.

Human airway epithelial cells (BEAS-2b) and mouse epidermal cells (JB6) were used to examine the effects of airborne particles on cell survival and its relationship to $\cdot\text{OH}$ generation. The highly sensitive technique was employed to quantify $\cdot\text{OH}$ produced by these particles in the presence of BEAS-2b or JB6 cells. Based on these studies, cell death does not correlate with $\cdot\text{OH}$ production for BEAS-2b and JB6 cells exposed to airborne particles.

For example:

- 1) Aerosil produced a high rate of cell death, but $\cdot\text{OH}$ was not detected in this system.
- 2) Although there was some production of $\cdot\text{OH}$ by urban dust, BEAS-2b and JB6 cells were viable and proliferated.

On the other hand, addition of NADPH to suspension of BEAS-2b and JB6 cells containing urban dust substantially increased $\cdot\text{OH}$ production and cell death. These results show that viability of the cells was decreased dramatically in the presence of high concentration of $\cdot\text{OH}$.

In conclusion, our studies suggest that $\cdot\text{OH}$ production is not the primary factor producing cell death during the short term exposure to these particles.

4.2. Future work

This research can be continued by using different types of airborne particulate matter, cell lines and techniques to find correlation of particulate matter with health effects.

4.2.1. Seasonal and regional studies on $\cdot\text{OH}$ production by PM

Epidemiological studies have shown an association between adverse health effects and mortality with PMs collected from different sources within different timescales. Although there are a few reports on determining $\cdot\text{OH}$ generated by particles obtained from different sources, they did not employ a sensitive and quantitative technique to measure $\cdot\text{OH}$ (Baulig et al. 2004). However, our technique can be used to determine $\cdot\text{OH}$ generated by various samples collected in different locations and times. In addition, the discussion can be continued by comparing the distribution of induced health effects by different PMs, which produce various amount of $\cdot\text{OH}$.

4.2.2. Screening $\cdot\text{OH}$ production by PMs in the presence of other reductants

In our studies, a linear production of $\cdot\text{OH}$ was observed only in the presence of biological reductants such as NADPH. It is important to investigate on $\cdot\text{OH}$ production in the presence of other reductants. Humic-like substances and sulfite

which are present in airborne particles are believed to reduce quinone moieties and metal ions, respectively. Therefore, it is valuable to study on these compounds to understand the mechanism of $\cdot\text{OH}$ production by different PMs.

4.2.3. Determining $\cdot\text{OH}$ produced by PM in the presence of macrophage or other cell lines

Our results suggest that different cell lines behaved differently when they were exposed to PM. Therefore, further research is needed to determine generated $\cdot\text{OH}$ by different airborne particles in the presence of different cell lines, such as primary lung epithelial cells and macrophage. The correlation between cell death, production of hydroxyl radical and increase in cytokines and chemokines for different cell lines also need to be investigated.

4.2.4. Physicochemical analysis for diesel particles

In this area of research, some studies have been done to characterize the chemical composition of diesel particulate matter by doing fluorescence or UV-Visible analysis. This work can be continued by analyzing the physical properties (particle size) as well as chemical composition (organic and inorganic) of different diesel particles. Morphological characterization can be performed to measure particles size. To determine chemical components, the soluble portion of diesel particles will be extracted and analyzed by various identification, separation and

quantification techniques and instruments. The analysis varies from determining diesel particles' metal contents to their organic components. Therefore, the correlation between ·OH production by diesel particles and particles' chemical compositions can help to elucidate the mechanism inducing adverse health effects.

4.2.5. Protein analysis for the cell lines exposed to PM

The current research shows that exposing BEAS-2b or JB6 cells to urban dust causes a proliferation effect. It is valuable to do further research to determine the proteins that are elevated or reduced while the BEAS-2b or JB6 are exposed to urban dust particles. The possible proteins are protein kinase C (PKC) which causes proliferation and high cell density. To obtain this purpose, the protein analysis will be done by using 2-D gel electrophoresis and mass spectrometry. The protein analysis will help to understand the mechanisms by which particles induced health effects.

Appendix A: Preliminary work on SRM 2975 analysis

Diesel particulate matter, SRM 2975, was extracted in solution containing 5 mM phosphate buffer and 0.9% NaCl at pH=7.5 (PBS) within 24 hours. pH of extracted solution was then adjusted from acidic to basic. Figure A-1 to A-7 show UV-Visible and excitation-emission fluorescence spectrums for extracted diesel particulate matter at different pHs.

To characterize the extracted diesel particulate matter in PBS, the aqueous solution was extracted in chloroform (CHCl_3), after adjusting pH in both 2.7 and 12. Figures A-8 and A-9 show UV-Vis spectrums for both aqueous and organic phase before and after the extraction. Based on the results, the best extraction in chloroform was obtained with a solution at acidic pH. The extraction was also repeated by using 5 mM phosphate buffer at pH=7.5, 100 mM phosphate buffer at pH=7.5 and water (Figure A-10 to A-12) in which pH was then adjusted to 2.8 prior to extraction in chloroform. In sum, the best condition to extract diesel particulate matter in aqueous solution is a buffer with higher ionic strength. Providing acidic pH for aqueous extracted solution prior to extraction in chloroform is also necessary.

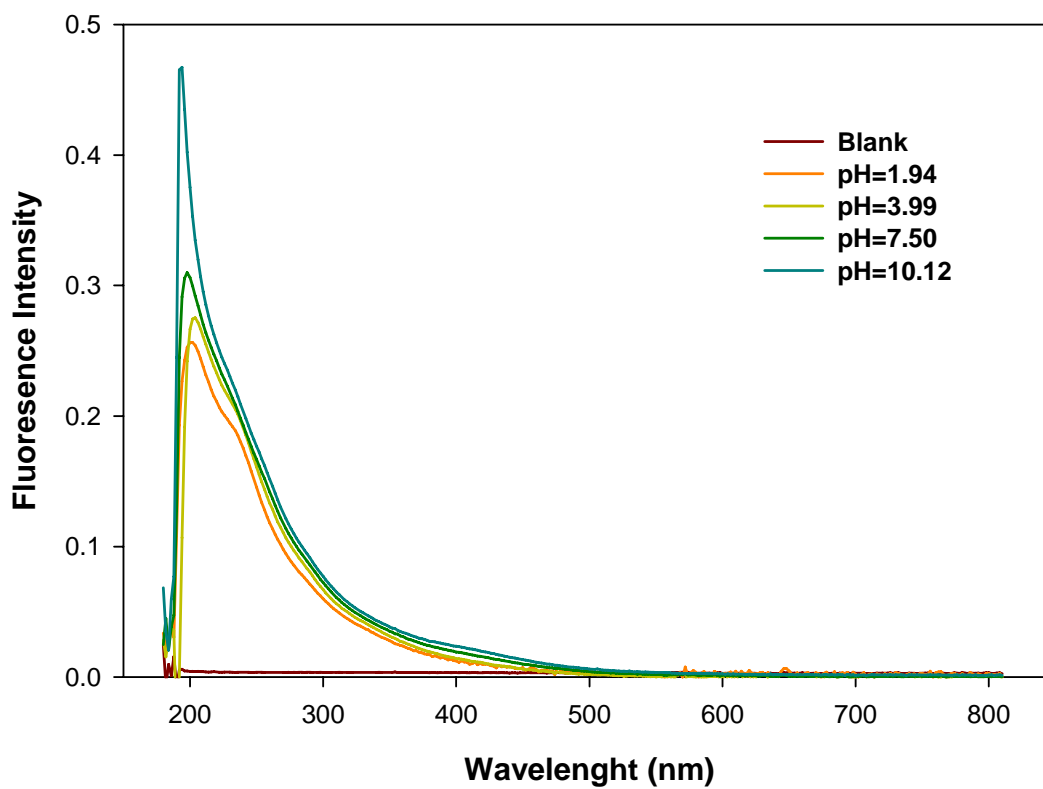


Figure A-1. UV-Visible spectrum of extracted diesel particulate matter in 5 mM phosphate buffer and 0.9% NaCl at pH 7.5 for 24 hours and then adjusting the pH to 1.94, 3.99, 7.50 and 10.12.

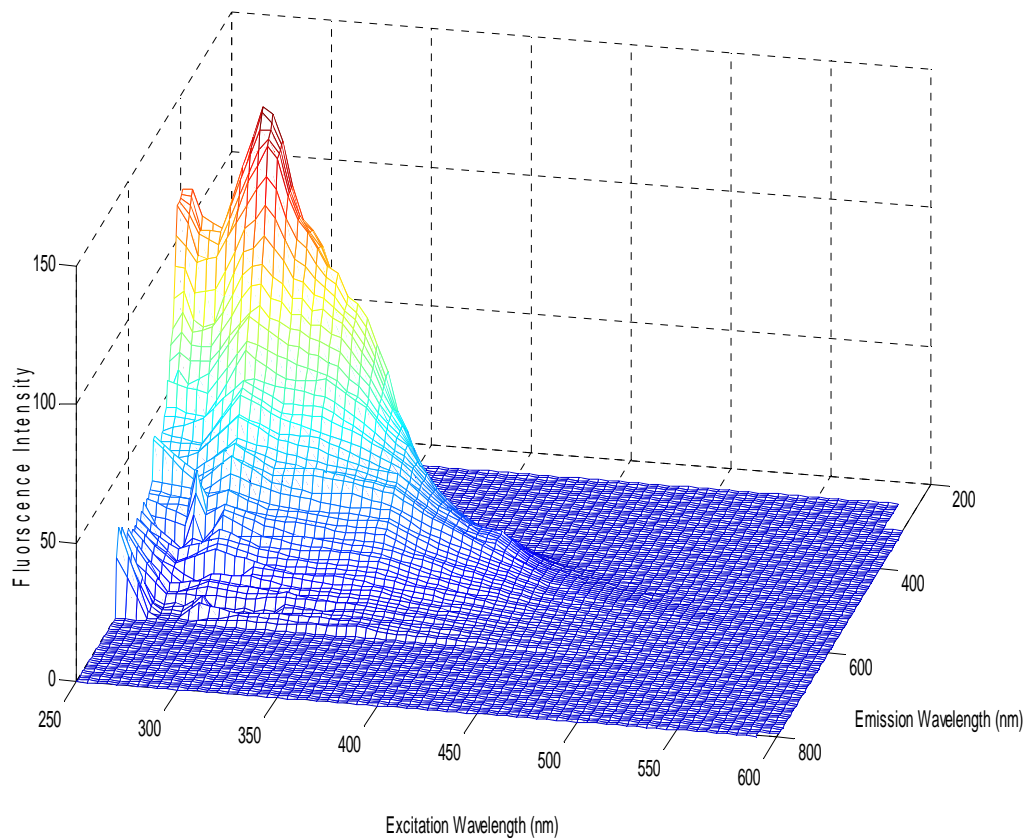


Figure A-2. 3-D fluorescence spectrum of extracted diesel particulate matter in 5 mM phosphate buffer and 0.9% NaCl at pH 7.5 for 24 hours. After the extraction the pH was adjusted to 2. Excitation is from 270 to 490 and emission is from 280 to 610. The vertical scale is emission intensity; units are arbitrary. Lines parallel to the emission axis correspond to single emission scans at different excitation wavelengths.

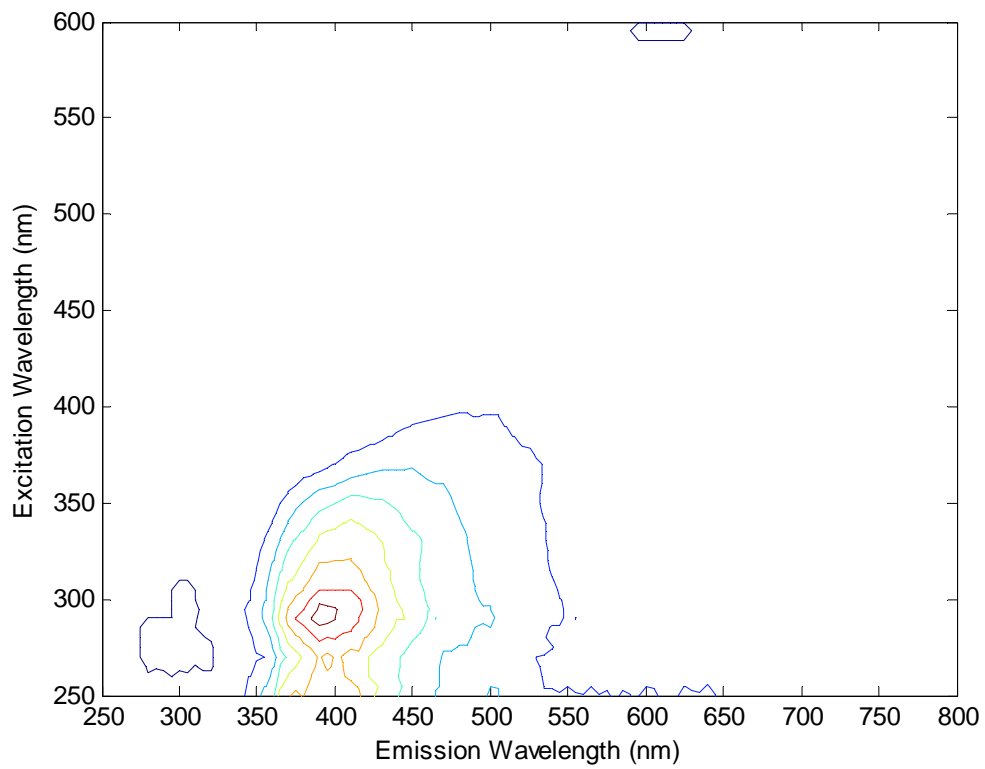


Figure A-3. Same spectrum as in previous figure, viewed in contour.

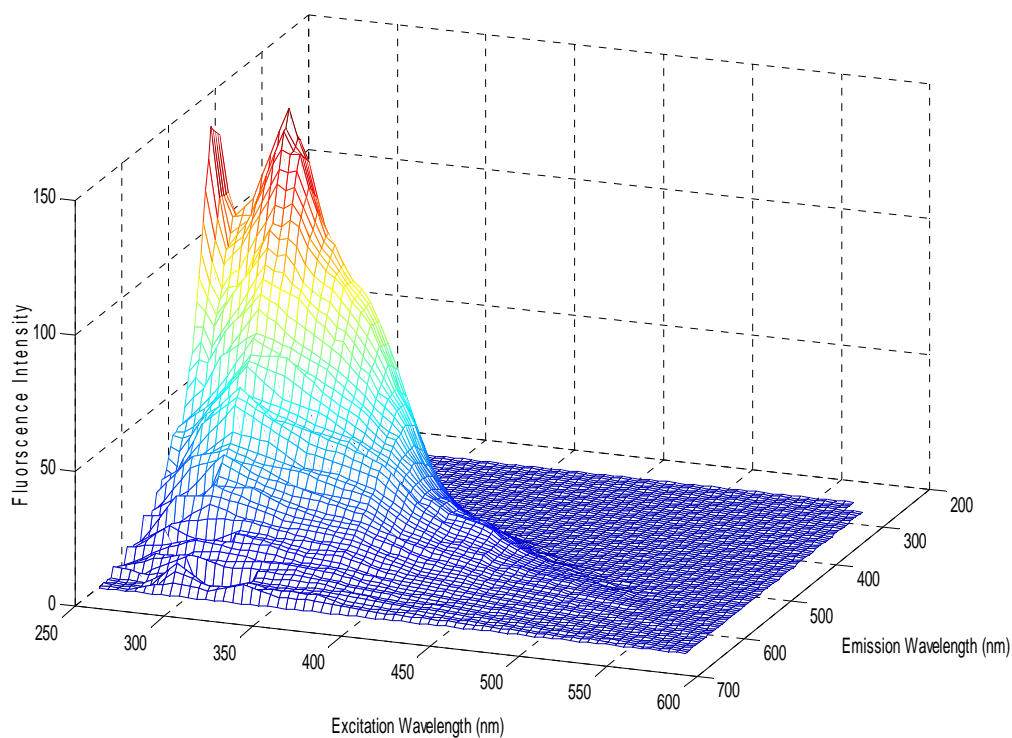


Figure A-4. 3-D fluorescence spectrum of extracted diesel particulate matter in 5 mM phosphate buffer and 0.9% NaCl at pH 7.5 for 24 hours. After the extraction pH was adjusted to 4. Excitation is from 270 to 490 and emission is from 280 to 610. The vertical scale is emission intensity; units are arbitrary. Lines parallel to the emission axis correspond to single emission scans at different excitation wavelengths.

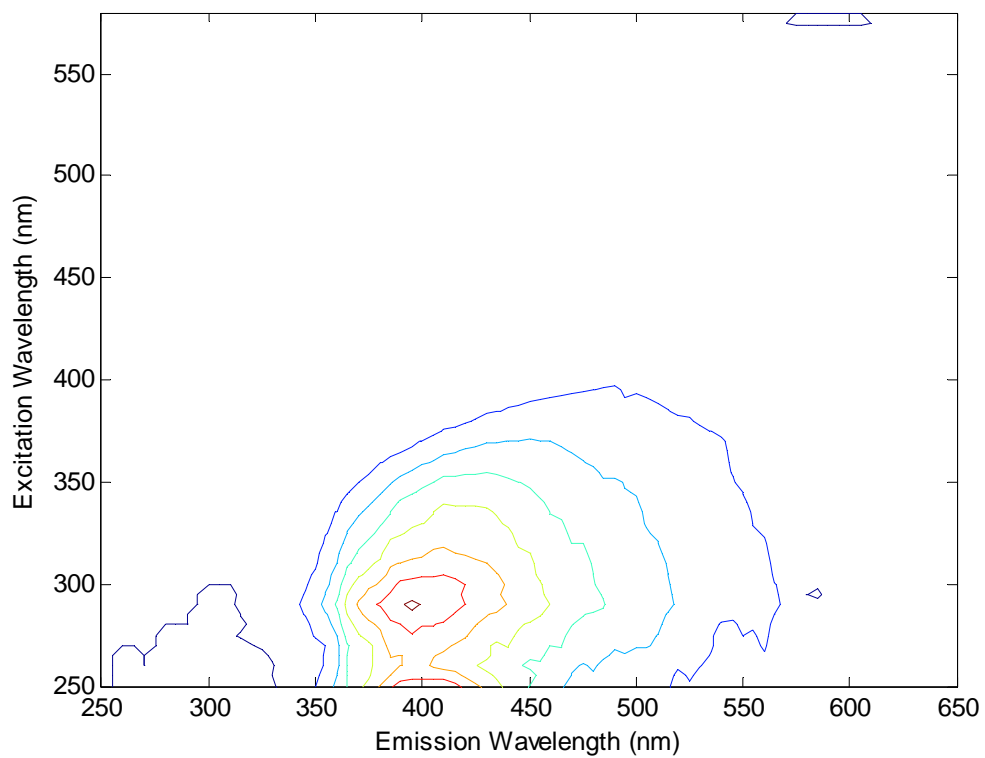


Figure A-5. Same spectrum as in previous figure, viewed in contour.

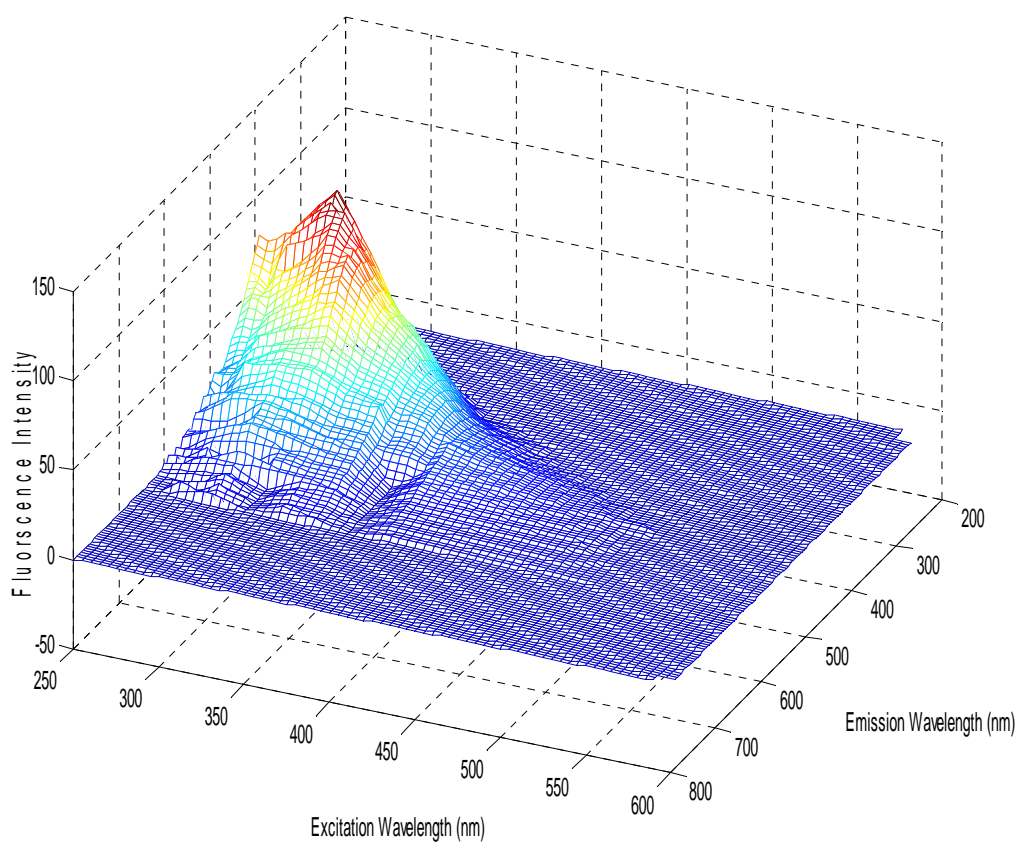


Figure A-6. 3-D fluorescence spectrum of extracted diesel particulate matter in 5 mM phosphate buffer and 0.9% NaCl at pH 7.5 for 24 hours. After the extraction pH was adjusted to 10. Excitation is from 270 to 490 and emission is from 280 to 610. The vertical scale is emission intensity; units are arbitrary. Lines parallel to the emission axis correspond to single emission scans at different excitation wavelengths.

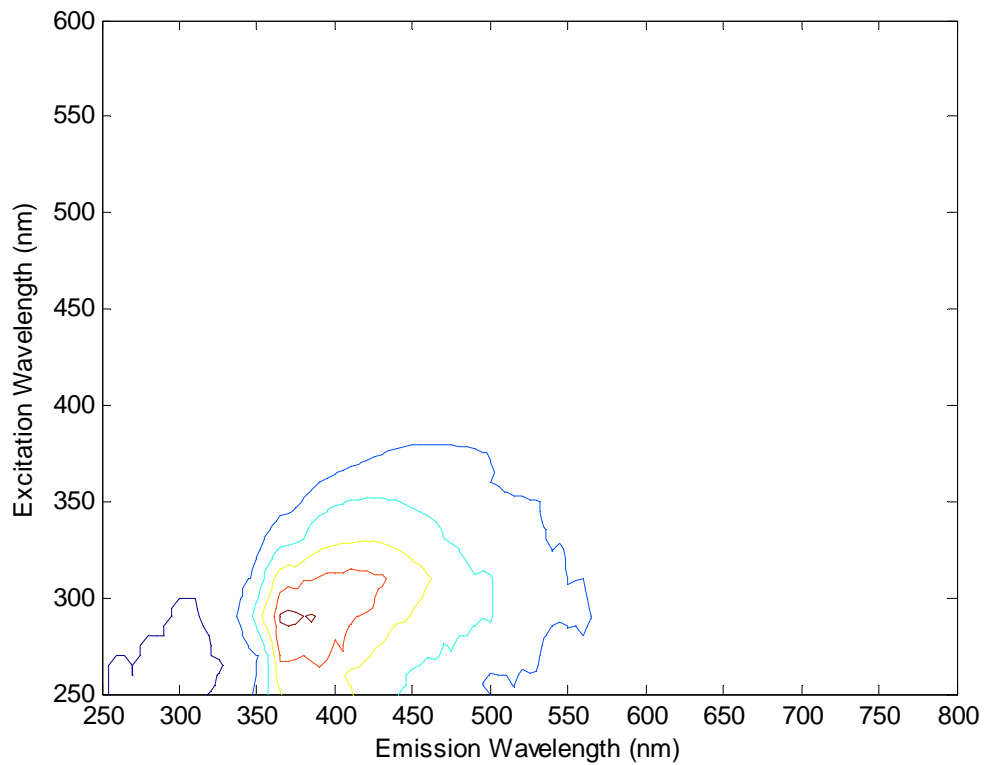


Figure A-7. Same spectrum as in previous figure, viewed in contour.

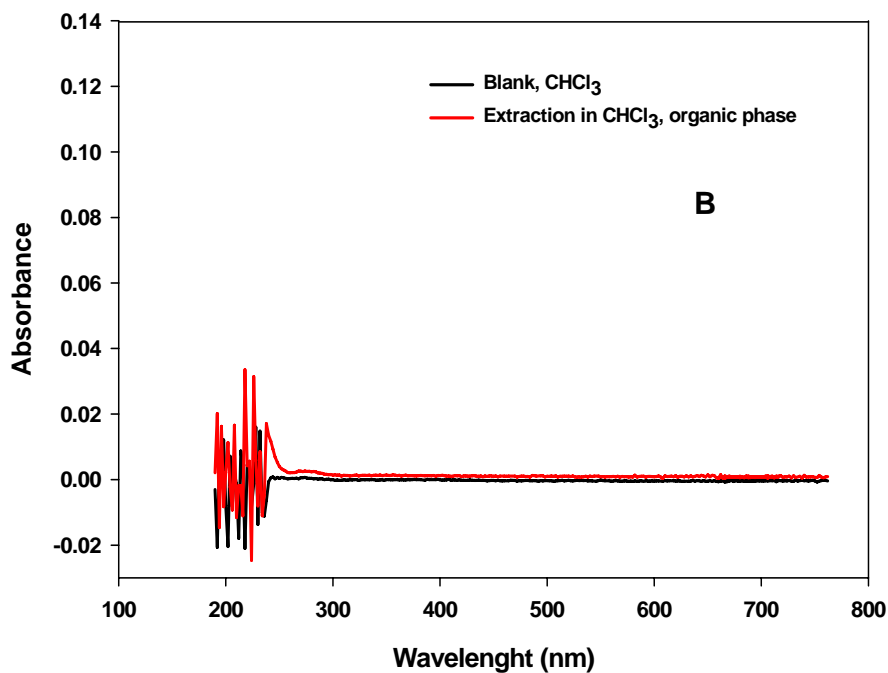
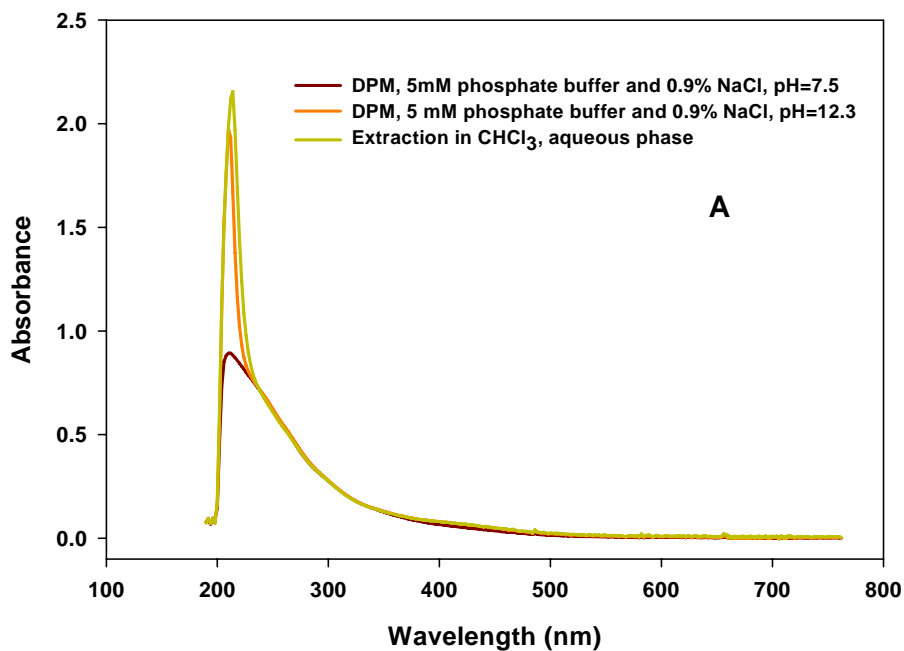


Figure A-8. (A) UV-Visible spectrum of extracted diesel particulate matter in 5 mM phosphate buffer and 0.9% NaCl at pH 7.5 for 24 hours (—); UV-Visible spectrum after the extraction and adjusting to pH=12.3 (—) and UV-Visible spectrum for aqueous phase after extraction in chloroform(—). (B) The UV-Visible spectrum for the chloroform phase after the extraction (—).

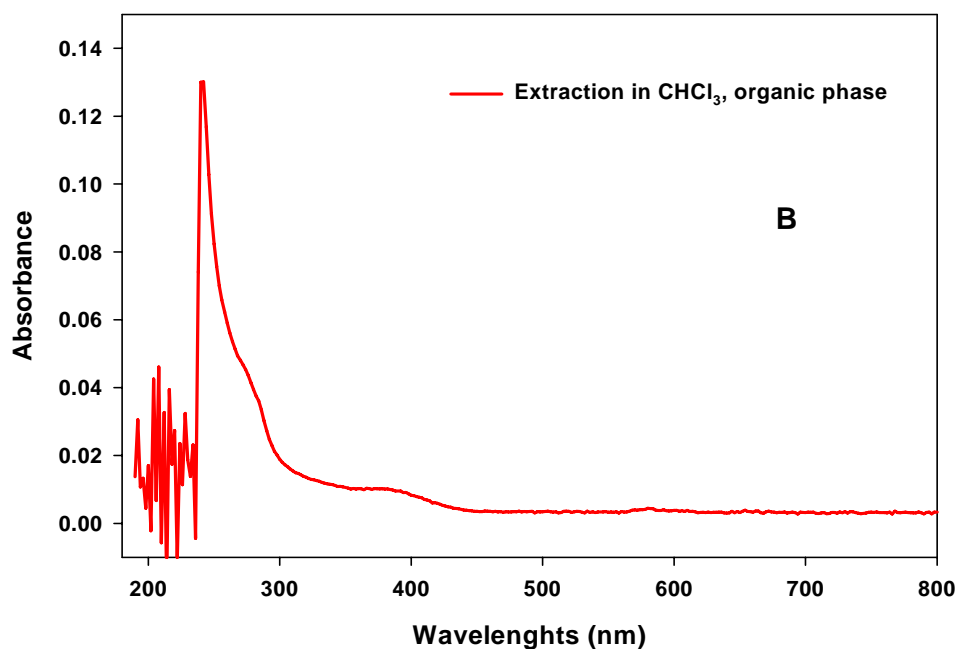
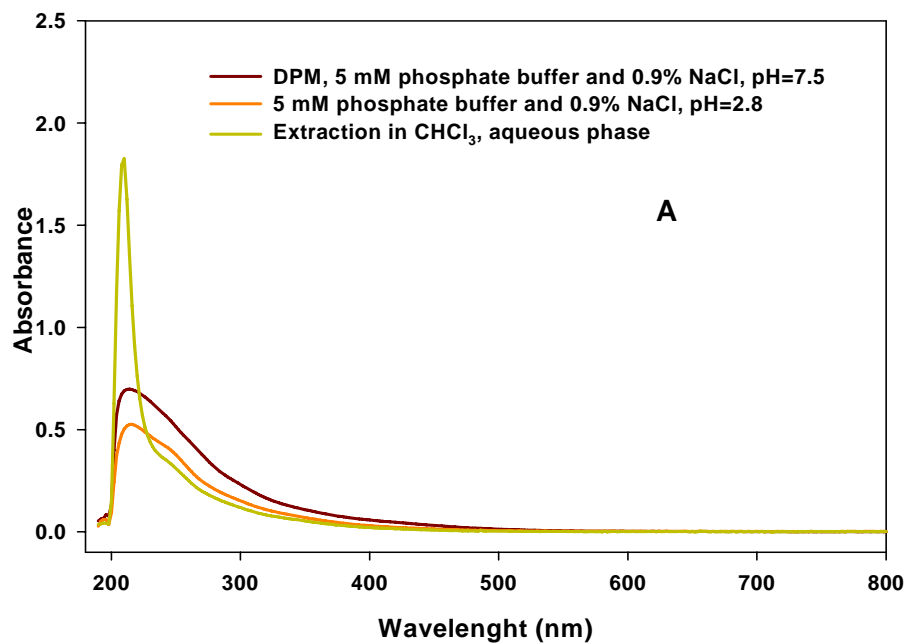


Figure A-9. (A) UV-Visible spectrum of extracted diesel particulate matter in 5 mM phosphate buffer and 0.9% NaCl at pH 7.5 for 24 hours (—); UV-Visible spectrum after the extraction and adjusting to pH=2.8 (—) and UV-Visible spectrum for aqueous phase after extraction in chloroform(—). (B) The UV-Visible spectrum for the chloroform phase after the extraction (—).

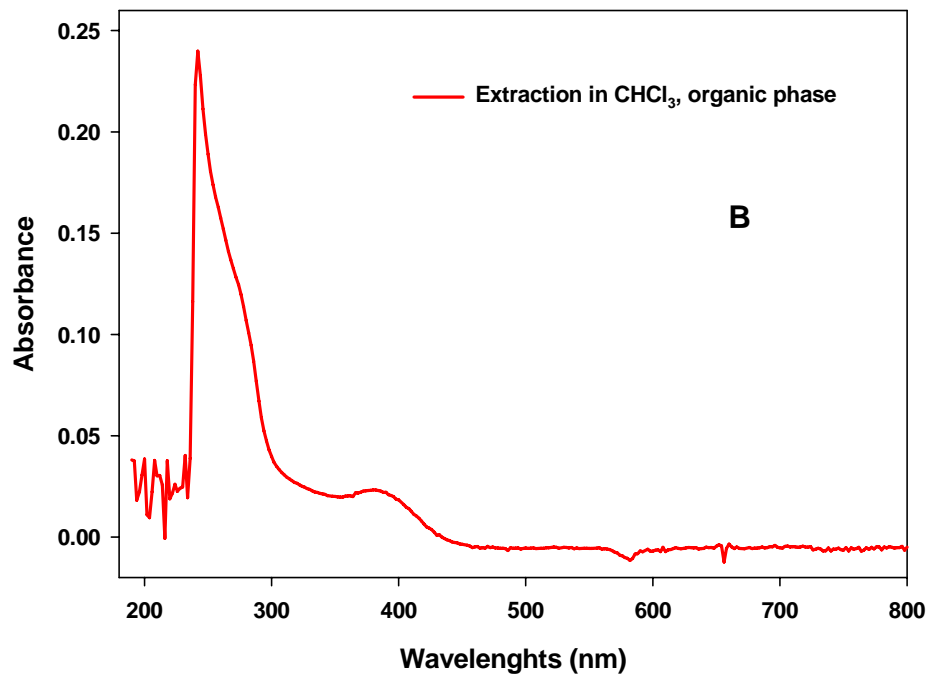
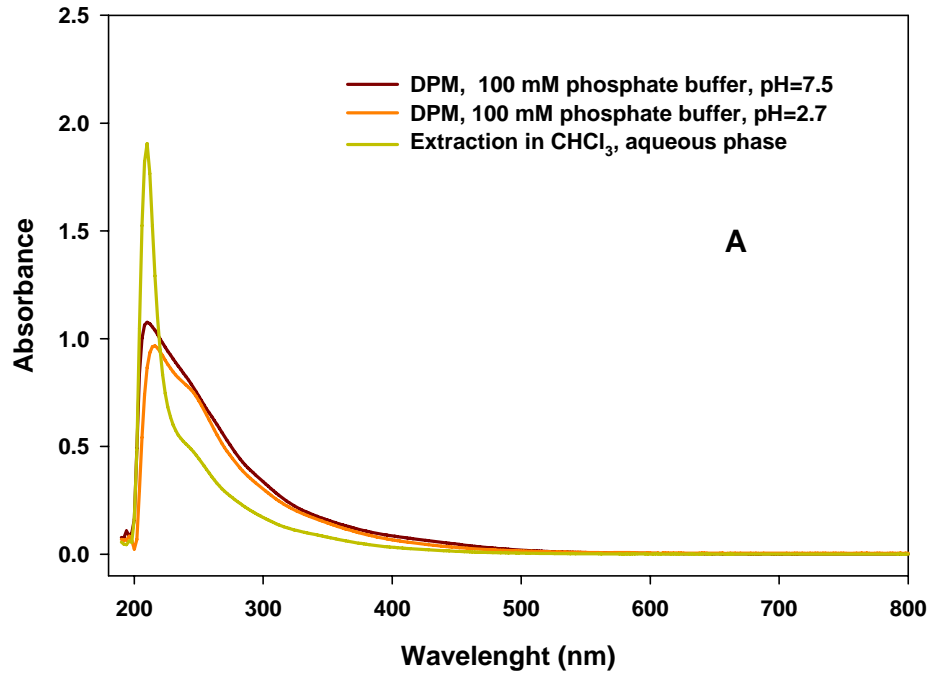


Figure A-10. (A) UV-Visible spectrum of extracted diesel particulate matter in 100 mM phosphate buffer at pH 7.5 for 24 hours (—); UV-Visible spectrum after the extraction and adjusting to pH=2.8 (—) and UV-Visible spectrum for aqueous phase after extraction in chloroform(—). (B) The UV-Visible spectrum for the chloroform phase after the extraction (—).

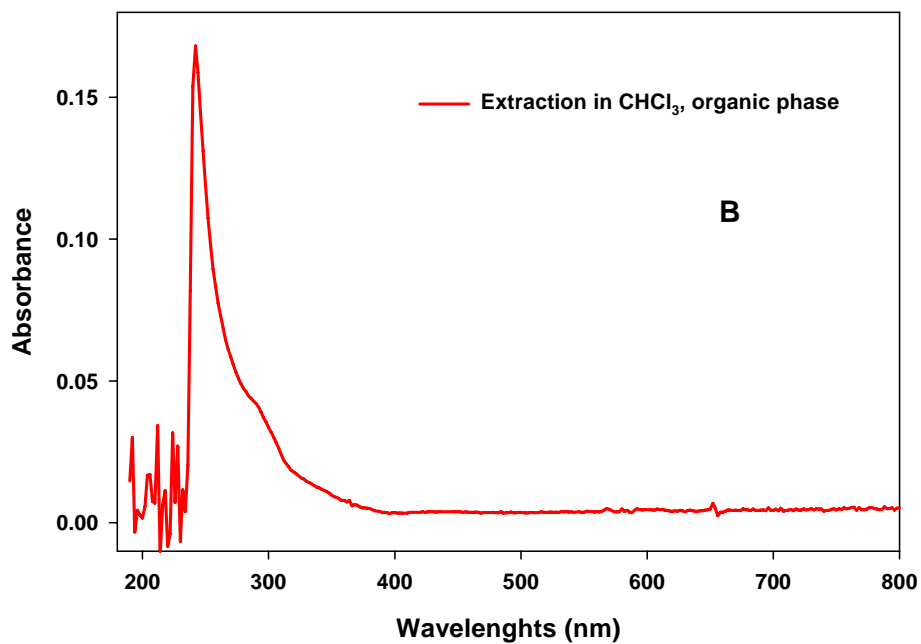
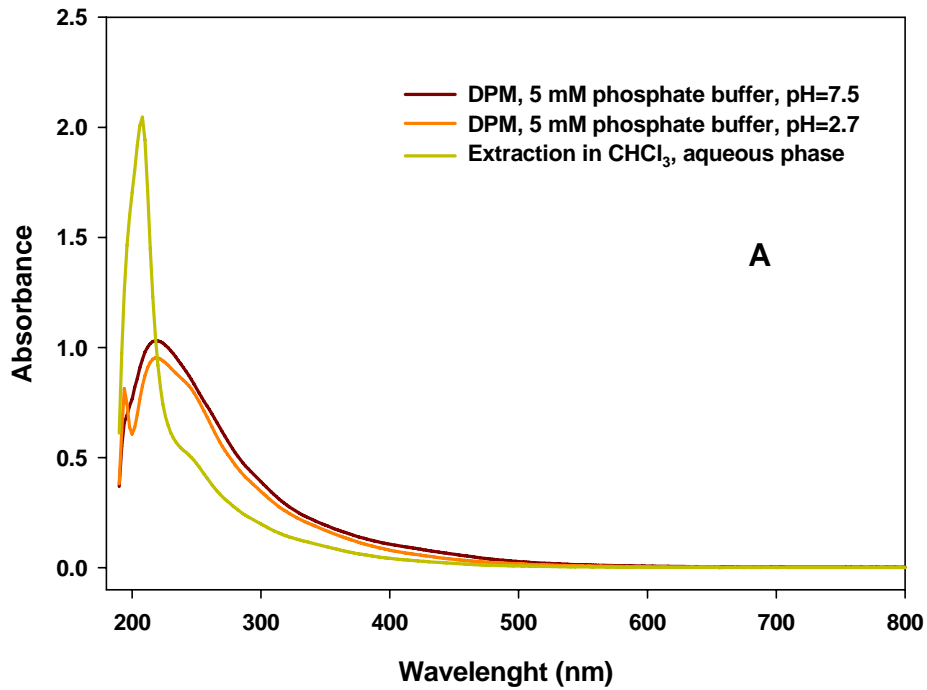


Figure A-11. (A) UV-Visible spectrum of extracted diesel particulate matter in 5 mM phosphate buffer for 24 hours (—); UV-Visible spectrum after the extraction and adjusting to pH=2.8 (—) and UV-Visible spectrum for aqueous phase after extraction in chloroform (—). (B) The UV-Visible spectrum for the chloroform phase after the extraction (—).

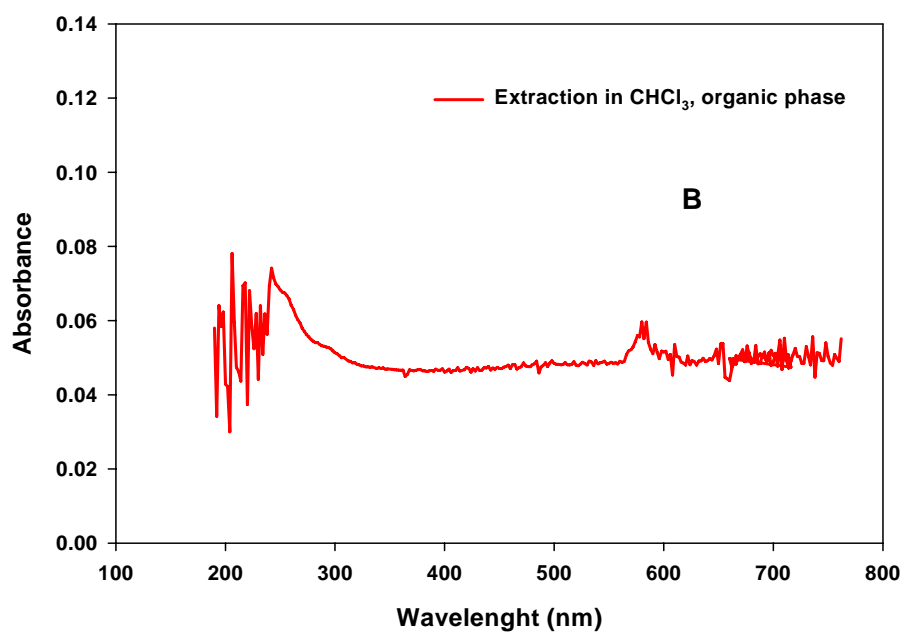
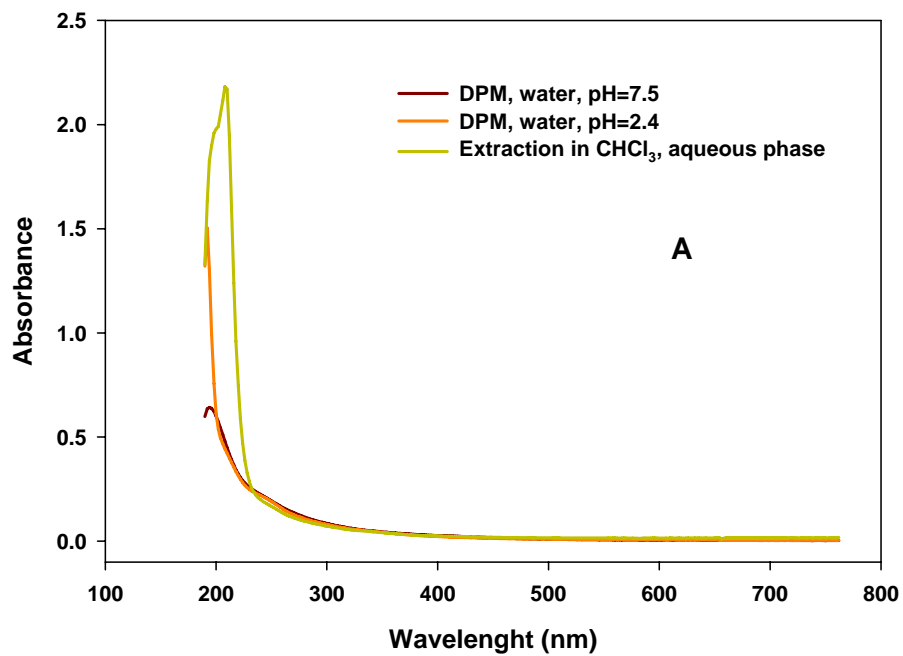


Figure A-12. (A) UV-Visible spectrum of extracted diesel particulate matter in water for 24 hours (—); UV-Visible spectrum after the extraction and adjusting to pH=2.8 (—) and UV-Visible spectrum for aqueous phase after extraction in chloroform (—). (B) The UV-Visible spectrum for the chloroform phase after the extraction (—).

Appendix B: Particles properties

In this section, available information for Standard Reference Material (SRM) 1649, 1648, 2975, 1632b and 2689 such as particles size, chemical (inorganic and organic) constituents and toxicity are reported.

B.1. Standard Reference Material 1649 (urban dust)

B.1.1. Sample collection and preparation

According to NIST report, SRM 1649 was prepared from atmospheric particles collected in the Washington DC area in 1976-1977. This particulate matter was collected over a period of one year from urban area in a special baghouse and the particles were removed from the baghouse filter bags by specially designed vacuum cleaner and combined in a single lot. This lot was passed through a 125 μm sieve and then thoroughly mixed and bottled.

B.1.2. Particle size

Here is the particle-size characteristics for SRM 1649 (NIST report, 2006).

Table B.1. Values for particle-size characteristics for SRM 1649

Particle Measurement	Value
Mean diameter (volume distribution, MV, μm)	34.6 ± 0.4
Mean diameter (area distribution, μm)	12.9 ± 0.3
Mean diameter (number distribution, μm)	1.50 ± 0.09
Surface Area (m^2/cm^3)	0.47 ± 0.01

B.1.3. Chemical constituents

Available information for chemical constituents of SRM 1649 is reported.

B.1.3.1. Organic constituents

Tables B-2, B-3, B-4, B-5, B-6 report the concentration of poly cyclic aromatic hydrocarbons (PAHs), polychlorinated biphenyls (PCBs), chlorinated pesticides in existing SRM 1649 (NIST 2006, Cho et al. 2004, Crimmins and Baker 2006, Karthikeyan et al. 2006, Poster et al. 1999, Bergvall and Westerholm 2006).

Table B-2. PAHs and nitro-PAHs and their concentrations in SRM 1649

PAHs	Mass Fractions (in $\mu\text{g}/\text{kg}$)
Phenanthrene	4.14 ± 0.37
Anthracene	0.432 ± 0.082
Fluoranthene	6.45 ± 0.18
Pyrene	5.29 ± 0.25
Benzoanthracene	2.208 ± 0.073
Chrysene	3.049 ± 0.069
Triphenylene	1.357 ± 0.054
Benzofluoranthene	6.45 ± 0.64
Benzopyrene	3.09 ± 0.19
Perylene	0.646 ± 0.075
Anthanthrene	0.450 ± 0.067
Benzoperylene	4.01 ± 0.91
Dibenzoanthracene	0.31 ± 0.034
Pentaphene	0.151 ± 0.035
Benzo-chrysene	0.315 ± 0.013
Picene	0.426 ± 0.022
Fluorene	230 ± 50
Dibenzothiophene	180 ± 10
1-Methylphenanthrene	370 ± 40
2-Methylphenanthrene	730 ± 120
3-Methylphenanthrene	500 ± 50
Benzophenanthrene	460 ± 30
Indenofluoranthene	230 ± 10
Benzo-chrysene	80 ± 4
Dibenzopyrene	630 ± 80
Dibenzofluoranthene	800 ± 100
1-nitronaphthlene	8.4
2-nitronaphthlene	12
2-nitrobiphenyl	2.5
3-nitrobiphenyl	4.7
2-nitrofluorene	2.6
9-nitroanthracene	70
9-nitrophenanthrene	14
2-nitrofluoranthene	190
1-nitropyrene	40
2-nitropyrene	7.0
7-nitroanthracene	15
6-nitrochrysene	2.5

Table B-3. PCBs and their concentrations in SRM 1649

Organic constituents	Mass Fractions (in mg/kg)
2,4'-Dichlorobiphenyl	12.28 ± 0.29
2,2',5-Trichlorobiphenyl	20.44 ± 0.84
2,4,4'-Trichlorobiphenyl	18.5 ± 1.2
2,2',5-Trichlorobiphenyl	17.3 ± 1.4
2,2',3,5'-Tetrachlorobiphenyl	15.4 ± 1.6
2,2',4,5'-Tetrachlorobiphenyl	12.2 ± 1.5
2,2',5,5'-Tetrachlorobiphenyl	24.65 ± 0.97
2,3',4,4'-Tetrachlorobiphenyl	65 ± 12
2,2',4,4',5-Pentachlorobiphenyl	9.58 ± 0.69
2,2',3,5',6-Pentachlorobiphenyl	51.6 ± 4.2
2,2',4,5,5'-Pentachlorobiphenyl	52.9 ± 1.0
2,3,3',4,4'-Pentachlorobiphenyl	8.63 ± 0.80
2,3,3',4',6-Pentachlorobiphenyl	26.6 ± 1.6
2,2',3,4,5'-Pentachlorobiphenyl	10.65 ± 0.62
2,3',4,4',5-Pentachlorobiphenyl	25.7 ± 1.5
2,2',3,3',4,4'-Hexachlorobiphenyl	6.35 ± 0.69
2,2',3,4,4',5'-Hexachlorobiphenyl	69.7 ± 7.5
2,2',3,4,4',5',6-Hexachlorobiphenyl	75.7 ± 1.3
2,2',3,5,5',6-Hexachlorobiphenyl	34.3 ± 3.9
2,2',4,4',5,5'-Hexachlorobiphenyl	82.5 ± 8.0
2,3,3',4,4',5-Hexachlorobiphenyl	16.25 ± 0.77
2,2',3,3',4,4',5-Heptachlorobiphenyl	30.8 ± 2.2
2,2',3,3',4,4',5-Heptachlorobiphenyl	78.7 ± 8.2
2,2',3,4,4',5',6-Heptachlorobiphenyl	20.34 ± 0.95
2,2',3,4',5,5',6-Heptachlorobiphenyl	40.1 ± 2.5
2,2',3,3',4,4',5,5'-Octachlorobiphenyl	28.9 ± 3.6
2,2',3,3',4,4',5,6-Octachlorobiphenyl	9.63 ± 0.37
2,2',3,3',4,4',5,5',6-Nonachlorobiphenyl	20.6 ± 4.6
Decachlorobiphenyl	8.04 ± 0.77

Table B-4. Dibenzo-*p*-dioxins & Dibenzofurans & their concentrations in SRM 1649

Dibenzo-<i>p</i>-dioxin & Dibenzofuran	Mass Fractions (in µg/kg)
2,3,7,8-Tetrachlorodibenzo- <i>p</i> -dioxin	0.011 ± 0.004
1,2,3,7,8-Pentachlorodibenzo- <i>p</i> -dioxin	0.091 ± 0.012
1,2,3,4,7,8-Hexachlorodibenzo- <i>p</i> -dioxin	0.26 ± 0.02
1,2,3,6,7,8-Hexachlorodibenzo- <i>p</i> -dioxin	0.68 ± 0.05
1,2,3,7,8,9-Hexachlorodibenzo- <i>p</i> -dioxin	0.64 ± 0.11
1,2,3,4,6,7,8-Heptachlorodibenzo- <i>p</i> -dioxin	18.8 ± 1.5
Octachlorodibenzo- <i>p</i> -dioxin	201 ± 20
2,3,7,8-Tetrachlorodibenzofuran	0.068 ± 0.15
1,2,3,7,8-Pentachlorodibenzofuran	0.090 ± 0.010
2,3,4,7,8-Pentachlorodibenzofuran	0.28 ± 0.03
1,2,3,4,7,8-Hexachlorodibenzofuran	0.87 ± 0.26
1,2,3,6,7,8-Hexachlorodibenzofuran	0.43 ± 0.06
2,3,4,6,7,8-Hexachlorodibenzofuran	0.69 ± 0.03
1,2,3,7,8,9-Hexachlorodibenzofuran	0.066 ± 0.029
1,2,3,4,6,7,8-Heptachlorodibenzofuran	3.8 ± 0.2
1,2,3,4,7,8,9- Heptachlorodibenzofuran	0.46 ± 0.07
Octachlorodibenzofuran	6.8 ± 0.8
Total Tetrachlorodibenzo- <i>p</i> -dioxins	0.16 ± 0.08
Total Pentachlorodibenzo- <i>p</i> -dioxins	0.88 ± 0.16
Total Hexachlorodibenzo- <i>p</i> -dioxins	6.0 ± 0.5
Total Heptachlorodibenzo- <i>p</i> -dioxins	36.4 ± 3.4
Total-Tetrachlorodibenzofurans	0.52 ± 0.13
Total-Pentachlorodibenzofurans	1.6 ± 0.2
Total-Hexachlorodibenzofurans	5.0 ± 0.6
Total-Heptachlorodibenzofurans	9.8 ± 0.8
Total Dibenzo- <i>p</i> -dioxins	244 ± 22
Total dibenzofurans	23.9 ± 1.9

Table B-5. Chlorinated Pesticides and their concentrations in SRM 1649

Chlorinated Pesticides	Mass Fractions (in $\mu\text{g}/\text{kg}$)
Hexachlorobenzene	16.3 ± 1.8
<i>trans</i> -Chlordane (γ -Chlordane)	40.3 ± 2.8
<i>cis</i> -Chlordane (α -Chlordane)	34.88 ± 0.42
<i>trans</i> -Nonachlor	27.6 ± 1.6
2,4'-DDE	5.79 ± 0.85
4,4'-DDE	40.4 ± 1.7
4,4'-DDD	34.01 ± 0.48
4,4'-DDT	212 ± 15

Table B-6. Quinones & their concentrations in SRM 1649

Quinones	Mass Fractions (in ng/kg)
1,2-Naphthoquinone	0.19 ± 0.03
1,4-Naphthoquinone	0.24 ± 0.05
9,10-Phenanthraquinone	1.18 ± 0.13
9,10-Anthraquinone	2.03 ± 0.19

B.1.3.2. Inorganic constituents

The majority of the inorganic constituents and their concentration in SRM 1649 are reported in Table B.7 (NIST report, 2006).

Table B-7. Concentration of inorganic constituents in SRM 1649

Inorganic constituents	Mass Fractions (in mg/kg)
Antimony	29.9 ± 0.7
Arsenic	67 ± 2
Barium	569 ± 21
Cadmium	26.5 ± 1.0
Cerium	52 ± 4
Cesium	2.84 ± 0.07

Chromium	211 ± 6
Cobalt	16.4 ± 0.4
Copper	223 ± 7
Europium	0.87 ± 0.07
Hafnium	4.4 ± 0.1
Lanthanum	33 ± 3
Manganese	237 ± 8
Molybdenum	13.5 ± 0.9
Nickel	166 ± 7
Rubidium	48 ± 3
Samarium	4.7 ± 0.4
Scandium	8.7 ± 0.2
Selenium	25.6 ± 0.7
Silver	3.5 ± 0.2
Thorium	6.6 ± 0.2
Tin	56 ± 13
Tungsten	3.8 ± 0.3
Uranium	2.65 ± 0.08
Vanadium	345 ± 13

Inorganic constituents	Mass Fractions (in %)
Bromine	0.119 ± 0.001
Chlorine	0.28 ± 0.01
Iron	2.98 ± 0.07
Lead	1.24 ± 0.04
Magnesium	0.92 ± 0.03
Sulfur	3.27 ± 0.09
Zinc	0.168 ± 0.004

B.1.4.Toxicity of SRM 1649

According to NIST report (2006), Durant et al. 1998, Gundel et al. 1993, Heimlg et al. 2004, chemicals associated with SRM 1649 are mutagenic. The reported mutagenic activity is 100-200 rev/mg. On the other hand, Karlsson et al. 2004 reported that the mutagenic activity is initiated by DNA oxidation. They measured 8-oxo-dG when the DNA was oxidized with SRM 1649.

B.2. Standard Reference Material 1648

B.2.1. Sample collection and preparation

According to NIST report (2006), SRM 1648 was prepared from urban particulate matter collected in the St. Louis, MO in a baghouse specially designed for this purpose. The particles were collected over a period of 12 months. The material was removed from the filter bags and combined in a single lot, passed through a fine mesh sieve to remove extraneous materials and blended in a v-blender. The particles then packed into numbered bottles.

B.2.2. Chemical constituents

Available information for chemical constituents of SRM 1648 is reported.

B.2.2.1. Inorganic constituents

The majority of the inorganic constituents and their concentration in SRM 1648 are reported in Table B-8 (NIST report, 2006).

Table B-8. Concentration of inorganic constituents in SRM 1648

Inorganic constituents	Mass Fractions (in mg/kg)
Antimony	45
Arsenic	115 ± 10
Barium	773
Bromine	500
Cadmium	75 ± 7
Cerium	55
Cesium	3
Chromium	403 ± 12
Cobalt	18
Copper	609 ± 27
Europium	0.8
Hafnium	4.4
Indium	1.0
Iodine	20
Lanthanum	42
Manganese	786 ± 17
Nickel	82 ± 3
Rubidium	52
Samarium	4.4 ± 0.4
Selenium	27 ± 1
Silver	6
Thorium	7.4
Tungsten	4.8
Uranium	5.1 ± 0.1
Vanadium	127 ± 7

Inorganic constituents	Mass Fractions (in %)
Aluminum	3.42 ± 0.11
Chlorine	0.45
Iron	3.91 ± 0.10
Potassium	1.05 ± 0.01
Lead	0.655 ± 0.008
Magnesium	0.8
Sulfur	5.0
Sodium	0.425 ± 0.002
Titanium	0.40
Zinc	0.168 ± 0.004

B.2.3. Toxicity of SRM 1648

Schneider et al. (2005) reported that SRM 1648 causes oxidative stress upon uptake by alveolar macrophage. Huang et al. (2004) reported that SRM 1648 cause inflammation and necrosis for human alveolar macrophage. They measured cytokine release to discuss about its toxicity.

B.3. Standard Reference Material 2975

B.3.1. Sample collection and preparation

According to NIST report (2006), SRM 2975 was prepared from diesel particulate matter, which was obtained from M.E. Wright of the Donaldson Company, INC. Minneapolis, MN. This particle was collected from a filtering system designed specifically for diesel-powdered forklifts. The material was homogenized in a V-blender for one hour and stored in polyethylene bags.

B.3.2. Particle size

Here are the particle-size characteristics for SRM 2975 (NIST report, 2006).

Table B-9. Values for particle-size characteristics for SRM 2975

Particle Measurement	Value
Mean diameter (volume distribution, MV, μm)	31.9 ± 0.6
Mean diameter (area distribution, μm)	11.2 ± 0.1
Mean diameter (number distribution, μm)	1.62 ± 0.01
Surface Area (m^2/cm^3)	0.538 ± 0.006

B.3.3. Chemical constituents

Available information for chemical constituents of SRM 2975 is reported.

B.3.3.1. Organic constituents

Table B-10 represents the concentration of poly cyclic aromatic hydrocarbons (PAHs) existing in SRM 2975 (NIST report, 2006; Bergvall and Westerholm 2006).

Table B-10. PAHs and their concentrations in SRM 2975

PAHs	Mass Fractions (in mg/kg)
Phenanthrene	17.0 ± 2.8
Anthracene	0.038 ± 0.008
Fluoranthene	26.6 ± 5.1
Pyrene	0.90 ± 0.24
Benzoanthracene	0.317 ± 0.066
Chrysene	4.56 ± 0.16
Triphenylene	5.22 ± 0.20
Benzo[a]fluoranthene	0.82 ± 0.11
Benzo[b]pyrene	1.11 ± 0.10
Perylene	0.054 ± 0.009
Benzo[perylene]	0.498 ± 0.044
Dibenzo[a,h]anthracene	0.37 ± 0.07
Pentaphene	0.038 ± 0.007
Benzo[k]chrysene	0.08 ± 0.03
Picene	1.0 ± 0.2
1-Methylphenanthrene	0.89 ± 0.11
2-Methylphenanthrene	2.0 ± 0.2
3-Methylphenanthrene	1.0 ± 0.2
Benzo[ghi]perylene	1.0 ± 0.4
Indeno[1,2,3-cd]fluoranthene	1.1 ± 0.2
Benzo[ghi]chrysene	0.08 ± 0.03
4- and 9-Methylphenanthrene	0.44 ± 0.09
1,2-Dimethylphenanthrene	0.05 ± 0.02
1,6-, 1,7-, 2,5-, and 2,9-Dimethylphenanthrene	0.57 ± 0.08
1,8-Dimethylphenanthrene	0.06 ± 0.02
2,6-Dimethylphenanthrene	0.25 ± 0.05

2,7- Dimethylphenanthrene	0.23 ± 0.05
3,6- Dimethylphenanthrene	0.18 ± 0.02
Benzofluoranthene	10.2 ± 0.5
8-Methylfluoranthene	0.68 ± 0.004
2-Methylpyre	0.040 ± 0.008
4-Methylpyrene	0.022 ± 0.005
Coronene	1.1 ± 0.2
1-Nitropyrene	36

B.3.4. Toxicity of SRM 2975

Arey (2004) reported that SRM 2975 showed mutagenic activity and lung injury on aspiration. Singh et al. (2004) reported that IL-6, IL-5 and TNF- α levels was increased when the macrophages were exposed to SRM 2975, but these cytokines levels are lower than cytokines increase levels for other diesel particles.

B.4. Standard Reference Material 2689

B.4.1. Sample collection and preparation

According to NIST report (2006), SRM 2689 was obtained from three different coal-fired power plants and is product of western Kentucky. The SRM 2986 was size classified using a Vortex C-13 air classifier and particles greater than 145 μm was removed for grinding. The coarse material consisted mostly of quartz and partially burned fragments. Once ground This material was blended back into the rest of the fly ash, the whole lot of material was homogenized in a ribbon blender, and sealed in glass vials and packaged The packaging was performed under controlled temperature and humidity.

B.4.2. Chemical Constituents

Available information for chemical constituents of SRM 2689 is reported.

B.4.2.1. Inorganic constituents

The majority of the inorganic constituents and their concentration in SRM 2689 are reported in Table B-11 (NIST report, 2006).

Table B-11. Concentration of inorganic constituents in SRM 2689

Inorganic constituents	Mass Fractions (in mg/kg)
Antimony	9
Arsenic	200
Barium	800
Beryllium	21
Cadmium	3
Cesium	11
Chromium	170
Cobalt	48
Europium	3
Hafnium	7
Lead	52
Manganese	300
Nickel	122
Mercury	<0.003
Scandium	32
Selenium	7
Strontium	700
Thorium	25
Zinc	240

Inorganic constituents	Mass Fractions (in %)
Aluminum	12.94 ± 0.21
Calcium	2.18 ± 0.06
Iron (Total)	9.32 ± 0.06
Potassium	2.20 ± 0.03
Magnesium	0.61 ± 0.05
Sodium	0.25 ± 0.03
Phosphorous	0.10 ± 0.01
Silicon	24.06 ± 0.08
Titanium	0.75 ± 0.01

B.5. Standard Reference Material 1632b

B.5.1. Sample collection and preparation

According to NIST report (2006), the coal for SRM 1632b was obtained from the Humphrey No. 7 mine and coal preparation plant of the Consolidated Coal Company, Christopher Coal Company Division, Osage, WV. The coal was obtained from an underground mine from the Pittsburg seam. The coal for SRM 1632b was almost oven dried prior to processing. The coal was passed from 60 mesh sieve prior to blending. The coal then blended in a stainless steel cone blender. After blending, the coal was packaged in polyethylene-lined aluminum cans. Homogeneity testing was performed on both the bulk and bottled samples using X-ray fluorescence spectroscopy.

B.5.2. Chemical constituents

Available information for chemical constituents of SRM 1632b is reported.

B.5.2.1. Inorganic constituent

The majority of the inorganic constituents and their concentration in SRM 1632b are reported in Table B-12 (NIST report, 2006).

Table B-12. Concentration of inorganic constituents in SRM 1632b

Inorganic constituents	Mass Fractions (in mg/kg)
Antimony	0.24
Arsenic	3.72 ± 0.09
Barium	67.5 ± 2.1
Bromine	17
Cadmium	0.0573 ± 0.0027
Cerium	9
Cesium	0.44
Chlorine	1260
Chromium	11
Cobalt	2.29 ± 0.17
Copper	6.28 ± 0.30
Europium	0.17
Fluorine	41.7 ± 3.2
Hafnium	0.43
Lanthanum	5.1
Lead	3.67 ± 0.26
Lithium	10
Manganese	12.4 ± 1.0
Mercury	0.07
Molybdenum	0.9
Nickel	6.10 ± 0.27
Rubidium	5.05 ± 0.11
Samarium	0.87
Scandium	1.9
Selenium	1.29 ± 0.11
Silicon	14000
Strontium	102
Thorium	1.342 ± 0.036
Tungsten	0.48

Uranium	0.436 ± 0.012
Vanadium	14
Zinc	11.89 ± 0.78

Inorganic constituents	Mass Fractions (in %)
Aluminum	0.855 ± 0.019
Calcium	0.204 ± 0.006
Carbon (Total)	76.86 ± 0.26
Hydrogen	4.94 ± 0.13
Iron	0.759 ± 0.045
Magnesium	0.0383 ± 0.0008
Nitrogen	1.56 ± 0.07
Potassium	0.0748 ± 0.0028
Sodium	0.0515 ± 0.0011
Sulfur	1.89 ± 0.06
Titanium	0.0454 ± 0.001

B.6. KGa-1b (kaolinite)

B.6.1. Particle source

The Clay Mineral Society standard was received from Professor Helz. This clay was originally purchased from the University of Missouri-Columbia Source Clay Repository. KGa-1b. The particle is a well-crystallized kaolinite from Washington County, Georgia (Vorlicek and Helz, 2002).

B.6.2. Chemical constituents

KGa-1b ($\text{Al}_2\text{Si}_2\text{O}_5[\text{OH}]_4$) has some trace amount of TiO_2 (1.64% w/w), Fe_2O_3 (0.21% w/w), quartz, micas, alkali, and alkaline earth oxides. KGa-1b has a Brunauer-Emmett-Teller (BET) surface area of $12.5 \text{ m}^2/\text{g}$ (Vorlicek and Helz, 2002).

B.7. Aerosil

B.7.1. Particle source and constituent

Aerosil is an amorphous, fumed, crystalline free silicon dioxide which was received from Professor Helz. This material was originally purchased from Degussa Corporation, NJ.

Bibliography

Adamson, I. Y. R., Prieditis, H., Vincent, R. (1999) Pulmonary toxicity of an atmosphere particulate sample is due to the soluble fraction. *Toxicol. Appl. Pharmacol.* 157, 43-50.

Agopyan, N., Bhatti, T., Yu, S., Simon, S. A. (2003) Vanilloid receptor activation by 2- and 10- μ m particles induces responses leading to apoptosis in human airway epithelial cells. *Toxicol. and applied pharmacol.* 192, 21-35.

Aljandali, A., Pollack, H., Yeldandi, A., Li, Y., Weitzman, S. A., Kamp, D. W. (2001) Asbestos causes apoptosis in alveolar epithelial cells: Role of iron-induced free radicals. *J. Lab Clin. Med.*, 137, 330-339.

Anderegg, G. (2005) IUPAC, Pure and Applied Chemistry 77, 1467-1468.

Andersson, P. J., Wilson, J. D., Hiller, F.C. (1990) Respiratory tract deposition of ultrafine particles in subjects with obstructive and restrictive lung disease. *Chest* 97, 1115-1120.

Andersson, H. R. (1997) Air pollution and trends in asthma, in: Chadwick, D. J., Cardew, G. (Eds), The rising trends in asthma. Wiley, Chichester, UK, 190-207.

Antonini, J. M., Lawryk, N. J., Murthy, G. G. K., Brain, J. D. (1999) Effect of welding fume solubility on lung macrophage viability and function in vitro. *J. Toxicol. Environ. Health, Part A.* 58, 343-363.

Antonini, J. M., Taylor, M. D., Leonard, S. S., Lawryk, N. J., Shi, X., Clarke, R. W., Roberts, J. R. (2004) Metal composition and solubility determine lung toxicity induced by residual oil fly ash collected from different sites within a power plant. *Molecular and Cellular Biochem.* 255, 257-265.

Arey, J. (2004) A tale of two diesels. *Environ. Health Perspect.* 112, 812-813.

Ball, J. C., Straccia, A. M., Young, W., Aust, A. E. (2000) The formation of reactive oxygen species catalyzed by neutral, aqueous extracts of NIST ambient particulate matter and diesel engine particles. *J Air & Waste Manage. Assoc.* 50, 1897-1903.

Baulig, A., Poirault, J., Ausset, P., Schins, R., Shi, T., Baralle, D., Dorlhene, P., Meyer, M., Lefevre, R., Baeza-Squiban, A., Marano, F. (2004) Physicochemical characteristics and biological activities of seasonal atmospheric particulate matter sampling in two locations of Paris. *Environ. Sci. Technol.* 38, 5985-5992.

Bergvall, C. and Westerholm, R. (2006) Deretmination of dibenzopyrenes in standard reference materials (SRM) 1649a, 1650, 2975 using ultrasonically assisted extraction and LC-GC-MS. *Anal. Bioanal. Chem.* 384, 438-447.

Blough, N. V. and Simpson, D. J. (1988) Chemically mediated fluorescence yield switching in nitroxide-fluorophore adducts: optical sensors of radical/redox reactions. *Am. Chem. Soc.* 110, 1915-1917.

Briedé, J. J., De Kok, T. M. C. M., Hogervorst, J. G. F., Moonen, E. J. C., Op Den Camp, C. L. B., Kleinjans, J. C. S. (2005) Development and application of an electron spin resonance spectroscopy method for the determination of oxygen free radical formation by particulate matter. *Environ. Sci. Technol.* 39, 2947-2953.

Brook R. D., Franklin B., Cascio W., Hong Y., Howard G., Lipsett M., Luepker R., Mittleman M., Samet J., Smith Jr S. C., Tager I. (2004) Air pollution and cardiovascular disease: A statement for healthcare of professionals from the expert panel on population and prevention science of the American heart association. *Circulation* 109, 2655-2671.

Brown, R. K., Wyatt, H., Price, J. F., Kelly, F.J. (1996) Pulmonary dysfunction in cystic fibrosis is associated with oxidative stress. *Eur. Respir. J.* 9, 334-339.

Brown, D. M., Wilson, M. R., MacNee, W., Stone V., Donaldson, K. (2001) Size-dependent proinflammatory effects of ultrafine polystyrene particles: A role for surface area and oxidative stress in the enhanced activity of ultrafine. *Toxicol. Appl. Pharmacol.* 175, 191-199.

Brunner, T. J., Wick, P., Manser, P., Spohn, P., Grass, R. N., Limbach, L. K., Bruinink, A., Stark, W. J. (2006) In vitro cytotoxicity of oxide nanoparticles: Comparison to asbestos, silica, and the effect of particles solubility. *Environ. Sci. Technol.* 40, 4374-4381.

Buxton, G. V.; Greenstock, C. L.; Helman, W. P.; Ross, A. B. (1988) Critical review of rate constants for reactions of hydroxylated electrons, hydrogen atoms and hydroxyl radical in aqueous solution. *J. Phys. Chem. Ref. Data*, 17, 513-886.

Carter, J. D., Ghio, A. J., Samet, J. M., Devlin, R. B. (1997) Cytokine production by human airway epithelial cells after exposure to an air pollution particles is metal-dependent. *Toxicol. Appl. Pharmacol.* 146, 180-188.

Chang, J., Chang, K. L. B., Hwang, D., Kong, Z. In vitro cytotoxicity of silica nanoparticles at high concentrations strongly depends on the metabolic type of the cell line. *Environ. Sci. & Technol.*, 41, 2064-2068.

Chao, C., Park, S., Aust, A.E. (1996) Participation of nitric oxide and iron in the oxidation of DNA in asbestos-treated human lung epithelial cells. *Arch. Biochem. Biophys.* 326, 152-157.

Cho, A. K., Di Stefano, E., You, Y., Rodriguez, C. E., Schmitz, D. A., Kumagai, Y., Miguel, A. H., Eiguren-Fernandez A., Kobayashi, T., Avol, E., Froines, J. R. (2004) Determination of four quinones in diesel exhaust particles, SRM 1649a, and atmospheric PM_{2.5}. *Aerosol Sci. Technol.* 38, 68-81.

Chen, F., Sun, S. C., Kuhn, D. C., Haydos, L. J. and Demers, L. M. (1995) Essential role of NF- κ B activation in silica induced inflammatory mediator production in macrophage. *Biochem. Biophys. Res. Commun.* 214, 985-992.

Collins, A. R., Cader, J., Möller, L., Poulsen, H. E., Viña, J. (2004) Are we sure we know how to measure 8-oxo-7, 8-dihydroguanine in DNA from human cells? *Arch. Biochem. Biophys.* 423, 57-65.

Crimmins, B. S. and Baker, J. E. (2006) Improved GC/MS methods for measuring hourly PAH and nitro-PAH concentrations in urban particulate matter. *Atmospheric Environment*, 40, 6764-6779.

Dalal, N. S., Shi, X., Vallyathan, V. (1990) Role of free radicals in the mechanisms of hemolysis and lipid peroxidation by silica: comparative ESR and cytotoxicity. *J. Toxicol. Environ. Health.* 29, 307-316.

Dalal, N. S., Newman, J., Pack, D., Leonard, S., Vallyathan, V. (1995) Hydroxyl radical generation by coal mine dust: possible implication to coal workers' pneumoconiosis (CWP). *Free radical in Biol. Med.* 18, 11-20.

Dawson (1986) In *Data for biochemical research handbook*, 3rd ed.; Oxford Press: New York p. 402-403.

Dellinger, B., Pryor, W. A., Cueto, R., Squadrito, G. L., Hegde, V., Deutsch W. A. (2001) Role of free radicals in the toxicology of airborne fine particulate matter. *Chem. Res. Toxicol.* 14, 1371-1377.

Ding, M., Shi, X., Lu, Y., Huang, C., Leonard, S., Roberts, J., Antonini, J., Castranova, V., Vallyathan, V. (2001) Induction of activator protein-1 through reactive oxygen species by crystalline silica in JB6 cells. 276, 9108-9114.

Ding, M., Shi, X., Dong, Z., Chen, F., Lu, Y., Castranova, V., Vallyathan, V. (1999) Freshly fractured crystalline silica induces activator protein-1 activation through ERKs and p38 MAPK. *J. Biol. Chem.* 274, 30611-30616.

Dockery, D. W., Schwartz, J., Spengler, J. D. (1992) Air pollution and daily mortality: associations with particulates and acid aerosols. *Environ. Res.* 59, 362-373.

Dockery, D. W., Pope, C. A., Xu, X., Spengler, J. D., Ware, J. H., Fay, M. E., Ferris, B. G., Speizer, F. E. (1993) An association between air pollution and mortality in six U.S. cities. *N Engl J Med.* 329, 1753-1759.

Doroshov, J. (2006) Redox modulation of chemotherapy-induced tumor cell killing and normal tissue toxicity. *JNCI*, 98, 223-225.

Durant, J. L., Lfleur, A. L., Plummer,, E. F., Taghizadeh, K., Busby Jr, W. F., Thilly, W. G. (1998) Human lymphoblast mutagens in urban airborne particles. *Environ. Sci. Technol.* 32, 1894-1906.

Duffin, R., Tran, C. L., Clouder, A., Brown, D. M., MacNee, W., Stone, V., Donaldson, K. (2002) The importance of surface area and specific reactivity in acute pulmonary inflammatory response to particles. *Ann. Occup. Hyg.* 46, 242-245.

Dye, J. A., Alder, K. B., Richards, J. H. and Dreher, K. L. (1997) Epithelial injury induced by exposure to residual oil fly-ash particles: Role of reactive oxygen species? *Am. J. Respir. Cell Mol. Boil.* 17, 625-633.

Felix, C. C., Sealy R. C. (1981) Electron spin resonance characterization of radicals from 3, 4 – dihydroxyphenylalanine: Semiquinone anions and their metal chelates. *J. Am. Chem. Soc.* 103, 2831-2836.

Finkelstein, E., Rosen, G. M., Rauckman, E. J., Paxton, J. (1979) Spin trapping of superoxide. *Mol. Pharmacol.* 16, 676-685.

Finkeistein, E., Rosen, G. M., Rauckman, E. J. (1980) Spin trapping. Kinetics of the reaction of superoxide and hydroxyl radicals with nitrones. *J. Am. Chem. Soc.* 102, 4994-4999.

Finkelstein, E., Rosen, G. M., Rauckman, E. J. (1982) Production of hydroxyl radical by decomposition of superoxide spin-trapped adducts. *Mol. Pharmacol.* 21, 262-265.

Firket J. (1931) The cause of the symptoms found in the Meune Valley during the fog of December. *Bull. Acad. R. Med. Belg.* 11, 683-741.

Flicker, T. M. and Green, S. A. (2001) Comparison of gas-phase free-radical populations in tobacco smoke and model systems by HPLC. *Environ Health Perspect.* 109, 765-771.

Frampton, M. W., Ghio, A. J., Samet, J. M., Carson, J. L., Carter, J. D., Devlin, R. B. (1999) Effects of aqueous extracts of PM10 filters from the Utah Valley on human airway epithelial cells. *AM. J. Physiol.* 277, 960-967.

- Gan, D.** (2005) Aqueous photochemistry of 1, 4-benzoquinones and their possible role in the photochemistry of natural organic matter. PhD dissertation.
- Gascoyne, P. Pethig, R. and Szent-Gyorgyi, A.** (1987) Electron spin resonance studies of the interaction of oxidoreductases with 2, 6-dimethoxy-p-quinone and semiquinone. *Biochim. Biophys. Acta* 923, 257-262.
- Gundel, L. A., Dalsey, J. M., De Carvalho, L. R. F., Kado, N. Y., Schuetzle, D.** (1993) Polar organic matter in airborne particles: Chemical characterization and mutagenic activity. *Environ. Sci. Technol.* 27, 2112-2119.
- Gutierrez, P. L.** (2000) The metabolism of quinone-containing alkylating agents: Free radical production and measurement. *Frontiers in Bioscience.* 5, d629-d638.
- Halliwell, B. and Gutteridge, J. M. C.** (1999) In Free radical in biology and medicine, 3rd ed.; Clarendon Press: New York.
- Hardy, J. A. and Aust, A. E.** (1995) Iron in asbestos chemistry and carcinogenicity. *Chem. Rev.* 95, 97-118.
- Heimlg, D., Lopez-Cancio, Jose, Arey, J., Harger, W. P., Atkinson, R.** (1992) Quantification of ambient nitrobenzopyranones: Further evidence for atmospheric mutagen formation. *Environ. Sci. Technol.* 26, 2207-2213.
- Hirano, S., Furuyama, A., Koike, E., Kobayashi, T.** (2003) Oxidative-stress potency of organic extracts of diesel exhaust and urban fine particles in rat heart microvessel endothelial cells. *Toxicology*, 187, 161-170.
- Hiura, T. S., Kaszubowski, M. P., Li, N., Nel, A. E.** (1999) Chemicals in diesel exhaust particles generate reactive radicals and induce apoptosis in macrophages. *J. Immunol.* 163, 5582-5591.
- Heunks, L. M., Dekhuijzen, P. N.** (2000) Respiratory muscle functions and free radicals: From cell to COPD. *Thorax* 55, 704-716.
- Huang, S. L., Cheng, W. L., Lee, C. T., Huang, S. L. and Chan, C. C.** (2002) Contribution of endotoxin in macrophage cytokine response to ambient particles in vitro. *J. Toxicol. Environ. Health, Part A* 65, 1261-1272.
- Huang, S., Hsu, M., Chan, C.** (2003) Effect of submicrometer particle composition on cytokine production and peroxidation of human bronchial epithelial cells. *Environ. Health Perspect.* 111, 478-482.
- Hwang, D., Chanmugam, P., Boudreau, M., Sohn, K. H., Stone, K. and Pryor W. A.** (1999) Activation and inactivation of cyclo-oxygenase in rat alveolar macrophage by aqueous cigarette tar extract. *Free Radical Biol. Med.* 27, 673-682.

Huang, Y. T., Li, Z., Harder, S. D., Soukup, J. M. (2004) Apoptotic and inflammatory effects induced by different particles in human alveolar macrophages. *Inhalation Toxicol.* *16*, 863-878.

Ichinose, T., Yajima, Y., Nagashima, M., Takenoshita, S., Nagamachi, Y., Sagai, M. (1997) Lung carcinogenesis and formation of 8-hydroxy-deoxyguanosine in mice by diesel exhaust particles. *Carcinogenesis*, *18*, 185-192.

Imrich, A., Ning, Y. Y. and Kobzik, L. (2000) Insoluble components of concentrated air particles mediate alveolar macrophage responses in vitro. *Toxicol. Appl. Pharmacol.* *167*, 140-150.

Janzen, E. G. (1984) Spin trapping. *Methods Enzym.* *105*, 188-198.

Janzen, E. G.; Krygsmann, P. H.; Lindsay, D. A.; Haire, D. L. (1990) Detection of alkyl, alkoxy, and alkyperoxy radicals from the thermolysis of azobis(isobutyronitrile) by EPR/spin trapping. Evidence for double spin adducts from liquid-phase chromatography and mass spectroscopy. *J. Am. Chem. Soc.* *112*, 8279-8284.

Jiménez, L. A., Thompson, J., Brown, D. A., Rahman, I., Antonicelli, F., Duffin, R., Drost, E. M., Hay, R. T., Donaldson, K., MacNee, W. (2000) Activation of NF- κ B by PM10 occurs via an iron-mediated mechanism in the absence of I κ B degradation. *Toxicol. Appl. Pharmacol.* *166*, 101-110.

Jung, H., Guo, B., Anastasio, C., Kennedy, I. M. (2006) Quantitative measurements of the generation of hydroxyl radicals by soot particles in a surrogate lung fluid. *Atmospheric Environment*, *40*, 1043-1052.

Kadiiska, M. B., Mason, R.P., Dreher, K. L., Costa, D. L., Ghio, A. J. (1997) In vivo evidence of free radical formation in the rat lung after exposure to an emission source air pollution particle. *Chem. Res. Toxicol.* *10*, 1104-1108.

Kang, J. L., Pack, I. S., Hong, S. M., Lee, H. S., Castranova, V. (2000) Silica-induced nuclear factor-kappa B activation: involvement of reactive oxygen species and protein tyrosine kinase activation. *J. Toxicol. Environ. Health, Part A* *60*, 27-46.

Karlsson, H. L., Nygren, J., Möller, L. (2004) Genotoxicity of airborne particulate matter: the role of cell-particle interaction and of substances with adduct-forming and oxidizing capacity. *Mutat. Res.* *565*, 1-10.

Karlsson, H. L., Nilsson, L., Möller, L. (2005) Subway particles are more genotoxic than street particles and induce oxidative stress in cultured human lung cells. *Chem. Res. Toxicol.* *18*, 19-23.

Karthikeyan, S., Balasubramanian, R., See, S. W. (2006) Optimization and validation of a low temperature microwave-assisted extraction method for analysis of polycyclic aromatic hydrocarbons in airborne particulate matter. *Talanta*, 69, 79-86.

Kelly F. J. (2003) Oxidative stress: its role in air pollution and adverse health effects. *Occup. Environ. Med.* 60, 612-616.

Kadiiska, M. B., Mason, R. P., Dreher, K. L., Costa, D. L., and Ghio, A. J. (1997) In vivo evidence of free radical formation in the rat lung after exposure to an emission source air pollution particle. *Chem. Res. Toxicol.* 10, 1104-1108.

Kieber, D. J., Blough, N. V. (1990a) Fluorescence detection of carbon-centered radicals in aqueous solution. *Free Radical Res. Comms.* 10, 109-117.

Kieber, D. J. and Blough, N. V. (1990b) Determination of carbon-centered radicals in aqueous solution by liquid chromatography with fluorescence detection. *Anal. Chem.* 62, 2275-2283.

Kiss, T. and Farkas, E., (1998) Metal-binding ability of Desferrioxamine B. *J. Inclusion Phenom. Molecul. Recogn. in Chem.* 32, 385-403.

Kleeman, M. J., Schauer, J. J. and Cass, G. R. (2000) Size and composition distribution of fine particulate matter emitted from motor vehicles. *Environ. Sci. Technol.* 34, 1132-1139.

Kocherginsky, N. and Swartz, H. M. (1995) In Nitroxide spin labels: Reactions in biology and chemistry. CRC press, Boca Raton, FL, 1995.

Krishna, M. C., Grahame, D. A., Samuni, A., Mitchell, J. B., Russo, A. (1992) Oxoammonium cation intermediate in the nitroxide-catalyzed dismutation of superoxide. *Proc. Natl. Acad. Sci. USA*, 89, 5537-5541.

Krishna, M. C. and Samuni, A. (1994) Nitroxides as antioxidants. *Methods Enzym.* 234, 580-589.

Knaapen, M., Shi, T., Borm, P. J. A., Schins, R. P. F. (2002) Soluble metals as well as the insoluble particles fraction are involved in cellular DNA damage induced by particulate matter. *234/235*, 317-326.

Kreyling, W. G., Semmler, M., Erbe, F., Mayer, P., Takenaka, S., Schultz, H., Oberdörster, G., Ziesenis, A. (2002) Translocation of ultrafine insoluble iridium particles from lung epithelium to extrapulmonary organs is size dependent but very low. *J. Toxicol. Environ. Health, Part A* 65, 1513-1530.

Kumagai, Y., Arimoto, T., Shinyashiki, M., Shimojo, N., Nakai, Y., Yoshikawa, T., Sagai, M. (1997) Generation of reactive oxygen species during interaction of

diesel exhaust particle components with NADPH-Cytochrome P540 reductase and involvement of the bioactivation in the DNA damage. *Free Radical Biol. Med.* 22, 479-487.

Lam, C. W., James, J. T., McClusky, R., Hunter, R. L. (2004) Pulmonary toxicity of single-wall carbon nanotubes in mice after 7 and 90 days after intratracheal instillation. *Toxicol. Sci.* 77, 126-134.

Lebowitz, M. D. (1996) Epidemiological studies of air pollution. *Eur. Respir. J.* 9, 1029-1054.

Li, B., Gutierrez, P. L., Blough, N. V. (1997) Trace determination of hydroxyl radical in biological systems. *Anal. Chem.* 69, 4295-4302.

Li, B., Gutierrez, P. L., Blough, N. V. (1999a) Trace determination of hydroxyl radical using fluorescence detection. *Methods of Enzymol.* 300, 202-216.

Li, B.; Gutierrez, P. L.; Amstad, P.; Blough, N. V. (1999b) Hydroxyl radical production by mouse epidermal cell lines in the presence of quinone anti-cancer compounds. *Chem. Res. Toxicol.* 12, 1042-1049.

Li, B., Blough, N. V., Gutierrez, P. L. (2000) Trace detection of hydroxyl radicals during the redox cycling of low concentrations of diaziquone: a new approach. *Free radical in Biol. Med.* 29, 548-556.

Li, N., Wang, M., Oberley T. D., Sempf, J. M., Nel, A. E. (2002) Comparison of the pro-oxidative and proinflammatory effects of organic diesel exhaust particle chemicals in bronchial epithelial cells and macrophage. *J. Immunol.* 169, 4531-4541.

Li, N., Sioutas, C., Cho, A., Schmitz, D., Misra, C., Sempf, J., Wang, M. Y., Oberely, T., Froines, J. and Nel, A. (2003) Ultrafine particulate pollutants induce oxidative stress and mitochondrial damage. *Environ. Health Prespect.* 111, 455-460.

Lind, C., Hochstein, P. and Ernster, L. (1982) DT-diaphorase as a quinone reductase: a cellular control devices against semiquinone and superoxide radical formation. *Arch. Biochem. Biophys.* 216, 178-185.

Logan WPD. (1953) Mortality in London fog incident. *Lancet*, 1, 336-338.

Lebowitz, M. D. (1996) Epidemiological studies of air pollution. *Eur. Respir. J.* 9, 1029-1054.

MacNee, W. and Donaldson, K. (2003) Mechanism of lung injury caused by PM₁₀ and ultrafine particles with special reference to COPD. *Eur. Respir. J.* 21, 47s-51s.

- Maynard, A. D. and Kuempel, E. D.** (2005) Airborne nanostructured particles and occupational health. *J. Nanoparticle Research* 7, 587-614.
- Mahadevan, B., Parsons, H., Musafia, T., Sharma, A. K., Amin, S., Pereira, C. and Baird, W. M.** (2004) Effect of artificial mixtures of environmental polycyclic aromatic hydrocarbons present in coal tar, urban dust and diesel exhaust particulates on MCF-7 cells in culture. *Environmental and molecular mutagenesis*, 44, 99-107.
- Mehlhorn, R. J. and Packer, L.** (1984) Electron spin resonance detection methods for radical detection. *Method Enzym.* 105, 215-220.
- Miller, D. M., Buettner, G. R., Aust, S. D.** (1990) Transition metals as catalysts of "autoxidation" reactions. *Free Radical Biol. Med.* 8, 95-108.
- Mitchell, J. B., Samuni, A., Krishna, M. C., DeGraff, W. G., Ahn, M. S., Samuni, U., Russo, A.** (1990) Biologically active metal-independent superoxide dismutase mimics. *Biochemistry* 29, 2802-2807.
- Molinelli, A. R., Madden M. C., McGee, J. K., Stonehuerner, J. G., Ghio, A. J.** (2002) Effect of metal removal on the toxicity of airborne particulate matter from the Utah valley. *Inhal. Toxicol.* 14, 1069-1086.
- Monteiro-Riviere, N. A., Nemanich, R. J., Inman, A. O., Wang, Y. Y. and Riviere, J. E.** (2005) Multi-walled carbon nanotube interactions with human epidermal keratinocytes. *Toxicol. Lett.* 155, 377-384.
- Möller, W., Hofer, T., Ziesenis, A., Karg, E., Heyder, J.** (2002) Ultrafine particles cause cytoskeletal dysfunctions in macrophages. *Toxicol. Appl. Pharmacol.* 182, 197-207.
- Mossman, B. T., Churg, A.** (1998) Mechanisms in the pathogenesis of asbestosis and silicosis. *Am. J. Respir. Crit. Care Med.* 157, 1666-1680.
- Mwebi, N.** (2005) Fenton and Fenton-like reactions: nature of oxidizing intermediate. PhD dissertation.
- Nemmar, A., Hoel, P. H. M., Vanquickenborne, B., Dinsdale, D., Thomeer, M., Hoylaerts, M. F., Vanbilloen, H., Mortelmans, L., Nemery, B.** (2002) Passage of inhaled particles into the blood circulation in humans. *Circulation*, 105, 411-414.
- Oberdörster, G., Ferin, R., Gelein, J., Soderholm, S. C. and Finkelstein, J.** (1992) Role of the alveolar macrophage in lung injury-studies with ultrafine particles. *Health Perspect.* 97, 193-199.
- Osornio-Vargas, A. R., Bonner, J. C., Alfaro-Moreno, E., Martinez, L., Garcia-Cuellar, C., Rosales, S. P., Miranda, J. and Rosas, I.** (2003) Proinflammatory and

cytotoxic effects of Mexico City air pollution particulate matter in vitro are dependent on particle size and composition. *Environ. Health Perspect.* 111, 1289-1293.

Pan, C. G., Schmitz, D. A., Cho, A. K., Froines, J., Fukuto, J. M. (2004) Inherent redox properties of diesel exhaust particles: Catalysis of the generation of reactive oxygen species by biological reductants. *Toxicol. Science* 81, 225-232.

Petigara, B. R., Blough, N. V., Mignerey, A. C. (2002) Mechanisms of hydrogen peroxide decomposition in soils. *Environ. Sci. Technol.* 36, 639-645.

Prahalad, A. K., Soukup J. M., Inmon J., Willis R., Ghio A. J., Becker S. and Gallagher J. E. (1999) Ambient air particles: Effect on cellular oxidant radical generation in relation to particulate elemental chemistry. *Toxicol. Appl. Pharmacol.* 158, 81-91.

Prahalad, A. K., Inmon, J., Ghio, A. J., Gallagher, J. E. (2000) Enhancement of 2'-Deoxyguanosine hydroxylation and DNA damage by coal and oil fly ash in relation to particulate metal content and availability. *Chem. Res. Toxicol.* 13, 1011-1019.

Prahalad, A. K., Inmon, J., Dailey, L. A., Madden, M. C., Ghio, A. J. and Gallagher, J. E. (2001) Air pollution particles mediated oxidative DNA base damage in a cell free system and in human airway epithelial cells in relation to particulate metal content and Bioreactivity. *Chem. Res. Toxicol.* 14, 879-887.

Prise, K. M., Davies, S., Micheal, B.D. (1993) Evidence for induction of DNA double-strand breaks at paired radical sites. *Radiat. Res.* 134, 102-106.

Pope III, C. A., Burnett, R. T., Thun, M. J., Calle, E. E., Krewski, D., Kazuhiko, I., Thurston, G. D. (2002) Lung cancer, cardiopulmonary, mortality, and long term exposure. *JAMA* 287, 1132-1141.

Porteney, P. R. and Mullahy, J. (1990) Urban air quality and chronic respiratory diseases. *Regional Sci. Urban Econ.* 20, 407-418.

Pou, S., Ramson, C. L., Gladwell, T. (1989) Problems associated with spin-trapping oxygen-centered free radicals in biological systems. *Anal. Biochem.* 177, 1.

Pou, S., Ramson, C. L., Gladwell, T., Renks, E., Centra, M., Young, D., Cohen, M.S., Rosen, M. (1994) A kinetic approach to the selection of a sensitive spin trapping system for the detection of hydroxyl radical. *Anal. Biochem.* 217, 76-83.

Powis, J. and Svingen, B. A. (1981) Pulse radiolysis measurement of one-electron reduction potential (E^1_7) of adriamycin derivatives. *Pharmacol.* 23, 181-187.

Powis, J. (1989) Free radical formation by antitumor quinones. *Free Rad. Biol. Med.* 6, 63-101.

Poster, D. L., Schantz, M. M., Wise, S. A., Vangel, M. G. (1999) Analysis of urban particulate standard reference materials for the determination of chlorinated organic contaminations and additional chemical and physical properties. *Fresenius J. Anal. Chem.* 363, 380-390.

Rosen, G. M. and Rauckman, E. J. (1984) Spin trapping of superoxide and hydroxyl radical. *Methods Enzym.* 105, 198-209.

Samet, J. M., Graves, L. M., Quay, J., Daily, L. A., Devlin, R. B., Ghio, A. J., Wu, W., Bromberg, P. A., Reed, W. (1998) Activation of MAPKs in human bronchial epithelial cells exposed to metals. *Am. J. Physiol. (Lung Cell. Mol. Physiol.)* 275, L551-L558.

Samet, J. M., DeMarini, D. M., Malling, H. V. (2004) Do airborne particles induce heritable mutations? *Science*, 304, 971-972.

Samet J. M. and Cohen, A. J. (1999) in *Air pollution and health*, Academic Press, San Diego, Chapter 36.

Samuni, A. Y., Samuni, A., Swartz, H. M. (1989) The cellular-induced decay of DMPO spin adducts of $\cdot\text{OH}$ and $\cdot\text{O}_2^-$. *Free radical Biol. Med.* 6, 179-183.

Schins, R. P. F., Duffin, R., Höhr, Knaapen, A. M., Shi, T., Weishaupt, C., Stone, V., Donaldson, K. and Borm, P. J. A. (2002) Surface modification of quartz inhibits toxicity, particle uptake and oxidative DNA damage in human lung epithelial cells.

Schmid P. and Ingold K. U. (1978) Kinetic application of EPR spectroscopy. 31. Rate constants for spin trapping. 1. Primary alkyl radicals. *J. Am. Chem. Soc.* 100, 2493-2500.

Schneider, J. C., Card, G. L., Pfau, J. C., Holian, A. (2005) Air pollution particulate SRM 1648 cause oxidative stress in RAW 264.7 macrophages leading to production of prostaglandin E2, a potential Th2 mediator. *Inhalation Toxicol.*, 17, 871-877.

Schwartz, J. and Dockery, D. W. (1992) Increased mortality in Philadelphia associated with daily air pollution concentrations. *Am Rev Respir Dis.* 145, 600-604.

Schwartz J. (1994) Air pollution and daily mortality: A review and meta-analysis *Environ. Res.* 64, 36-52.

Shi, X., Dalal, N. S., Vallyathan, V. (1988) ESR evidence for the hydroxyl radical formation in aqueous suspension of quartz particles and its possible significance to lipid peroxidation in silicosis. *Toxicol. Environ. Health.* 25, 237-245.

Shi, X., Dong, Z., Huang, C., Ma, W., Kejian, L., Ye, J., Chen, F., Leonard, S. S., Ding, M., Castranova, V., Vallyathan, V. (1999) The role of hydroxyl radical as a messenger in the activation of nuclear transcription factor NF- κ B. *Mol Cell. Biochem.* 194, 63-70.

Shi, T., Schins, R. P. F., Knaapen, A. M., Kuhlbusch, T., Pitz, M., Heinrich, J., Borm, P. J. A. (2003a) Hydroxyl radical generation by electron paramagnetic resonance as a new method to monitor ambient particulate matter composition. *Journal of Environmental Monitoring* 5, 550-556.

Shi, T., Knaapen, A. M., Begerow, J., Birmili, W., Borm, P. J. A., Schin, R. P. F. (2003b) Temporal variation of hydroxyl radical generation and 8-hydroxy-2'-deoxyguanosine formation by coarse and fine particulate matter. *Occup. Environ. Med.* 60, 315-321.

Shukla, A., Timblin, C. R., Berube, Gordon, T., McKinney, W., Driscoll, K., Vacek, P., J., Mossman, B. T., (2000) Inhaled particulate matter causes expression of Nuclear Factor (NF)- κ B-related genes and oxidant-dependent NF- κ B activation in vitro. *Am. J. Respir. Cell Mol. Biol.* 23, 182-187.

Shukla, A., Timblin, C. R., Hubbard, A. K., Bravman, J., Mossman, B. (2001) Silica-induced activation of c-Jun-NH₂-terminal amino kinases, protracted expression of the activator protein-1 proto-oncogene, *fra-1*, and S-Phase alterations are mediated via oxidative stress. *Cancer Res.* 61, 1791-1795.

Shvedova, A. A., Kisin, E. R., Murray, A. R., Gandelsman, V. Z., Maynard, A. D., Baron, P. A., Castranova, V. (2003) Exposure to carbon nanotube material: Assessment of the biological effects of nanotube materials using human keratinocyte cells. *J. Toxicol Environ. Health* 66, 1909-1926.

Singh, P., Demarini, D. M., Dick, C. A. J., Tabor, D. G., Ryan, J. V., Linak, W. P., Kobayashi, T., Gilmour, M. I. (2004) Sample characterization of Automobile and forklift diesel exhaust particles and comparative pulmonary toxicity in mice. *Environ. Health Perspect.* 112, 820-825.

Smith, K. R., Aust, A. E. (1997) Mobilization of iron from urban particulates leads to generation of reactive oxygen species in vitro and induction of ferritin synthesis in human lung epithelial cells. *Chem. Res. Toxicol.* 10, 828-834.

Somers, C. M., McCarry, B. E., Malek F., Quinn J. S. (2004) Reduction of particulate air pollution lowers the risk of heritable mutations in mice. *Science* 304, 1008-1010.

Squadrito, G. L., Cueto, R.; Dellinger, B., Pryor, W. A. (2001) Quinoid redox cycling as a mechanism for sustained free radical generation by inhaled airborne particulate matter. *Free Radical Biol. Med.* 31, 1132-1138.

Sunyer, J. and Basagaña, X. (2001) Particles, and not gases, are associated with the risk of death in patients with chronic obstructive pulmonary disease. *Intern. J. Epidemiol.* 30, 1138-1140.

Swartz, H. M. Sentjurc, M. and Morse P. D. II. (1986) Cellular metabolism of water-soluble nitroxides effect on rate of reduction of cell/nitroxide ratio, oxygen concentration and permeability of nitroxides. *Biochim. Biophys. Acta*, 888, 82-90.

Swartz, H. M. (1987) Use of nitroxides to measure redox metabolism in cells and tissues. *J. Chem. Soc. Faraday Trans. I*, 83, 191-202.

Swartz, H. M. (1990) Principles of the metabolism of nitroxides and their implication for spin trapping. *Free Rad. Res. Commun.* 9, 399-405.

Tao, F. and Kobzik, L. (2002) Lung macrophage-epithelial cell interactions amplify particle-mediated cytokine release. *Am. J. Respir. Cell Mol. Biol.* 26, 499-505.

Tao, F., Gonzalez-Flecha, B., Kobzik L. (2003) Reactive oxygen species in pulmonary inflammation by ambient particulates. *Free Radical Biol. Med.* 35, 327-340.

Takizawa, H., Ohtoshi, T., Kawaski, S., Kohyama, T., Desaki, M., Kasama, T., Kobayashi, K., Nakahara, K., Yamamoto, K., Matsushima, K., Kudoh, S. (1999) Diesel exhaust particles induce NF-kappa B activation in human bronchial epithelial cells in vitro: importance in cytokine transcription. *J. Immunol.* 162, 4705-4711.

Takizawa, H., Abe, S. Okazaki, H., Kohyama, T., Kawaski, S., Sugewara, I., Saito, Y., Ohtoshi, T., Kawasaki, S., Desaki, M., K., Nakahara, Yamamoto, K., K., Matsushima, Tanaka, M. Sagai, M., Kudoh, S. (2003) Diesel exhaust particles upregulate eotaxin gene expression in human bronchial epithelial cells via nuclear factor- κ B-dependent pathway. *Am. J. Physiol. Lung Cell Mol. Physiol.* 284, L1055-L1062.

Thomas-Smith, T. E., Blough, N. V. (2001) Photoproduction of hydrated electron from constituents of natural water. *Environ. Sci. Technol.* 35, 2721-2726.

- Tran, C. L., Buchanan, D., Cullen, R. T., Searl, A., Jones, A. D., Donaldson, K.** (2000) Inhalation of poorly soluble particles. II. Influence of particle surface area on inflammation and clearance. *Inhal. Toxicol.* 12, 1113-1126.
- Tseny R. Y., Li C. K., Spiky J.** (1992) Particulate air pollution and hospitalization for asthma. *Ann. Allergy* 68, 425-432.
- Upadhyay, D., Panduri, V., Ghio, A., Kamp, D. W.** (2003) Particulate matter induces alveolar epithelial cell DNA damage and apoptosis: Role of free radicals and the mitochondria. *Am. J. Respir. Cell Mol. Biol.*, 29, 180-187.
- Utell, M.J., Frampton, M. W.** (2000) Acute health effects of ambient air pollution: the ultrafine particle hypothesis. *J Aerosol Med.* 13, 355-359.
- Vallyathan, V., Shi, X., Dalal, N. R., Irr, W., Castranova, V.,** (1988) Generation of free radicals from freshly fractured silica dust; potential role in acute silica-induced lung injury. *American Review of Respiratory Diseases*, 138(5), 1213-1219.
- Vaughan, P. P., Blough, N. V.** (1998) Photochemical formation of hydroxyl radical by constituents of natural water. *Environ. Sci. Technol.* 32, 2974-2953.
- Veranth J. M., Reilly, C. A., Veranth, M. M., Moss, T. A., Langelier, C. R.** (2004) Inflammatory cytokines and cell death in BEAS-2b lung cells treated with soil dust, lipopolysaccharide, and surface-modified particles. *Toxicol. Sci.* 82, 88-96.
- Valavanidis, A., Fiotakis, K., Bakeas, E., Vlahogianni, T.** (2005) Electron paramagnetic resonance study of the generation of reactive oxygen species catalysed by transition metals and quinoid redox cycling by inhalable particulate matter. *Redox Report*, 10, 37-51.
- Valavanidis, A.; Fiotakis, K.; Vlahogianni, T.; Papadimitriou, V.; Pantikaki, V.** (2006) Determination of selective quinones and quinoid radicals in airborne particulate matter and vehicular exhaust particles. *Environmental chemistry*, 3, 118-123.
- Vallyathan, V., Shi, X., Dalal, N. S., Irr, W. and Castranova, V.** (1988) Generation of free radicals from freshly fractured silica dust; potential role in acute silica-induced injury. *American Review of Respiratory Disease*, 138, 1213-1219.
- Vorlicek, T. P. and G. R. Helz** (2002) Catalysis by mineral surfaces: Implications for Mo geochemistry in anoxic environment. *Geochimica et Cosmochimica ACTA*, 66, 3679-3692.
- Warheit, D. B., Laurence, B. R., Reed, K. L., Roach, D. H., Reynolds, G. A. M., Webb, T. R.** (2004) Comparative pulmonary toxicity assessment of single-wall carbon nanotubes in rats. *Toxicol. Sci.* 77, 117-125.

Welch, K. D.; Davis, T. Z.; Aust, S. D. (2002) Iron autoxidation and free radical generation effects of buffers, ligands and chelators. *Arch. Biochem. Biophys.* 397, 360-369.

Whittemore, A. S.; Korn, E. L. (1980) Asthma and air pollution in the Los Angeles area. *Am J Public Health.* 70, 687-696.

Wilson, R. L. (1971) Pulse radiolysis studies on reaction of triacetoneamine-N-oxyl with radiation-induced free radicals. *Trans, Faraday Soc.* 67, 3008-3019.

Wilson, M. R., Lightbody, J. H., Donaldson, K., Sales, J. and Stone, V. (2002) Interaction between ultrafine particles and transition metals in vivo and in vitro. *Toxicol. Appl. Pharmacol.* 184, 172-179.

Xu, A., Wu, L. J., Santella, R. M. (1999) Role of oxyradicals in mutagenicity and DNA damage induced by crocidolite asbestos in mammalian cells. *Cancer Res.* 59, 5922-5926.